Mammalian SWI/SNF collaborates with a polycomb-associated protein to regulate male germ line transcription in the mouse

Debashish U. Menon, Yoichiro Shibata, Weipeng Mu and Terry Magnuson

Department of Genetics, and Lineberger Comprehensive Cancer Center, The University of North Carolina at Chapel Hill, Chapel Hill, North Carolina, NC 27599-7264, USA

*Correspondence: trm4@med.unc.edu, Tel 919-962-1319, Fax 919-843-4682

Abstract:

A deficiency in BRG1, the catalytic subunit of the SWI/SNF chromatin remodeling complex, results in a meiotic arrest during spermatogenesis. Here, we explore the causative mechanisms. BRG1 is preferentially enriched at active promoters of genes essential for spermatogonial pluripotency and meiosis. In contrast, BRG1 is also associated with the repression of somatic genes. Chromatin accessibility at these target promoters is dependent upon BRG1. These results favor a model where BRG1 coordinates spermatogenic transcription to ensure meiotic progression. In spermatocytes, BRG1 interacts with SCML2, a testes specific PRC1 factor that is associated with the repression of somatic genes. We present evidence to suggest that BRG1 and SCML2 concordantly regulate genes during meiosis. Furthermore, BRG1 is required for the proper localization of SCML2 and its associated deubiquitinase, USP7, to the sex chromosomes during pachynema. SCML2 associated, mono ubiquitination of histone H2A lysine 119 (H2AK119ub1) and acetylation of histone lysine 27 (H3K27ac) are elevated in *Brg1*^{cKO} testes. Coincidentally, the PRC1 ubiquitin ligase, RNF2 is activated while a histone H2A/H2B deubiquitinase, USP3 is repressed. Thus, BRG1 impacts the male epigenome by influencing the localization and expression of epigenetic modifiers. This mechanism highlights a novel paradigm of co-operativity between SWI/SNF and PRC1.

Keywords: SWI/SNF chromatin remodeling,BRG1, transcriptional regulation, SCML2

Summary statement

BRG1, a catalytic subunit of SWI/SNF chromatin remodeling complex, interacts with SCML2 (Sex comb on midleg-like 2), a member of the polycomb repressive 1 (PRC1) complex, to regulate transcription during spermatogenesis. This represents a novel paradigm of co-operativity between SWI/SNF and PRC1 that is critical to gametogenesis.

41 **Introduction:**

42

43 Spermatogenesis is a developmental cascade in which genetic information is passed on from
44 mitotic precursors to meiotically derived haploid gametes. This process is particularly sensitive to
45 the activity of several epigenetic regulators, known to influence meiotic recombination. Examples
46 include the role of the meiosis specific H3K4 methyltransferase PRDM9 (PR domain zinc finger
47 protein9) in double stranded break (DSB) formation and the roles of polycomb repressive
48 complex2 (PRC2) and the H3K9 methyl transferases, EHMT2- Euchromatic histone lysine N-
49 methyltransferase 2 (G9a); Suppressor of variegation 3-9 1 or 2 (SUV39H1/H2) in homolog
50 pairing (synapsis) (Brick et al., 2012; Diagouraga et al., 2018; Hayashi et al., 2005; Mu et al.,
51 2014; Tachibana et al., 2007; Takada et al., 2011). In addition to meiotic recombination, the
52 temporal regulation of transcription is also essential for normal spermatogenesis. Defects in male
53 fertility have been attributed to the mis-regulation of genes governed by polycomb repressive
54 complexes, PRC1 and PRC2 (Hasegawa et al., 2015; Mu et al., 2014). Put together, these
55 studies illustrate the importance of proteins that catalyze or respond to specific histone
56 modifications in the germ line. Another class of proteins that modulate chromatin accessibility,
57 have also been shown to be essential for spermatogenesis. These include the INO80, SWI/SNF
58 and CHD5 family of ATP dependent nucleosome remodeling complexes. Their impact spans the
59 gamut of spermatogenesis, beginning at meiosis and ending at spermiogenesis (Kim et al., 2012;
60 Li et al., 2014; Serber et al., 2015).

61

62 Our lab previously reported the role of BRG1 (SMARCA4 – SWI/SNF catalytic subunit) during
63 meiosis-I in males (Kim et al., 2012). Normally, meiosis-I is initiated by the formation of DSBs
64 induced by the SPO11 endonuclease at leptonema, following which, an orderly process of
65 chromosomal synapsis during zygonema, crossover formation at pachynema and asynapsis at
66 diplonema ensues, culminating in DNA repair and recombination (reviewed in Handel and
67 Schimenti, 2010). The germ line depletion of BRG1 results in a pachytene arrest. Briefly, mutant
68 spermatocytes display unrepaired DNA DSBs evidenced by persistent γH2Ax, chromosomal
69 asynapsis and reduced MLH1 foci, a marker of crossovers (Wang et al. 2012). Additionally,
70 mutant pachytene spermatocytes also display enhanced levels of repressive chromatin, which
71 could either be a physiological consequence of apoptotic initiation or a product of perturbed
72 epigenetic processes. SWI/SNF influences chromatin accessibility by either sliding or evicting

73 nucleosomes (Clapier et al., 2017). It is therefore plausible that the meiotic defects seen in the
74 *Brg1*^{cKO} testes might be a consequence of altered chromatin structure, which may either perturb
75 transcription or DNA repair. Both processes are known to be influenced by SWI/SNF.
76
77 SWI/SNF is associated with both gene activation and repression. In mouse embryonic fibroblasts,
78 BRG1 and the core SWI/SNF member, SNF5 are known to co-ordinate nucleosome occupancy
79 at promoters to achieve transcriptional regulation (Tolstorukov et al., 2013). The transcriptional
80 outcome is often dictated by the subunit composition of the complex, which in turn can influence
81 its genome-wide association and interactions with other gene regulators (Euskirchen et al., 2011;
82 Raab et al., 2015; Raab et al., 2017). SWI/SNF complexes are biochemically heterogeneous and
83 are broadly categorized into the *Brahma* Associated Factor (BAF) and *polybromo*-BAF (PBAF)
84 complex, based on the identity of mutually exclusive DNA binding subunits and associated
85 ATPase (BRG1/BRM) (Masliah-Planchon et al., 2015). This SWI/SNF heterogeneity is a theme
86 that features frequently in the regulation of tissue and cell type specific transcriptional programs
87 that impact critical processes such as embryonic stem (ES) cell pluripotency and differentiation,
88 neuronal and cardiac cell fate specification (Ho and Crabtree, 2010). SWI/SNF subunits also
89 constitute some of the most frequently mutated genes in various cancers (Masliah-Planchon et
90 al., 2015). Thus, SWI/SNF directed gene regulation plays a critical role in development and
91 disease.
92
93 Apart from gene regulation, SWI/SNF has also been implicated in several DNA repair
94 mechanisms. In Yeast and cell culture models, SWI/SNF is recruited to sites of DNA damage to
95 promote accessibility and stimulate γH2Ax, a key component of the DNA damage response
96 (DDR) signaling pathway (Kwon et al., 2015; Lee et al., 2010; Ogiwara et al., 2011). Other
97 activities include the recruitment of homologous recombination (HR) and non-homologous end
98 joining (NHEJ) repair factors (Ogiwara et al., 2011; Qi et al., 2014; Watanabe et al., 2014), the
99 transcriptional silencing of regions adjacent to DNA DSB (Kakarougkas et al., 2013). Unlike its
100 role in mitotic cells, BRG1 is dispensable for γH2Ax formation during meiosis but has been
101 reported to affect the distribution of DDR factors like RAD51 (DNA recombinase) and RPA
102 (Replication protein A1) (Kim et al., 2012).
103
104 In this study we present evidence to show that BRG1 influences spermatogenesis by
105 coordinating germ line transcription. BRG1 activates genes that are essential for maintaining

106 spermatogonial pluripotency and meiotic progression and represses somatic genes. Our data
107 suggest that gene repression is achieved through an interaction with SCML2 (Sex comb on
108 midleg-like 2), a known testis specific PRC1(Polycomb Repressive Complex 1) member known
109 to regulate somatic genes (Luo et al., 2015). We show that that loss of BRG1 results in the
110 activation of somatic genes that are normally repressed by SCML2. Additionally, mutant
111 pachytene spermatocytes display the mis-localization of SCML2 and its interacting partner,
112 USP7 (Ubiquitin Specific Peptidase 7) from the sex body (sub nuclear γH2Ax enriched
113 compartment containing the sex chromosomes), indicating a failure in recruitment. Furthermore,
114 histone modifications associated with SCML2, such as the repressive mono ubiquitination of
115 histone H2A lysine 119 (H2AK119ub1) and activating acetylation of histone lysine 27 (H3K27ac)
116 are perturbed in *Brg1*^{cKO} testes. Coincidentally, BRG1 also activates the expression of the H2A
117 ubiquitin ligase, RNF2 (Ring Finger Protein 2) and represses the histone H2A/H2B
118 deubiquitinase, USP3 (Ubiquitin Specific Peptidase 3). Thus SWI/SNF can potently shape the
119 epigenetic landscape, in an SCML2 dependent and independent fashion to regulate germ line
120 transcription.
121

122 **Results:**

123

124 **BRG1 associates with transcriptionally active and poised chromatin**

125 To understand the functions of SWI/SNF activity during meiosis, we determined the genome-wide
126 association of BRG1 by ChIP-seq. We reasoned that the examination of BRG1 binding dynamics
127 concurrent to critical meiotic processes such as DSB repair and homologous chromosome
128 synapsis would yield insight into the molecular mechanisms underlying the meiotic defects
129 observed in the *Brg1*$^{fl/\Delta}$*; Mvh-cre*$^{Tg/0}$ (*Brg1*^{cKO}; see materials and methods) males. For this purpose
130 we isolated chromatin from spermatogenic cells obtained from P12 (mostly pre-pachytene germ
131 cells) and P18 testes (predominantly pachytene spermatocytes) (Bellve et al., 1977; Goetz et al.,
132 1984). At both P12 and P18, BRG1 appears to be enriched promoter proximally (Fig. 1A, panels
133 1 & 4). This is consistent with the fact that more than 50% of BRG1 peaks occupy promoters of
134 genes in P12 and P18 spermatogenic cells, with only a minority mapping to distal sites (Fig. S1A).
135 By performing K-means clustering we were able to categorize transcription start sites (TSS) into
136 three different classes (class1: Cl-1, class2: Cl-2, class: Cl-3) based upon their association with
137 BRG1. These TSS's are characterized by high (Cl-1), medium (Cl-2) and negligible (Cl-3) BRG1
138 enrichment.

139

140 To gain insight into the activity of genes associated with promoters occupied by BRG1 in
141 spermatogenic cells, we surveyed the chromatin environment surrounding these TSS. We
142 specifically monitored the enrichment of trimethylation of histone H3 lysine 4 (H3K4me3),
143 associated with gene activation and trimethylation of histone H3 lysine 27 (H3K27me3),
144 associated with gene repression. We compared BRG1 ChIP profiles from P12 and P18 testes to
145 stage-equivalent H3K4me3 and H3K27me3 ChIP profiles generated from P12 and P17 testes
146 (Mu et al., 2014) (Fig. 1A). Robust H3K4me3 enrichment appeared to be associated stably with
147 Cl-1 and Cl-2 promoters and was near-absent at Cl-3 promoters from P12 to P17 (Fig. 1A, panels
148 2 & 5). On the other hand, H3K27me3 levels at P12 and P17 appear depleted at Cl-1 (high BRG1)
149 promoters. Such antagonism is a well-established feature of SWI/SNF and PRC2 genomic
150 associations (Wilson et al., 2010). Cl-3 (low to no BRG1) promoters only displayed basal levels
151 of H3K27me3, which is particularly discernable at P17. In contrast to Cl-1 and Cl-3, Cl-2 promoters
152 that feature medium BRG1 enrichment display significantly higher levels of H3K27me3, which
153 appears progressively enhanced from P12 to P17 (Fig. 1A, panels 3 & 6). The co-occurrence of
154 H3K27me3 and H3K4me3 at Cl-2 promoters resemble features of bivalent promoters, which are

155 usually associated with transcriptionally quiescent genes poised to be reactivated at later stages
156 of development (Bernstein et al., 2006; Hammoud et al., 2014; Lesch et al., 2013). Thus genes
157 associated with Cl-2 promoters likely represent repressed target genes. In contrast potential
158 activated gene targets appear to be associated with Cl-1 BRG1 promoters.
159
160 To understand BRG1 directed gene regulation in the context of spermatogenesis, we categorized
161 the genes associated with each K-means cluster (Fig. 1A), by their temporal expression profiles,
162 previously determined from whole-testes RNA seq data (Margolin et al., 2014). The genes were
163 split between the five major categories, which include those maximally expressed in testes, at P6
164 (pre-meiotic: Pmei), from P8-P20 (meiotic: Mei), at P38 (Late, adult testis), from P6-P38
165 (Constantly; Const) and those expressed at low levels in testes from P6-P38 (Low, < 2 Reads per
166 Kilobase per Million of Reads; RPKM). The majority of Cl-1 associated genes were meiotic with
167 relatively fewer pre-meiotic genes. In contrast, Cl-2 and Cl-3 were mostly comprised of pre-meiotic
168 and low genes (Fig. S1B). This is particularly interesting given that Cl-1 gene promoters appear
169 to be exclusively marked by H3K4me3 indicative of transcriptional activation, while the Cl-2
170 promoters display bivalent chromatin modifications (H3K4me3/H3K27me3), which is indicative of
171 transcriptional silencing. We observed similar trends when monitoring H3K4me3 and H3K27me3
172 dynamics, specifically at BRG1 target promoters (P12 peaks) categorized by their temporal
173 expression profile during meiosis (P12 to P17) (Fig. 1B). Over this duration all target gene
174 categories experience a 4-fold decrease in BRG1 enrichment in the presence of relatively
175 abundant levels of H3K4me3 (Fig. 1B, top and middle row). Only pre-meiotic and low gene targets
176 display elevated levels of H3K27me3 from P12 to P17 (Fig. 1B, bottom row), distinguishing them
177 from, meiotic, constant and late gene targets, that appear exclusively marked by H3K4me3 (Fig.
178 1B, middle and bottom row). Candidate pre-meiotic targets such as *Zbtb16* and *Id4*, which are
179 markers of undifferentiated spermatogonial cells along with *Pdgfra*, a somatic signaling receptor,
180 that are normally repressed during meiosis, display promoters bivalently modified with H3K4me3
181 and H3K27me3 (Basciani et al., 2002; Green et al., 2018; Hammoud et al., 2014). In contrast, the
182 promoter of BRG1 target, *Sycp1*, which is expressed during meiosis and is essential for
183 synaptonemal complex assembly is marked exclusively by H3K4me3 (Fig. S1C) (De Vries et al.,
184 2005). Thus BRG1 might co-ordinate the expression of genes over the measured course of
185 spermatogenesis.
186

187 Given its robust association with active (H3K4me3) and poised (H3K4me3/H3K37me3)
188 chromatin, we were curious to examine BRG1 localization to the sex chromosomes, which are
189 transcriptionally silenced during pachynema (reviewed in Turner, 2007). We examined BRG1
190 occupancy at the TSS's of X – linked genes in P12 (Pre-pachytene stages) and P18 (Pachytene
191 stages) spermatogenic cells. BRG1 enrichment at X – linked TSS's appeared reduced at P18
192 relative to P12, but not absent (Fig. 1C). Thus BRG1 associates with regions that are subject to
193 transcriptional repression during meiosis.
194
195 Apart from TSS's, H3K4me3 is also enriched at DSB/recombination hotspots, known to be
196 associated with a meiosis specific histone methyl transferase, PRDM9 (Brick et al., 2012;
197 Diagouraga et al., 2018; Hayashi et al., 2005). We therefore examined BRG1 association at these
198 PRDM9 sites previously mapped by ChIP-seq in P12 testes (Baker et al., 2015). The lack of any
199 association with PRDM9 peaks makes it unlikely that BRG1 directly affects DSB formation (Fig.
200 S1D). Thus BRG1 might play a major role in gene regulation during meiosis.
201
202
203 **BRG1 co-ordinates spermatogenic gene expression**
204 The promoter centric association of BRG1 prompted us to examine its influence on the
205 transcription of target genes by RNA-seq. We compared transcript abundance between
206 spermatogenic cells isolated from P12 *Brg1*$^{fl/+}$ (*Brg1*^{WT}) and *Brg1*$^{fl/\Delta}$*; Mvh-cre*$^{Tg/0}$ (*Brg1*^{cKO}) testes.
207 The quantification of spermatocytes per tubule present at various stages of prophase I from
208 *Brg1*^{WT} and *Brg1*^{cKO} testes cryosections, staged by γH2Ax staining, revealed similar proportions
209 of pre-pachytene populations up to P13 (Fig. S2A, left panel). Beyond this stage we began to
210 notice differences in the cellular profiles between *Brg1*^{WT} and *Brg1*^{cKO} testes at P14 (Fig. S2A,
211 left panel). This is consistent with the incidence of pachytene arrest induced apoptosis in
212 previously reported in *Brg1*^{cKO} testes (Kim et al., 2012). Thus we considered P12 to be an
213 appropriate stage at which RNA-seq could be performed between *Brg1*^{WT} and *Brg1*^{cKO} testes. In
214 agreement with the cell quantification, an examination of prophase I substage specific protein
215 coding transcripts (Ball et al., 2016) revealed no significant differences in the abundance of pre-
216 pachytene staging markers between P12 *Brg1*^{WT} and *Brg1*^{cKO} testes (Fig. S2A). Only, early and
217 late pachytene specific transcripts were slightly less abundant in the P12 *Brg1*^{cKO} relative to
218 *Brg1*^{WT} testes (Fig. S2A, right panel). This is suggestive of a minor difference in the onset of

219 pachynema. Overall we do not expect the analysis of gene expression to be impacted significantly
220 by secondary effects such as developmental delays.
221
222 To identify genes significantly mis-expressed (FDR ≤ 0.05) upon the loss of BRG1, we performed
223 an edgeR analysis on the RNA-seq data. An equivalent number of genes are either
224 transcriptionally down regulated (n=1100) or up regulated (n=983) in P12 *Brg1*^{cKO} relative to
225 *Brg1*^{WT} testes (Fig. 2A). More genes were down regulated (n=310) by a magnitude of 2-fold or
226 higher, relative to those up regulated (n=75), upon the loss of BRG1 (Fig. 2A) . Nearly half of all
227 the differentially regulated genes are occupied by BRG1 peaks (P12 peaks). The down regulated
228 genes were associated with transcripts normally expressed in gonadal tissue and the nervous
229 system and were enriched for Gene ontology (GO) terms relevant to meiotic processes (Fig. 2B).
230 In contrast ,the up regulated genes are normally expressed in limb and muscle and were enriched
231 for GO terms relevant to somatic developmental processes (Fig. 2B). Thus, BRG1 coordinates
232 germ line transcription by activating meiotic genes while concomitantly repressing somatic genes.
233 Since BRG1 is essential for meiotic progression (Kim et al., 2012), we monitored the expression
234 of genes associated with abnormal spermatogonia proliferation and meiotic arrest phenotypes,
235 curated from the mouse genome database (Blake et al., 2003). We integrated the expression
236 data into a heatmap that displays z-scores associated with transcript abundance of each
237 candidate gene, measured across P12 *Brg1*^{WT} and *Brg1*^{cKO} replicates (Fig. 2C). With the
238 exception of *Androgen receptor* (*Ar*) and *Microtubule associated protein 7* (*Map7*), all other germ
239 cell factors appeared less abundant upon the loss of BRG1 (Fig. 2C). Next, we adopted a reverse
240 genetic approach to test whether the mis-expression of candidate genes were associated with
241 specific phenotypes in the *Brg1*^{cKO}. To do this we choose a pre-meiotic candidate, *Zbtb16* and
242 meiotic candidate, *Sycp2*.
243
244 *Zbtb16* is essential for the maintenance of a pool of undifferentiated spermatogonia (typeA, SpgA)
245 (Buaas et al., 2004) . While BRG1 has been shown to be dispensable for the establishment of
246 spermatogonia, its role in the maintenance of SpgA is unknown (Kim et al., 2012). We quantified
247 the number of SpgA in P10 *Brg1*^{WT} and *Brg1*^{cKO} testes cryosections by immunofluorescence
248 staining for ZBTB16. The *Brg1*^{cKO} testes contain 46% fewer SpgA, when compared to *Brg1*^{WT}
249 testes (Fig. 2D). Since a reduction in the number of SpgA in the *Brg1*^{cKO} can skew the measured
250 abundance of *Zbtb16* mRNA, we performed qRT-PCR to measure transcript abundance in
251 purified, THY1^{+} fraction containing spgA cells obtained from P8 *Brg1*^{WT}, *Brg1*^{Het} (*Brg1*$^{fl/+}$*;Mvh-*

252 *cre*$^{Tg/0}$) and *Brg1*^{cKO} testes. In addition to *Zbtb16*, we also monitored the expression of other
253 established stem cell factors such as, *Inhibitor of DNA binding 4* (*Id4*), *POU domain, class 5,*
254 *transcription factor 1* (*Pou5f1*, also known as *Oct4*)*, POU domain, class 3, transcription factor 1*
255 (*Pou3f1, also known as Oct6*) and *Forkhead box O1* (*Foxo1*) (Dann et al., 2008; Goertz et al.,
256 2011; Oatley et al., 2011; Wu et al., 2010). The loss of BRG1 resulted in a significant decrease in
257 the abundance of transcripts associated with *Zbtb16*, *Id4* and *Pou5f1* in the purified THY1^{+}
258 fractions (Fig. S2B). The fact that *Thy1* mRNA levels remain abundant argues against a loss of
259 spermatogonial cells early in development (Fig. S2B). Thus, BRG1 influences the maintenance
260 of a pool of undifferentiated spermatogonial cells by activating the expression of critical stem cell
261 factors.
262
263 The meiotic gene candidate, *Sycp2*, constitutes the structural component of the lateral element
264 of meiotic chromosomal axes and is essential for synapsis (Yang et al., 2006). Coincidentally,
265 *Brg1*^{cKO} spermatocytes display an increase in asynapsis (Kim et al., 2012). In the *Brg1*^{cKO}, SCYP2
266 levels are distinctly lower relative to the controls (Fig. 2E, Fig. S2C) and abnormally assemble
267 into short lateral filaments and aggregates in about 37% of the mutant zygotene spermatocytes
268 (Fig. 2F, Fig. S2D). While *Sycp2*$^{-/-}$ spermatocytes fail to form SYCP3 elements , we did not
269 observe a similar defect in the *Brg1*^{cKO} spermatocytes (Fig. S2D) (Yang et al., 2006). We reason
270 that the reduced levels of SYCP2 might be sufficient to facilitate apparently normal SYCP3
271 assembly. Thus, a paucity in SYCP2 may limit meiotic progression by potentially compromising
272 the formation of a functional synaptonemal complex. In addition to the mis-regulation of essential
273 germ cell factors, we also identified a significant increase in the expression of several somatic
274 genes in the *Brg1*^{cKO} (Table S1). *Pdgfra* a signaling receptor, generally associated with somatic
275 (Basciani et al., 2018; Schmahl et al., 2008) and pre-meiotic spermatogonia (Hammoud et al.,
276 2014) , was up-regulated by more than 2-fold over a period spanning meiosis-I in the *Brg1*^{cKO} (Fig.
277 S2E).
278
279
280 **BRG1 is required to maintain chromatin accessibility at promoters**
281 Chromatin remodelers reposition nucleosomes, consequently regulating accessibility to
282 transcription factors. Thus BRG1 might influence transcription by modulating the structure of the
283 germ line epigenome. To investigate this, we performed Assay for Transposase-Accessible
284 Chromatin (ATAC)-seq to map open chromatin in pre-pachytene and pachytene spermatogenic

285 cells isolated from P12 and P18 testes respectively. Similar to the RNA-seq data, we surveyed
286 differences in chromatin accessibility between P12 *Brg1*^{WT} and *Brg1*^{cKO} testes (Fig. S3A, left
287 panel). Since P18 *Brg1*^{cKO} testes are characterized by severe pachytene arrest, we compared
288 chromatin accessibility between P18 *Brg1*^{WT} and *Brg1*^{Het} (*Brg1*$^{fl/\Delta}$) testes (Fig. S3A, right panel).
289 In normal spermatogenic cells, strong ATAC read coverage was detected promoter proximally at
290 both P12 and P18 (Fig. S3A). This promoter accessibility is significantly diminished in P12
291 *Brg1*^{cKO} testes and also under conditions of haploinsufficiency in P18 *Brg1*^{Het} testes (FigS3A).
292
293 Since promoter proximal chromatin responds to the loss of BRG1, we first monitored the changes
294 in chromatin accessibility at promoters of target genes differentially regulated by BRG1 (Fig. 3A).
295 Promoters of BRG1 target genes that are normally activated (down regulated upon BRG1 loss),
296 display a significant decrease in promoter accessibility in the *Brg1*^{cKO} relative to *Brg1*^{WT} testes.
297 While the promoters of repressed gene targets (up regulated upon BRG1 loss) are less accessible
298 relative to their activated counterparts in *Brg1*^{WT} testes, their accessibility appears further reduced
299 in the *Brg1*^{cKO} testes, albeit at levels that fail to meet statistical significance (Fig. 3A). Thus only
300 activated gene promoters experience a significant change in accessibility.
301
302 To identify genome-wide changes in chromatin accessibility at P12, we performed edgeR on the
303 ATAC read counts obtained from wild type and mutant samples. The vast majority of regions that
304 displayed significant differences in chromatin accessibility appear to be less accessible (Closed;
305 n= 549), leaving only a few regions that acquire greater accessibility (Opened; n= 99) in the
306 *Brg1*^{cKO} relative to the *Brg1*^{WT} testes (Fig. 3B). Consistent with the general decrease in promoter
307 accessibility in the *Brg1*^{cKO} (Fig. S3A), the closed regions are overwhelmingly associated with
308 promoters (Fig. 3C, Fig. S3B; panel 1). In contrast, the opened regions were prominently featured
309 within introns and intergenic regions (Fig. 3C, Fig. S3B, panel 2 & 3). This overall decrease in
310 chromatin accessibility genome-wide is consistent with the previously observed increase in
311 repressive epigenetic modifications in *Brg1*^{cKO} spermatocytes (Kim et al., 2012). The genes
312 associated with closed promoters in *Brg1*^{cKO} testes were mostly meiotic in function (Fig. 3D, Table
313 S2). Thus BRG1 probably activates meiotic genes by maintaining chromatin accessibility at
314 cognate promoters. In contrast a few genes associated with the distal sites that appear more
315 accessible in the *Brg1*^{cKO} testes, represent somatic factors (Fig. 3D, Table S2).
316
317

318 **BRG1 physically interacts with SCML2, a non-canonical PRC1 factor**

319 To investigate further mechanisms governing SWI/SNF mediated epigenetic regulation, we
320 monitored BRG1 interactions during meiosis. BRG1 Immuno-pulldowns (IP) were prepared from
321 nuclear extracts obtained from 3-week-old testes (Fig. 4A). Proteins isolated from a BRG1 IP and
322 control nonspecific (ns) IgG pulldown were identified by mass spectrometry (MS). Peptides
323 belonging to known SWI/SNF sub-units were identified only in the BRG1 IP, which demonstrates
324 the efficacy of this procedure (Fig. 4A, Fig. S4A). Furthermore the presence of both SWI/SNF sub
325 complexes; *Brahma* Associated Factor (BAF) and *polybromo*-BAF (PBAF) are detected in the
326 germ line (Fig. 4A,Fig. S4A). More interestingly we identified peptides associated with SCML2, a
327 known testes specific PRC1 factor (Hasegawa et al., 2015; Luo et al., 2015) (Fig. 4A). Since
328 candidate peptides were also detected in the non-specific IgG IP, we validated these interactions
329 by performing a reverse IP with an antibody against SCML2 (Fig. 4B). The IP was conducted on
330 nuclear lysates treated with universal nuclease (benzonase) to eliminate the possibility of non-
331 specific, DNA mediated interactions. BRG1 was specifically detected in the SCML2 IP, compared
332 to the nsIgG (Fig. 4B, lane 2 & 3). Furthermore we also detected a previously established
333 interaction between SCML2 and RNF2 (Fig. 4B, lane3) (Hasegawa et al., 2015), which builds
334 our confidence in the results. However, the smear like appearance of SCML2 in the nuclear
335 extracts (Fig 4B) prompted us to confirm the specificity of the SCML2 antibody. We did this by
336 performing western blots on nuclear extracts obtained from spermatogenic cells and ovaries.
337 Consistent with its male specific expression pattern, we fail to detect a SCML2 signal in nuclear
338 extracts obtained from ovaries (Fig.S4B, lane 2). Hence the smearing might be a product of
339 protein instability or indicative of isoforms.

340

341 In pachytene spermatocytes, SCML2 is also known to interact with USP7, a known deubiquitinase
342 and non-canonical member of the mammalian PRC1.4 complex (Lecona et al., 2015; Luo et al.,
343 2015). Hence we were curious to determine its interaction with BRG1. We were unable to detect
344 an interaction between USP7 and BRG1 (Fig. S4C, lane 2-4). Thus the BRG1 interaction appears
345 to be limited to SCML2 during meiosis.

346

347

348 **BRG1 and SCML2 concordantly regulate genes during meiosis**

349 In pachytene spermatocytes, SCML2 is known to repress somatic and spermatogonial genes,
350 while concurrently activating certain meiotic and late spermatogenic genes (Hasegawa et al.,

351 2015). This is similar to the epigenetic role of BRG1 in the germ line. Hence it might be possible
352 that BRG1 interacts with SCML2 to mutually regulate the germ line transcriptome. In support of
353 such a possibility, we identified robust enrichment of BRG1 at TSS's of genes differentially
354 regulated (FDR < 0.05) by SCML2, during pachynema (Fig. 4C). The relative enrichment was
355 greater at P12 (8 fold over input) compared to P18 (6 fold over input), indicating that BRG1
356 localizes prior to pachytene at this sites. Furthermore, chromatin accessibility at TSS's associated
357 with SCML2 regulated genes is reduced upon the loss of BRG1 at P12 (Fig. S5A).
358 Next, we looked for commonly mis-expressed genes (FDR<0.05) between the P12 BRG1 and
359 pachytene SCML2 RNA-seq data. About 65% (n=597) of genes commonly mis-expressed in the
360 absence of either BRG1 or SCML2 exhibited concordant expression changes that were highly
361 correlated (r^2=0.72). The remaining 35% (n=330) showed discordant changes (r^2=0.51) (Fig. 4D).
362 Of the concordantly regulated genes, 64% (n=388) were repressed, while the remainder (n=209)
363 were activated. The concordantly repressed genes accounted for 40% of the genes up-regulated
364 in the P12 *Brg1*^{cKO} testes. In contrast, only 19% of genes down regulated in the P12 *Brg1*^{cKO} testes
365 overlapped with concordantly activated genes. The commonly repressed genes were mostly
366 somatic in function (Fig. S5B) and included the somatic signaling receptor, PDGFRA, associated
367 with BRG1 (Fig. S1C, Fig. S2E). Thus during normal prophase-I, BRG1 might achieve gene
368 repression by recruiting SCML2. On the other hand the co-activated genes were associated with
369 GO terms relevant to the mitotic spindle checkpoint (Fig S5B). Previous studies have
370 demonstrated the existence of a meiotic spindle checkpoint in spermatocytes, and candidate
371 genes such as *Smc2*, a member of the condensin I and II complexes, is known to influence female
372 meiosis (Eaker et al., 2001; Lee et al., 2011). Thus SCML2 might activate these spindle
373 checkpoint factors, at later stages of meiosis I, in a BRG1 dependent manner.
374
375
376 **BRG1 influences SCML2 and USP7 localization to the sex body**
377 During pachynema, both SCML2 and its interacting partner, USP7 paint the sex body, a γH2Ax
378 enriched, sub-nuclear compartment containing the sex linked chromosomes (Hasegawa et al.,
379 2015; Luo et al., 2015). Therefore we determined whether SCML2 localization to the sex body
380 was dependent on BRG1.
381

382 We first compared SCML2 localization in *Brg1*^{WT} and *Brg1*^{cKO} testes cryo-sections from 2- and
383 3-week-old males by IF (Fig. 5A,Fig. S6A). Mutant pachytene spermatocytes were identified by
384 staining for γH2Ax, given that its association with the sex body remains unperturbed in the *Brg1*^{cKO}
385 (Kim et al., 2012). The loss of BRG1 appeared to impact the localization of SCML2 in *Brg1*^{cKO}
386 pachytene spermatocytes (Fig. 5A). The SCML2 signal in the mutants appeared abnormally
387 distributed genome-wide, without displaying the strong sex body association, typically observed
388 in *Brg1*^{WT} (Fig. 5A, panel 3 insets). We confirmed these defects, by co-staining for ATR (Ataxia
389 Telangiectasia and Rad3 Related), a DDR factor enriched on the sex body (Royo et al., 2013)
390 and also stained for BRG1, to demonstrate protein loss in pachytene spermatocytes displaying
391 SCML2 mis localization (Fig. S6A). Given that SCML2 is known to be physically associated with
392 γH2Ax (Hasegawa et al., 2015; Luo et al., 2015), it may be that in the absence of BRG1, it is de-
393 localized to autosomal sites harboring persistent γH2Ax (Fig 5A, panel insets). Surprisingly, subtle
394 defects in SCML2 localization were also seen in *Brg1*^{Het} pachytene spermatocytes, where it
395 appeared more homogenously distributed genome-wide (Fig. S6B, panel insets).
396
397 We next examined SCML2 localization in *Brg1*^{WT} and *Brg1*^{cKO} meiotic spreads, co-stained with
398 a synaptonemal complex marker, SYCP3, to visualize chromosomes. Mutant meiotic spreads
399 were obtained from *Brg1*^{cKO} testes generated using two independent germ line specific CRE's,
400 namely the *Mvh-cre* and *Stra8-cre*. Similar to the cryosections, SCML2 association with the sex
401 chromosomes was perturbed in *Brg1*^{cKO} pachytene spreads (Fig. S7). However, *Brg1*^{cKO}
402 pachytene spermatocyte generated with *Stra8-cre*, exhibited a less severe defect in SCML2
403 localization to the sex chromosomes, relative to their *Mvh-cre* derived counterparts (Fig. S7).
404 Such differences might be a consequence of the distinct temporal activity of each CRE (see
405 materials and methods) (Gallardo et al., 2007; Sadate-Ngatchou et al., 2008).
406
407 In addition to SCML2 we also monitored the localization of USP7 in pachytene spermatocytes
408 obtained from *Brg1*^{WT} and *Brg1*^{cKO} testes. Even though BRG1 does not directly interact with USP7
409 (Fig. S4C), we posited that the mis-localization of SCML2 in *Brg1*^{cKO} pachytene spermatocytes
410 might also affect USP7 enrichment on the sex body. In fact this seems to be the case in *Brg1*^{cKO}
411 pachytene spermatocytes immunofluorescently stained for USP7 and γH2Ax (Fig. 5B).
412
413 From previous studies it is clear that the mis localization of SCML2 does not affect processes,
414 critical to the initiation of meiotic sex chromosome inactivation (MSCI) (Hasegawa et al., 2015).

415 Since the loss of BRG1 has been previously reported to influence MSCI (Wang et al., 2012), we
416 examined its impact on the localization of known MSCI factors such as BRCA1, ATR and MDC1
417 to the sex body (Ichijima et al., 2011; Turner et al., 2004). By immunofluorescence, BRCA1, ATR
418 and MDC1 appeared stably associated with the sex body in the *Brg1*^{cKO} pachytene spermatocytes
419 (Fig. 5C). Thus BRG1 like SCML2 does not affect the initiation of MSCI. Interestingly, it was
420 previously reported that the loss of MDC1 abrogates SCML2 recruitment to the sex chromosomes
421 (Hasegawa et al., 2015). Therefore, the stable association of MDC1 with the sex body in *Brg1*^{cKO}
422 spermatocytes (Fig. 5C), suggests that SWI/SNF may function downstream MDC1 in the
423 recruitment of SCML2 to the sex body.
424
425
426
427 **BRG1 influences the abundance of SCML2 associated histone modifications**
428 Since SCML2 has been shown to regulate both H2AK119ub1 and H3K27ac during meiosis
429 (Adams et al., 2018; Hasegawa et al., 2015), we investigated whether BRG1 influences these
430 histone post translational modifications (PTM). We first, monitored the abundance of
431 H2AK119ub1 and H3K27ac in P12 *Brg1*^{WT}, *Brg1*^{Het} and *Brg1*^{cKO} spermatogenic cells by
432 performing western blots on acid extracted histones (Fig. 6A, top panel). In addition to these
433 histone PTM's, we also examined the abundance of H3K4me3, associated with BRG1 target
434 promoters and PRC2 catalyzed H3K27me3 (Fig. 6A, bottom panel). While neither H3K4me3 nor
435 H3K27me3 levels were perturbed, both H2AK119ub1 and H3K27ac were dramatically elevated
436 in P12 *Brg1*^{Het} and *Brg1*^{cKO}, relative to the *Brg1*^{WT} spermatogenic cells (Fig. 6A, top panel).
437 Interestingly, these epigenetic perturbations were undetectable at P8 and P10, which coincide
438 with the initiation of meiosis and pairing (Leptonema to zygonema) (Fig. S8A). Thus BRG1
439 suppresses H2AK119ub1 and H3K27ac prior to the onset of pachynema. The dose dependency
440 of such epigenetic regulation, prompted us to verify whether it was a consequence of the *Brg1*
441 hypomorph or due to the mere presence of the *Mvh-cre*. The former scenario seems to be true,
442 as evidenced by lack of any difference in the levels of H2AK119ub1, between males with the CRE
443 and their littermate control (Fig. S8B). Another cause for concern was that, the H2AK119ub1
444 antibody (clone E6C5) used in this study was recently reported to recognize non-histone epitopes
445 (Hasegawa et al., 2015). Hence, we validated the specificity of clone E6C5 by performing western
446 blots on acid-extracted histones obtained from RNF2 (PRC1 E3-ubiquitiun ligase) knock out
447 (*Rnf2*^{KO}) embryonic stem (ES) cells, engineered using CRISPR-CAS9. The near-absence of

448 H2AK119ub1 signal in the *Rnf2*^{KO} relative to *Rnf2*^{WT} ES cell histone extracts confirms the
449 specificity of clone E6C5 (Fig. S8C). Furthermore, H2AK119ub1 is clearly detected in chromatin
450 fractions obtained from P12 *Brg1*^{WT}, *Brg1*^{Het} and *Brg1*^{cKO} testes (Fig. S8D). Thus the changes in
451 H2AK119ub1 reported here are genuine.
452
453
454
455 **BRG1 suppresses H2AK119ub1 and enhances H3K27ac at target promoters**
456 Based on the genome-wide increase in H2AK119ub1 and H3K27ac in *Brg1*^{cKO} testes, we were
457 encouraged to survey the changes in these histone PTM's at BRG1 target promoters by ChIP-
458 seq. We compared the enrichment of H2AK119ub1 and H3K27ac between P12 *Brg1*^{WT} and
459 *Brg1*^{cKO} spermatogenic cells at promoters normally associated with BRG1 peaks. First, we
460 categorized the BRG1 targets by their chromosomal location, the rationale being that both
461 H2AK119ub1 and H3K27ac are known to be differentially regulated between the autosomes and
462 sex chromosomes at pachynema (Adams et al., 2018). The BRG1 target promoters displayed
463 contrasting changes in H2AK119ub1 and H3K27ac enrichment in the *Brg1*^{cKO} spermatogenic
464 cells. Irrespective of chromosomal location, target promoters displayed enhanced H2AK119ub1
465 combined with reduced H3K27ac in the *Brg1*^{cKO} relative to *Brg1*^{WT} spermatogenic cells (Fig. 6B,
466 top panel). This mirrors the changes in H2AK119ub1 and H3K27ac that occur on the sex
467 chromosomes in *Scml2*^{KO} pachytene spermatocytes (Adams et al., 2018; Hasegawa et al., 2015).
468 Thus, the regulation of H2AK119ub1 and H3K27ac at regions occupied by BRG1 may be
469 influenced by SCML2, with which it is physically associated.
470
471 Next, we analyzed the changes in H2AK119ub1 and H3K27ac at the promoters of BRG1 target
472 genes that are differentially expressed. We hypothesized that these epigenetic modifications
473 might influence the transcriptional status of genes regulated by BRG1. Consistent with changes
474 observed at all BRG1 occupied promoters (Fig. 6B, top panel), H2AK119ub1 was elevated while
475 H3K27ac was reduced at promoters of mis-expressed target genes, irrespective of their
476 transcriptional status in the *Brg1*^{cKO} relative to *Brg1*^{WT} spermatogenic cells (Fig. 6B, bottom panel).
477 These epigenetic changes are typically associated with gene repression and thus only account
478 for the silencing of mis-expressed genes in *Brg1*^{cKO} spermatogenic cells. Therefore, the activation
479 of mis-expressed target genes occurs by mechanisms independent of H2AK119ub1 or H3K27ac.
480

481 The loss of H3K27ac at promoters normally occupied by BRG1 in *Brg1*^{cKO} spermatogenic cells is
482 inconsistent with its genome-wide increase (Fig.6A; top panel , Fig. 6B). To determine whether
483 other genomic regions acquire greater H3K27ac enrichment upon the loss of BRG1, we
484 performed a differential peak calling analysis using the macs2 bdgdiff algorithm (Zhang et al.,
485 2008). This analysis revealed several intronic and intergenic regions that lost, gained or
486 maintained (common) H3K27ac peaks in *Brg1*^{cKO} relative to the *Brg1*^{WT} spermatogenic cells (Fig
487 6C; left panel, Fig. S9). Compared to the common peaks, regions that loose or gain H3K27ac are
488 normally depleted of BRG1 (Fig. 6C, right panel). Thus while total H3K27ac levels are elevated,
489 its local distribution appears more heterogeneous upon the loss of BRG1.
490
491
492
493
494 **BRG1 can also influence the epigenome in a SCML2 independent manner**
495 While our data suggest that BRG1 regulates H2AK119ub1 and H3K27ac, through its interaction
496 with SCML2, we cannot rule out the possibility that BRG1 might also influence these histone
497 PTM's by directly regulating the expression of cognate epigenetic modifiers. In fact, our ChIP-seq
498 data identifies BRG1 peaks at promoters of epigenetic modifiers known to influence H2AK119ub1,
499 H2BK120ub1 and H3K27ac (Fig. S10A). These include the H2A ubiquitin ligase, RNF2 (Wang et
500 al., 2004), USP3 a H2A/H2B deubiquitinase (Nicassio et al., 2007) and the histone deacetylases,
501 HDAC1 and HDAC2 (Gallinari et al., 2007) (Fig. S10A). The transcript abundances of all these
502 targets are significantly altered in response to the loss of BRG1 (Fig.S10B).
503
504 In the case of the histone ubiquitin modifiers, *Rnf2* and *Usp3*, the former displayed an increase
505 while the latter displayed a decrease in transcript abundance in *Brg1*^{cKO} relative to the *Brg1*^{WT}
506 spermatogenic cells at P12 (Fig. S10B, row 1). This is consistent with significant increases in
507 protein levels in *Brg1*^{cKO} (RNF2: 88% increase, USP3:59% decrease) relative to the *Brg1*^{WT}
508 chromatin fractions prepared from testes (Fig. 6D, lane 4-6). Thus BRG1 may influence
509 H2AK119ub1 by maintaining a balanced expression of RNF2 and USP3. Furthermore this
510 represents an SCML2 independent mechanism of epigenetic regulation. Since USP3 has also
511 been associated with mono ubiquitinylated H2B (Nicassio et al., 2007), we monitored the levels
512 of mono ubiquitination of H2B lysine 120 (H2BK120ub1), a mark associated with gene activation
513 and chromatin relaxation (Fierz et al., 2011; Minsky et al., 2008; Pavri et al., 2006). At P12,

514 H2BK120ub1 appeared elevated genome-wide in *Brg1*^{cKO}, relative to *Brg1*^{WT} spermatogenic cells
515 (Fig. S10C). The changes in the *Brg1*^{Het} spermatogenic cells appear to be a product of unequal
516 protein loading.
517
518 Similar to the histone ubiquitin modifiers, H3K27ac associated modifiers, *Hdac1* and *Hdac2*
519 displayed reduced transcript abundance in the *Brg1*^{Het} and *Brg1*^{cKO} (Fig. S10B, row 2). At least
520 in the case of *Hdac1*, we were unable to identify a corresponding depletion in nuclear protein
521 levels by western blot (Fig. 6D, lane 1-6). Since HDAC1 has been shown to compensate for
522 HDAC2 in various developmental scenarios (Ma et al., 2012; Montgomery et al., 2009; Yamaguchi
523 et al., 2010) it is unlikely that the perturbation in H3K27ac levels in the *Brg1*^{cKO} spermatogenic
524 cells, is associated with mis-expression of histone deacetylases.
525

526 **Discussion:**

527

528 In this study we integrate genomic and proteomic approaches to show that SWI/SNF directed
529 regulation of transcription, influences meiotic progression in males. In spermatogenic cells, BRG1
530 is overwhelmingly promoter associated which is distinct from what has been observed in other
531 mammalian cell types and embryonic tissue (Alexander et al., 2015; Alver et al., 2017; Attanasio
532 et al., 2014). This re-enforces the notion that cell or tissue specific associations influence
533 SWI/SNF function during development (reviewed in Ho and Crabtree 2010). We propose a model
534 in which the SWI/SNF ATPase, activates essential spermatogenic genes, while maintaining the
535 repression of somatic genes. We show that BRG1 facilitates chromatin accessibility at the
536 promoters of these differentially regulated genes, which is consistent with the generally accepted
537 role of SWI/SNF chromatin remodeling (reviewed in Clapier et al., 2017). The activated genes
538 play critical roles in the maintenance of undifferentiated spermatogonial cell populations and
539 facilitate meiotic progression. Target stem cell factors include, *Zbtb16* and *Id4*. The latter
540 specifically identifies a self-renewing population of spermatogonia, generally referred to as
541 spermatogonial stem cells (SSC) (Green et al., 2018; Oatley et al., 2011). Thus BRG1 might
542 influence SSC maintenance. The role of BRG1 in the maintenance of pluripotency while not novel,
543 was previously unknown in the germ line, thus demonstrating a conserved role for SWI/SNF
544 across various stem cell lineages (Ho et al., 2009; Lessard et al., 2007) . In the case of meiotic
545 gene targets, several of these have been associated with meiotic arrest phenotypes. The role of
546 BRG1 in the activation of *Sycp2*, which is associated with synaptonemal complex assembly and
547 homolog synapsis (Yang et al., 2006), potentially explains the incomplete synapsis and
548 subsequent meiotic arrest seen in *Brg1*^{cKO} spermatocytes (Kim et al., 2012). Thus the male sterility
549 associated with *Brg1*^{cKO} adults is a consequence of a shortage of germ line progenitors and
550 essential meiotic factors.

551

552 The repression of the somatic transcriptome during meiosis is a feature shared with two other
553 epigenetic regulators, namely, PRC2 and SCML2, a testes specific PRC1 factor (Hasegawa et
554 al., 2015; Mu et al., 2014). Here we propose that BRG1 achieves the repression of its target
555 genes by recruiting SCML2 activity. This is supported by the following observations; BRG1 (i)
556 physically interacts with SCML2, (ii) is enriched at the promoters of genes regulated by SCML2
557 (iii) concordantly represses most genes commonly regulated by SCML2 and (iv) influences
558 SCML2 localization during pachynema, based on a pronounced effect on sex body association.

559 Interestingly, the transition to pachynema is accompanied by a reduction but not depletion of
560 BRG1 from the X chromosome. This reduced level of BRG1 might be sufficient to recruit SCML2
561 to the sex body. Alternatively, the enrichment of SCML2 on the sex body may be dependent on a
562 temporally defined interaction with BRG1 that precedes pachynema. In contrast to the repressed
563 genes, BRG1 concordantly activates fewer SCML2 regulated genes. Most of these are associated
564 with the regulation of mitotic spindle checkpoints, which in the context of meiosis occurs late into
565 meiosis-I (Eaker et al., 2001).
566
567 In addition to these observations, BRG1 also appears to influence SCML2 associated histone
568 PTM's, H2AK119ub1 and H3K27ac in the male germ line (Adams et al., 2018; Hasegawa et al.,
569 2015). Similar to SCML2, we find that BRG1 is required to suppress H2AK119ub1 and enhance
570 H3K27ac at target promoters in pre-pachytene spermatogenic cells. However unlike SCML2,
571 BRG1 did not appear to differentially regulate autosomal and sex linked chromatin (Hasegawa et
572 al., 2015). It is possible that such differential regulation does not manifest at pre pachytene stages.
573 Alternatively, this may be indicative of distinct epigenetic outcomes associated with SCML2
574 dependent and independent mechanisms. The latter is demonstrated by the effect of BRG1 on
575 the expression of potent H2AK119ub1 modifiers, such as RNF2 and USP3.
576
577 As counter-intuitive as it may seem, repressed BRG1 targets genes are associated with low
578 H2AK119ub1 and higher H3K27ac levels. Hence, the repression of target genes might occur by
579 alternative mechanisms. Several BRG1 target promoters are bivalently modified
580 (H3K4me3/H43K27me3) during the course of meiosis from P12 to P17. These bivalent promoters
581 appear to distinguish somatic and pre-meiotic targets from meiotic targets. Hence, the silencing
582 of these genes might occur through the formation of bivalent promoters, which are commonly
583 associated with somatic developmental genes in the germ line (Hammoud et al., 2014; Lesch et
584 al., 2013; Lesch et al., 2016). Interestingly, SCML2 has been recently shown to influence the
585 formation of bivalent domains during germ line development (Maezawa et al., 2018). Hence, such
586 SCML2 activity might potentially influence the repression of BRG1 target genes.
587
588 In addition to H2AK119ub1, BRG1 also suppresses H2BK120ub1, which is associated with
589 transcriptional activation and chromatin relaxation (Fierz et al., 2011; Minsky et al., 2008; Pavri et
590 al., 2006). Hence, an increase in H2BK120ub1 might potentially activate genes mis-expressed in
591 the *Brg1*^{cKO} spermatogenic cells. This might occur due to the mis-regulation of USP3 or mis-

592 localization of USP7, two deubiquitinases, whose activities have been shown to influence mono
593 ubiquitination of H2B (Nicassio et al., 2007; Van Der Knaap et al., 2005). The evidence for USP7
594 is based on its function in *Drosophila* (Van Der Knaap et al., 2005). In contrast, mammalian USP7
595 does not seem to catalyze the deubiquitnation of H2B (Lecona et al., 2015; Maertens et al., 2010).
596 However there appears to be an effect on H2BK120ub1 that is independent of its enzymatic
597 activity (Huether et al., 2014).
598
599 In conclusion we reveal the transcriptional basis for the meiotic defects previously described in
600 *Brg1*^{cKO} males, and present a new paradigm for studying co-operation between SWI/SNF and
601 PRC1 factors in the regulation of the epigenome. While recent studies have illustrated the
602 propensity of BRG1 to evict canonical PRC1 members from chromatin in normal and oncogenic
603 cell culture models (Kadoch et al., 2016; Stanton et al., 2016), the relationship between SWI/SNF
604 and variant PRC1 factors remain unexplored. More recent reports have described the roles of
605 variant PRC1 factors in gene activation in ES cells and the central nervous system (CNS) (Creppe
606 et al., 2014; Gao et al., 2014). Whether SWI/SNF influences these activities in the germ line
607 remains a topic of future investigation. Interestingly, a recent report has revealed a role for PRC1
608 in gene activation in spermatogonial cells (Maezawa et al., 2017).
609

610 **Materials and Methods:**

611

612 **Generation of *Brg1* conditional deletion and genotyping:**

613 *Brg1 floxed* (Sumi-Ichinose et al., 1997) , *Mvh-Cre* (activated at ~ E15) (Gallardo et al., 2007) and
614 *Stra8-Cre* (activated only in males at P3) (Sadate-Ngatchou et al., 2008) were maintained on a
615 outbred background genetic background using CD-1 mice. *Brg1*$^{fl/fl}$ females were crossed to
616 *Brg1*$^{fl+}$;*Mvh-Cre*$^{Tg/0}$ males to obtain *Brg1*$^{fl\Delta}$;*Mvh-Cre*$^{Tg/0}$ (*Brg1*^{cKO},) , *Brg1*$^{fl+}$;*Mvh-Cre*$^{Tg/0}$ (*Brg1*^{Het})
617 and *Brg1*$^{fl+}$ (*Brg1*^{WT}) littermate controls. Similar crosses were made to generate the *Stra8-Cre*
618 induced conditional knockouts and littermate controls. Genotyping primers used in this study
619 include: *Brg1*$^{fl/+}$ alleles - (F)- 5' -CCTAGCCAAGGTAGCGTGTCCTCAT-3' ; (R) 5' -
620 CCAGGACCACATACAAGGCCTTGTCT-3', the excised allele (Δ)- reverse primer used above in
621 combination with (F) 5' -CTAACCGTGTATGTAGCCAGTTCTGCCT-3', *Mvh-Cre* - (F) 5' -
622 CACGTGCAGCCGTTTAAGCCGCGT-3', (R) 5' -TTCCCATTCTAAACAACACCCTGAA-3' and
623 *Stra8-Cre* - (F) 5' -GTGCAAGCTGAACAACAGGA-3', (R) 5' -AGGGACACAGCATTGGAGTC-3'.
624 All animal work was carried out in accordance with approved IACUC protocols at the University
625 of North Carolina at Chapel Hill.

626

627 **Disruption of Rnf2 by CRISPR-Cas9:**

628 The sequences of sgRNAs for Rnf2 are 5'CACCGTGTTTACATCGGTTTTGCG3' and
629 5'AAACCGCAAAACCGATGTAAACAC3'. sgRNAs were cloned into pX330-U6-Chimeric_BB-
630 CBh-hSpCas9 (42230, Addgene) using Golden Gate assembly cloning strategy (Bauer et al.,
631 2015). Briefly, 5 x 10^4 E14 ES cells were cultured on 60 mm dishes for one day and then
632 transfected with plasmids expressing Cas9 and sgRNAs, along with a plasmid expressing PGK-
633 PuroR (Addgene, cat. no. 31937) using FuGENE HD reagent (Promega) according to the
634 manufacturer's instructions. The cells were treated with 2 µg/ml puromycin for two days and
635 recovered in normal culture medium until ES cell colonies grew up. *Ezh1* targeted colonies were
636 verified by DNA sequencing.

637

638 **Immunofluorescence staining:**

639 Spermatocyte spreads were prepared as described (Peters et al., 1997) or by using a protocol
640 adapted from (Wojtasz et al., 2009) , that was used to generate "3D-preserved" spermatocytes.
641 The latter entails a detergent spreading technique in which single- cell preparations obtained as
642 described (Biswas 2018) were treated with 0.25% NP-40 for not more than 2 minutes. These

643 spreads were used to view SYCP2 staining. All spermatocyte spreads were generated from 2- to
644 3-week-old mice. Prepared slides were either dried down and stored at -80^0 C or stored in
645 phosphate buffered saline (PBS) at 4^0 C in the case of "3D-preserved" spermatocytes.
646 Testis cryosections were prepared essentially as described before (Kim et al., 2012) with a few
647 modifications. Briefly, juvenile/adult testes were fixed in 10% neutral buffered formalin at 4^{0}C.
648 After 20 minutes of incubation in NBF the tissue was sliced into half and then fixed up to 1 hour.
649 Fixed tissue were washed 3 times in PBS at room temperature and then saturated through a
650 sucrose series - 10% (30 min), 20% (30 min) and 30% (1 hr). The tissue were then incubated
651 overnight in 30% sucrose/optimum cutting temperature (OCT) formulation at 4^0 C and
652 subsequently embedded in OCT. Frozen sections were cut at 9 µm thickness. Antigen retrieval
653 was performed for all antibodies used in this study. Briefly slides were incubated in boiling 10mM
654 citric acid (pH6.0) for 10 minutes. Over this period, citrate buffer was replaced every 2 minutes
655 with fresh boiling buffer and then allowed to cool down gradually for up to 20 minutes.
656 Tissue section and spreads were washed in PBS followed by permeabilization in 0.1% Triton-X
657 100 and then blocked in Antibody dilution buffer (10% bovine serum albumin; 10% goat/donkey
658 serum; 0.05% Triton-X 100) diluted 1:10 in PBS for 20 minutes before incubation with primary
659 antibody overnight at 4^{0}C. The following day, samples were again washed, permeabilized and
660 blocked in ADB/PBS after which they were incubated for 1 hour with Alexa fluor- conjugated
661 secondary antibodies. Immuno-stained slides were finally washed twice in PBS/0.32% photoflo
662 (Kodak), once in H_2O/ 0.32% photoflo and then counterstained with DAPI before mounting in
663 Prolong Gold antifade medium (P-36931; Life Technologies). A list of all the primary antibodies
664 used in this study are provided (Table S4). We used alexa fluor conjugated secondary antibodies
665 at a dilution of 1:500. All imaging in this study was done on a Zeiss AxioImager-M2.
666
667 **Isolation of Spermatogonial stem cells and RNA extraction:**
668 Testes cell suspension was generated from 8-day-old *Brg1*^{WT} (n=5), *Brg1*^{Het} (n=1), *Brg1*^{cKO} (n=2)
669 mice as described previously (Kubota and Brinster, 2008). Conditional deletions were generated
670 using the *Mvh-Cre* transgene. Spermatogonial stem cells (SSC) were enriched using THY1$^+$
671 microbeads (Miltenyi Biotec; 131-049-101) followed by their isolation on magnetic activated cell
672 sorting (MACS) columns (Miltenyi Biotec; 131-090-312). RNA from SSC's were isolated and
673 purified using the PicoPure™ RNA isolation kit (Life technologies; KIT0204).
674
675

676 **RT-PCR and qPCR:**

677 cDNA was synthesized using random primer mix (NEB) and ProtoScript® II reverse transcriptase
678 (NEB). Real time qPCR was performed using Sso Fast EvaGreen supermix (Bio-Rad) on a CFX96
679 thermocycler (Bio-Rad). A list of qRT-PCR primers used in this study are provided (Table S5).

680

681 **Isolation of spermatogenic cells:**

682 Spermatocyte enriched populations were isolated by methods described previously (Chang et al.,
683 2011; Mu et al., 2014). Spermatocyte populations were enriched using percoll and cell strainers.
684 Cell populations were then used for downstream applications such as RNA-seq, ATAC-seq, ChIP-
685 seq and nuclear lysate preparations for immunoprecipitations.

686

687

688 **RNA-seq:**

689 RNA was extracted from spermatogenic cells obtained from 4 biological replicates of P12 *Brg1*^{WT}
690 and *Brg1*^{cKO} mice each. Conditional deletions were generated using the *Mvh-Cre* transgene. Cells
691 were treated with the TRIzol reagent (Invitrogen) and total RNA was isolated and cleaned up
692 using the Direct-zol RNA kit (Zymo). Sequencing libraries were prepared using a Kapa mRNA
693 library kit as per manufacturer's instruction and then sequenced on a Illumina Hiseq 4000 (50 bp
694 reads, single end). Scml2 RNA-seq was previously published and is publically available under
695 GEO accession number GSE55060 (Hasegawa et al., 2015).

696

697 **RNA-seq data analysis:**

698 Gene expression was quantified using kallisto (Bray et al., 2016). Transcript levels (counts) were
699 summarized per gene using tximport (Soneson et al., 2016) and then imported to perform a
700 differential analysis of gene expression using edgeR (Robinson et al., 2010). The mouse (mm9)
701 gene/transcript annotations were retrieved using the ensembldb R package
702 (https://github.com/jotsetung/ensembldb). Low abundance genes (counts per million <1 across
703 4 replicates) were filtered out in edgeR and significant differences in counts were called at a false
704 discovery rate (FDR)≤ 0.05. The lists of differentially expressed genes are provided (Table S1).
705 Anatomy ontology terms were curated from EMAPA (The Edinburgh Mouse Atlas Project)
706 (Hayamizu et al., 2013) and the analysis was done on MouseMine (www.mousemine.org)

707 (Motenko et al., 2015). Gene ontology analysis were performed using clusterProfiler (Yu et al.,
708 2012).
709
710 **ChIP-seq:**
711 BRG1 ChIP was performed exactly as described previously (Raab et al., 2015). We performed
712 the ChIP in duplicates on $4x10^7$ wild type (CD-1) spermatogenic cells obtained from P12 and P18
713 mice each. H2AK119ub1 and H3K27ac ChIPs were also performed in duplicate on spermatogenic
714 cells obtained from P12 *Brg1*^{WT} and *Brg1*^{cKO} mice using a method described previously for low
715 chromatin inputs (Brind'Amour et al., 2015), with minor modifications (See supplemental materials
716 for details). The BRG1 ChIP samples were sequenced on a Hiseq 2500 using v4 chemistry (50
717 bp reads, single end), whereas the H3K27ac and H2AK119ub1 ChIP samples were sequenced
718 on an Illumina Hiseq 4000 (50 bp reads, single end). The antibodies used for ChIP are listed
719 (table S4). H3K4me3, H3K27me3 ChIP-seq data were previously published and are publically
720 available under GEO accession number GSE61902 (Mu et al., 2014). ChIP data analysis methods
721 can be found in the supplemental materials.
722
723
724 **ATAC-seq:**
725 ATAC-seq was performed on spermatogenic cells isolated from 2 biological replicates of P12
726 *Brg1*^{WT} and *Brg1*^{cKO} mice each. Only a single sample from 18 day old *Brg1*^{WT} and *Brg1*^{Het} mice
727 were processed for ATAC-seq. Conditional deletions were generated using the *Mvh-Cre*
728 transgene. ATAC-seq libraries were made as previously reported (Buenrostro et al., 2013) , with
729 the exception of a double-sided SPRI bead size selection step of each library, using 0.5x and 1x
730 ratio of SPRI beads to obtain a library size range of ~150bp to ~2kb. All libraries were combined
731 and sequenced on a single lane of Illumina Hiseq 2500 using v4 chemistry (50bp reads, single).
732
733
734 **Preparation of nuclear lysates:**
735 Nuclear extracts were prepared from spermatocyte enriched preparations as previously described
736 (Chandler et al., 2012; Li et al., 1991) with minor modifications. These nuclear lysates were used
737 for co-immunoprecipitations (co-IP) and for the mass spectrometric analysis of BRG1
738 immunopulldowns (supplemental materials).
739

740

741 **Identification of BRG1 interacting proteins by mass spectrometry:**

742 Proteins isolated from BRG1 IP and IP with a non-specific rabbit IgG were run approximately 2
743 cm below the bottom of the well of a precast SDS polyacrylamide gel (short gel). The short gel
744 was stained with GelCode blue protein stain (ThermoFisher) and the lanes containing each
745 sample were cut out and analyzed by mass spectrometry at the University of Massachusetts
746 Medical School Mass spectrometry Core Facility (see supplemental materials).

747

748

749 **Preparation of sub cellular protein fractions:**

750 Cytosolic, nucleoplasmic (soluble) and chromatin (insoluble) fractions were prepared as
751 described (Méndez and Stillman, 2000) from spermatogenic cells obtained from P12 and P21
752 *Brg1*^{WT} ,*Brg1*^{Het} and *Brg1*^{cKO} mice. Conditional deletions were generated using the *Mvh-Cre*
753 transgene.

754

755 **Preparation of acid extracted histones:**

756 Histones were extracted from spermatogenic cells obtained from P12 *Brg1*^{WT} ,*Brg1*^{Het} and *Brg1*^{cKO}
757 mice using acid extraction protocol described previously (Shechter et al., 2007). Conditional
758 deletions were generated using the *Mvh-Cre* transgene.

759

760 **Western blotting:**

761 Protein samples were separated by polyacrylamide gel electrophoresis and then transferred to
762 PVDF (Polyvinylidene Difluoride) membranes (Bio-Rad) using wet/ semi-dry transfer apparatus
763 (Bio-Rad). Western blots were generated using the Li-COR Bioscience Odyssey fluorescent
764 western blotting reagents. All the antibodies used in this study and their corresponding dilutions
765 are listed (Table S4).

766

Acknowledgements

We thank all members of the Magnuson laboratory for helpful comments on manuscript preparation. This work was supported by National Institutes of Health grants R01GM101974 and U42OD010924.

Competing interests statement

The authors declare no competing financial interests.

Data availability:

Raw and processed data have been deposited under GEO accession number GSE119179 (For access, please enter token number: wjyxqkgozrgrpir).

781 **References:**

782 **Adams, S. R., Maezawa, S., Alavattam, K. G., Abe, H., Sakashita, A., Shroder, M., Broering, T.**
783 **J., Sroga Rios, J., Thomas, M. A., Lin, X., et al.** (2018). RNF8 and SCML2 cooperate to
784 regulate ubiquitination and H3K27 acetylation for escape gene activation on the sex
785 chromosomes. *PLoS Genet.* **14**,.

786 **Alexander, J. M., Hota, S. K., He, D., Thomas, S., Ho, L., Pennacchio, L. A. and Bruneau, B. G.**
787 (2015). Brg1 modulates enhancer activation in mesoderm lineage commitment.
788 *Development* **142**, 1418–1430.

789 **Alver, B. H., Kim, K. H., Lu, P., Wang, X., Manchester, H. E., Wang, W., Haswell, J. R., Park, P. J.**
790 **and Roberts, C. W. M.** (2017). The SWI/SNF chromatin remodelling complex is required for
791 maintenance of lineage specific enhancers. *Nat. Commun.* **8**, 1–10.

792 **Attanasio, C., Nord, A. S., Zhu, Y., Blow, M. J., Biddie, S. C., Mendenhall, E. M., Dixon, J.,**
793 **Wright, C., Hosseini, R., Akiyama, J. A., et al.** (2014). Tissue-specific SMARCA4 binding at
794 active and repressed regulatory elements during embryogenesis. *Genome Res.* **24**, 920–
795 929.

796 **Baker, C. L., Kajita, S., Walker, M., Saxl, R. L., Raghupathy, N., Choi, K., Petkov, P. M. and**
797 **Paigen, K.** (2015). PRDM9 Drives Evolutionary Erosion of Hotspots in Mus musculus
798 through Haplotype-Specific Initiation of Meiotic Recombination. **11**,.

799 **Ball, R. L., Fujiwara, Y., Sun, F., Hu, J., Hibbs, M. A., Handel, M. A. and Carter, G. W.** (2016).
800 Regulatory complexity revealed by integrated cytological and RNA-seq analyses of meiotic
801 substages in mouse spermatocytes. *BMC Genomics* **17**, 1–17.

802 **Basciani, S., Mariani, S., Arizzi, M., Ulisse, S., Rucci, N., Jannini, E. A., Rocca, C. Della,**
803 **Manicone, A., Carani, C., Spera, G., et al.** (2002). Expression of Platelet-Derived Growth
804 Factor-A (PDGF-A), PDGF-B, and PDGF Receptor-α and -β during Human Testicular
805 Development and Disease. *J. Clin. Endocrinol. Metab.* **87**, 2310–2319.

806 **Basciani, S., Mariani, S., Arizzi, M., Ulisse, S., Rucci, N., Jannini, E. A., Rocca, C. Della,**
807 **Manicone, A., Carani, C., Spera, G., et al.** (2018). Expression of Platelet-Derived Growth
808 Factor-A. **87**, 2310–2319.

809 **Bellve, a R., Cavicchia, J. C., Millette, C. F., O'Brien, D. a, Bhatnagar, Y. M. and Dym, M.**

810 (1977). Spermatogenic cells of the prepubertal mouse. Isolation and morphological
811 characterization. *J Cell Biol* **74**, 68–85.
812 **Bernstein, B. E., Mikkelsen, T. S., Xie, X., Kamal, M., Huebert, D. J., Cuff, J., Fry, B., Meissner,**
813 **A., Wernig, M., Plath, K., et al.** (2006). A Bivalent Chromatin Structure Marks Key
814 Developmental Genes in Embryonic Stem Cells. *Cell* **125**, 315–326.
815 **Blake, J. A., Richardson, J. E., Bult, C. J., Kadin, J. A., Eppig, J. T., Baldarelli, R. M., Beal, J. S.,**
816 **Bradt, D. W., Burkart, D. L., Butler, N. E., et al.** (2003). MGD: The mouse genome
817 database. *Nucleic Acids Res.* **31**, 193–195.
818 **Bray, N. L., Pimentel, H., Melsted, P. and Pachter, L.** (2016). Near-optimal probabilistic RNA-
819 seq quantification. *Nat. Biotechnol.* **34**, 525–527.
820 **Brick, K., Smagulova, F., Khil, P., Camerini-Otero, R. D. and Petukhova, G. V.** (2012). Genetic
821 recombination is directed away from functional genomic elements in mice. *Nature* **485**,
822 642–645.
823 **Brind'Amour, J., Liu, S., Hudson, M., Chen, C., Karimi, M. M. and Lorincz, M. C.** (2015). An
824 ultra-low-input native ChIP-seq protocol for genome-wide profiling of rare cell
825 populations. *Nat. Commun.* **6**,.
826 **Buaas, F. W., Kirsh, A. L., Sharma, M., McLean, D. J., Morris, J. L., Griswold, M. D., De Rooij, D.**
827 **G. and Braun, R. E.** (2004). Plzf is required in adult male germ cells for stem cell self-
828 renewal. *Nat. Genet.* **36**, 647–652.
829 **Buenrostro, J. D., Giresi, P. G., Zaba, L. C., Chang, H. Y. and Greenleaf, W. J.** (2013).
830 Transposition of native chromatin for fast and sensitive epigenomic profiling of open
831 chromatin, DNA-binding proteins and nucleosome position. *Nat. Methods* **10**, 1213–8.
832 **Chandler, R. L., Brennan, J., Schisler, J. C., Serber, D., Patterson, C. and Magnuson, T.** (2012).
833 ARID1a-DNA Interactions Are Required for Promoter Occupancy by SWI/SNF. *Mol. Cell.*
834 *Biol.* **33**, 265–280.
835 **Chang, Y. F., Lee-Chang, J. S., Panneerdoss, S., MacLean, J. a. and Rao, M. K.** (2011). Isolation
836 of Sertoli, Leydig, and spermatogenic cells from the mouse testis. *Biotechniques* **51**, 341–
837 344.
838 **Clapier, C. R., Iwasa, J., Cairns, B. R. and Peterson, C. L.** (2017). Mechanisms of action and

839 regulation of ATP-dependent chromatin-remodelling complexes. *Nat. Rev. Mol. Cell Biol.*
840 **Creppe, C., Palau, A., Malinverni, R., Valero, V. and Buschbeck, M.** (2014). A Cbx8-Containing
841 Polycomb Complex Facilitates the Transition to Gene Activation during ES Cell
842 Differentiation. *PLoS Genet.* **10**,.
843 **Dann, C. T., Alvarado, A. L., Molyneux, L. A., Denard, B. S., Garbers, D. L. and Porteus, M. H.**
844 (2008). Spermatogonial Stem Cell Self-Renewal Requires OCT4, a Factor Downregulated
845 During Retinoic Acid-Induced Differentiation. *Stem Cells* **26**, 2928–2937.
846 **De Vries, F. A. T., De Boer, E., Van Den Bosch, M., Baarends, W. M., Ooms, M., Yuan, L., Liu, J.**
847 **G., Van Zeeland, A. A., Heyting, C. and Pastink, A.** (2005). Mouse Sycp1 functions in
848 synaptonemal complex assembly, meiotic recombination, and XY body formation. *Genes*
849 *Dev.* **19**, 1376–1389.
850 **Diagouraga, B., Clément, J. A. J., Duret, L., Kadlec, J., de Massy, B. and Baudat, F.** (2018).
851 PRDM9 Methyltransferase Activity Is Essential for Meiotic DNA Double-Strand Break
852 Formation at Its Binding Sites. *Mol. Cell* **69**, 853–865.e6.
853 **Eaker, S., Pyle, A., Cobb, J. and Handel, M. A.** (2001). Evidence for meiotic spindle checkpoint
854 from analysis of spermatocytes from Robertsonian-chromosome heterozygous mice. *J. Cell*
855 *Sci.* **114**, 2953–2965.
856 **Euskirchen, G. M., Auerbach, R. K., Davidov, E., Gianoulis, T. a., Zhong, G., Rozowsky, J.,**
857 **Bhardwaj, N., Gerstein, M. B. and Snyder, M.** (2011). Diverse roles and interactions of the
858 SWI/SNF chromatin remodeling complex revealed using global approaches. *PLoS Genet.* **7**,.
859 **Fierz, B., Chatterjee, C., McGinty, R. K., Bar-Dagan, M., Raleigh, D. P. and Muir, T. W.** (2011).
860 Histone H2B ubiquitylation disrupts local and higher-order chromatin compaction. *Nat.*
861 *Chem. Biol.* **7**, 113–119.
862 **Gallardo, T., Shirley, L., John, G. B. and Castrillon, D. H.** (2007). Generation of a germ cell-
863 specific mouse transgenic Cre line, Vasa-Cre. *Genesis* **45**, 413–7.
864 **Gallinari, P., Di Marco, S., Jones, P., Pallaoro, M. and Steinkühler, C.** (2007). HDACs, histone
865 deacetylation and gene transcription: From molecular biology to cancer therapeutics. *Cell*
866 *Res.* **17**, 195–211.
867 **Gao, Z., Lee, P., Stafford, J. M., Schimmelmann, M. Von, Schaefer, A. and Reinberg, D.** (2014).

868 An AUTS2 – Polycomb complex activates gene expression in the CNS. *Nature* **516**, 349–
869 354.
870 **Goertz, M. J., Wu, Z., Gallardo, T. D., Hamra, F. K. and Castrillon, D. H.** (2011). Foxo1 is
871 required in mouse spermatogonial stem cells for their maintenance and the initiation of
872 spermatogenesis. *J. Clin. Invest.* **121**, 3456–3466.
873 **Goetz, P., Chandley, a C. and Speed, R. M.** (1984). Morphological and temporal sequence of
874 meiotic prophase development at puberty in the male mouse. *J. Cell Sci.* **65**, 249–263.
875 **Green, C. D., Ma, Q., Manske, G. L., Shami, A. N., Zheng, X., Marini, S., Moritz, L., Sultan, C.,**
876 **Gurczynski, S. J., Moore, B. B., et al.** (2018). A Comprehensive Roadmap of Murine
877 Spermatogenesis Defined by Single-Cell RNA-Seq. *Dev. Cell* **46**, 651–667.e10.
878 **Hammoud, S. S., Low, D. H. P., Yi, C., Carrell, D. T., Guccione, E. and Cairns, B. R.** (2014).
879 Chromatin and Transcription Transitions of Mammalian Adult Germline Stem Cells and
880 Spermatogenesis. *Cell Stem Cell* **15**, 239–253.
881 **Handel, M. A. and Schimenti, J. C.** (2010). Genetics of mammalian meiosis: regulation,
882 dynamics and impact on fertility. *Nat. Rev. Genet.* **11**, 124–136.
883 **Hasegawa, K., Sin, H., Hasegawa, K., Sin, H., Maezawa, S., Broering, T. J., Kartashov, A. V and**
884 **Alavattam, K. G.** (2015). SCML2 Establishes the Male Germline Epigenome through
885 Regulation of Histone H2A Ubiquitination Article SCML2 Establishes the Male Germline
886 Epigenome through Regulation of Histone H2A Ubiquitination. *Dev. Cell* **32**, 574–588.
887 **Hayamizu, T. F., Wicks, M. N., Davidson, D. R., Burger, A., Ringwald, M. and Baldock, R. A.**
888 (2013). Open Access EMAP / EMAPA ontology of mouse developmental anatomy : 2013
889 update. *J. Biomed. Semantics* 1–5.
890 **Hayashi, K., Yoshida, K. and Matsui, Y.** (2005). A histone H3 methyltransferase controls
891 epigenetic events required for meiotic prophase. *Nature* **438**, 374–378.
892 **Ho, L. and Crabtree, G. R.** (2010). Chromatin remodelling during development. *Nature* **463**,
893 474–484.
894 **Ho, L., Ronan, J. L., Wu, J., Staahl, B. T., Chen, L., Kuo, A., Lessard, J., Nesvizhskii, A. I., Ranish,**
895 **J. and Crabtree, G. R.** (2009). An embryonic stem cell chromatin remodeling complex,
896 esBAF, is essential for embryonic stem cell self-renewal and pluripotency. *Proc. Natl. Acad.*

897 *Sci. U. S. A.* **106**, 5181–5186.
898 **Huether, R., Dong, L., Chen, X., Wu, G., Parker, M., Wei, L., Ma, J., Edmonson, M. N., Hedlund,**
899 **E. K., Rusch, M. C., et al.** (2014). The landscape of somatic mutations in epigenetic
900 regulators across 1,000 paediatric cancer genomes. *Nat. Commun.* **5**, 1–7.
901 **Ichijima, Y., Ichijima, M., Lou, Z., Nussenzweig, A., Daniel Camerini-Otero, R., Chen, J.,**
902 **Andreassen, P. R. and Namekawa, S. H.** (2011). MDC1 directs chromosome-wide silencing
903 of the sex chromosomes in male germ cells. *Genes Dev.* **25**, 959–971.
904 **Kadoch, C., Williams, R. T., Calarco, J. P., Miller, E. L., Weber, C. M., Braun, S. M. G., Pulice, J.**
905 **L., Chory, E. J. and Crabtree, G. R.** (2016). Dynamics of BAF–Polycomb complex opposition
906 on heterochromatin in normal and oncogenic states. *Nat. Genet.* **49**, 213–222.
907 **Kakarougkas, A., Ismail, A., Chambers, A., Riballo, E., Herbert, A., Künzel, J., Löbrich, M.,**
908 **Jeggo, P. and Downs, J.** (2013). Requirement for PBAF in Transcriptional Repression and
909 Repair at DNA Breaks in Actively Transcribed Regions of Chromatin. *Mol. Cell* 1–10.
910 **Kim, Y., Fedoriw, A. M. and Magnuson, T.** (2012). An essential role for a mammalian SWI/SNF
911 chromatin-remodeling complex during male meiosis. *Development* **139**, 1133–1140.
912 **Kubota, H. and Brinster, R. L.** (2008). Culture of Rodent Spermatogonial Stem Cells, Male
913 Germline Stem Cells of the Postnatal Animal. *Methods Cell Biol.* **86**, 59–84.
914 **Kwon, S.-J., Park, J.-H., Park, E.-J., Lee, S.-A., Lee, H.-S., Kang, S. W. and Kwon, J.** (2015). ATM-
915 mediated phosphorylation of the chromatin remodeling enzyme BRG1 modulates DNA
916 double-strand break repair. *Oncogene* **34**, 303–313.
917 **Lecona, E., Narendra, V. and Reinberg, D.** (2015). USP7 Cooperates with SCML2 To Regulate
918 the Activity of PRC1. *Mol. Cell. Biol.* **35**, 1157–1168.
919 **Lee, H.-S., Park, J.-H., Kim, S.-J., Kwon, S.-J. and Kwon, J.** (2010). A cooperative activation loop
920 among SWI/SNF, gamma-H2AX and H3 acetylation for DNA double-strand break repair.
921 *EMBO J.* **29**, 1434–1445.
922 **Lee, J., Ogushi, S., Saitou, M. and Hirano, T.** (2011). Condensins I and II are essential for
923 construction of bivalent chromosomes in mouse oocytes. *Mol. Biol. Cell* **22**, 3465–3477.
924 **Lesch, B. J., Dokshin, G. a, Young, R. a, McCarrey, J. R. and Page, D. C.** (2013). A set of genes
925 critical to development is epigenetically poised in mouse germ cells from fetal stages

926 through completion of meiosis. *Proc. Natl. Acad. Sci. U. S. A.* **110**, 16061–6.
927 **Lesch, B. J., Silber, S. J., McCarrey, J. R. and Page, D. C.** (2016). Parallel evolution of male
928 germline epigenetic poising and somatic development in animals. *Nat. Genet.* **48**, 1–10.
929 **Lessard, J., Wu, J. I., Ranish, J. a., Wan, M., Winslow, M. M., Staahl, B. T., Wu, H., Aebersold,**
930 **R., Graef, I. a. and Crabtree, G. R.** (2007). An Essential Switch in Subunit Composition of a
931 Chromatin Remodeling Complex during Neural Development. *Neuron* **55**, 201–215.
932 **Li, Y. C., Ross, J., Scheppler, J. A. and Franza Jr., B. R.** (1991). An in vitro transcription analysis
933 of early responses of the human immunodeficiency virus type 1 long terminal repeat to
934 different transcriptional activators. *Mol Cell Biol* **11**, 1883–1893.
935 **Li, W., Wu, J., Kim, S.-Y., Zhao, M., Hearn, S. a, Zhang, M. Q., Meistrich, M. L. and Mills, A. a**
936 (2014). Chd5 orchestrates chromatin remodelling during sperm development. *Nat.*
937 *Commun.* **5**, 3812.
938 **Luo, M., Zhou, J., Leu, N. A., Abreu, C. M., Wang, J., Anguera, M. C., de Rooij, D. G., Jasin, M.**
939 **and Wang, P. J.** (2015). Polycomb Protein SCML2 Associates with USP7 and Counteracts
940 Histone H2A Ubiquitination in the XY Chromatin during Male Meiosis. *PLoS Genet.* **11**, 1–
941 17.
942 **Ma, P., Pan, H., Montgomery, R. L., Olson, E. N. and Schultz, R. M.** (2012). Compensatory
943 functions of histone deacetylase 1 (HDAC1) and HDAC2 regulate transcription and
944 apoptosis during mouse oocyte development. *Proc. Natl. Acad. Sci.* **109**, E481–E489.
945 **Maertens, G. N., El Messaoudi-Aubert, S., Elderkin, S., Hiom, K. and Peters, G.** (2010).
946 Ubiquitin-specific proteases 7 and 11 modulate Polycomb regulation of the INK4a tumour
947 suppressor. *EMBO J.* **29**, 2553–2565.
948 **Maezawa, S., Hasegawa, K., Yukawa, M., Sakashita, A., Alavattam, K. G., Andreassen, P. R.,**
949 **Vidal, M., Koseki, H., Barski, A. and Namekawa, S. H.** (2017). Polycomb directs timely
950 activation of germline genes in spermatogenesis. *Genes Dev.* **31**, 1693–1703.
951 **Maezawa, S., Hasegawa, K., Yukawa, M., Kubo, N. and Sakashita, A.** (2018). Polycomb protein
952 SCML2 facilitates H3K27me3 to establish bivalent domains in the male germline [Genetics].
953 *Pnas* 3–8.
954 **Margolin, G., Khil, P. P., Kim, J., Bellani, M. a and Camerini-Otero, R. D.** (2014). Integrated

955 transcriptome analysis of mouse spermatogenesis. *BMC Genomics* **15**, 39.
956 **Masliah-Planchon, J., Bièche, I., Guinebretière, J.-M., Bourdeaut, F. and Delattre, O.** (2015).
957 SWI/SNF Chromatin Remodeling and Human Malignancies. *Annu. Rev. Pathol. Mech. Dis.*
958 **10**, 145–171.
959 **Méndez, J. and Stillman, B.** (2000). Chromatin association of human origin recognition
960 complex, cdc6, and minichromosome maintenance proteins during the cell cycle: assembly
961 of prereplication complexes in late mitosis. *Mol. Cell. Biol.* **20**, 8602–12.
962 **Minsky, N., Shema, E., Field, Y., Schuster, M., Segal, E. and Oren, M.** (2008).
963 Monoubiquitinated H2B is associated with the transcribed region of highly expressed
964 genes in human cells. *Nat. Cell Biol.* **10**, 483–488.
965 **Montgomery, R. L., Hsieh, J., Barbosa, A. C., Richardson, J. A. and Olson, E. N.** (2009). Histone
966 deacetylases 1 and 2 control the progression of neural precursors to neurons during brain
967 development. *Proc. Natl. Acad. Sci.* **106**, 7876–7881.
968 **Motenko, H., Neuhauser, S. B., O'Keefe, M. and Richardson, J. E.** (2015). MouseMine: a new
969 data warehouse for MGI. *Mamm. Genome* **26**, 325–330.
970 **Mu, W., Starmer, J., Fedoriw, A. M., Yee, D. and Magnuson, T.** (2014). Repression of the soma-
971 specific transcriptome by Polycomb-repressive complex 2 promotes male germ cell
972 development. *Genes Dev.* **28**, 2056–2069.
973 **Nicassio, F., Corrado, N., Vissers, J. H. A., Areces, L. B., Bergink, S., Marteijn, J. A., Geverts, B.,**
974 **Houtsmuller, A. B., Vermeulen, W., Di Fiore, P. P., et al.** (2007). Human USP3 Is a
975 Chromatin Modifier Required for S Phase Progression and Genome Stability. *Curr. Biol.* **17**,
976 1972–1977.
977 **Oatley, M. J., Kaucher, A. V, Racicot, K. E. and Oatley, J. M.** (2011). Inhibitor of DNA binding 4
978 is expressed selectively by single spermatogonia in the male germline and regulates the
979 self-renewal of spermatogonial stem cells in mice. *Biol. Reprod.* **85**, 347–356.
980 **Ogiwara, H., Ui, A., Otsuka, A., Satoh, H., Yokomi, I., Nakajima, S., Yasui, A., Yokota, J. and**
981 **Kohno, T.** (2011). Histone acetylation by CBP and p300 at double-strand break sites
982 facilitates SWI/SNF chromatin remodeling and the recruitment of non-homologous end
983 joining factors. *Oncogene* **30**, 2135–2146.

984 **Pavri, R., Zhu, B., Li, G., Trojer, P., Mandal, S., Shilatifard, A. and Reinberg, D.** (2006). Histone
985 H2B Monoubiquitination Functions Cooperatively with FACT to Regulate Elongation by
986 RNA Polymerase II. *Cell* **125**, 703–717.
987 **Peters, A. H. F. M., Plug, A. W., Van Vugt, M. J. and De Boer, P.** (1997). A drying-down
988 technique for the spreading of mammalian melocytes from the male and female germline.
989 *Chromosom. Res.* **5**, 66–68.
990 **Qi, W., Wang, R., Chen, H., Wang, X., Xiao, T., Boldogh, I., Ba, X., Han, L. and Zeng, X.** (2014).
991 BRG1 promotes the repair of DNA double-strand breaks by facilitating the replacement of
992 RPA with RAD51. *J. Cell Sci.* **128**, 317–330.
993 **Raab, J. R., Resnick, S. and Magnuson, T.** (2015). Genome-Wide Transcriptional Regulation
994 Mediated by Biochemically Distinct SWI/SNF Complexes. *PLoS Genet.* **11**, 1–26.
995 **Raab, J. R., Runge, J. S., Spear, C. C. and Magnuson, T.** (2017). Co-regulation of transcription by
996 BRG1 and BRM, two mutually exclusive SWI/SNF ATPase subunits. *Epigenetics and*
997 *Chromatin* **10**, 1–15.
998 **Robinson, M. D., McCarthy, D. J. and Smyth, G. K.** (2010). edgeR: a Bioconductor package for
999 differential expression analysis of digital gene expression data. *Bioinformatics* **26**, 139–40.
1000 **Royo, H., Prosser, H., Ruzankina, Y., Mahadevaiah, S. K., Cloutier, J. M., Baumann, M.,**
1001 **Fukuda, T., Höög, C., Tóth, A., de Rooij, D. G., et al.** (2013). ATR acts stage specifically to
1002 regulate multiple aspects of mammalian meiotic silencing. *Genes Dev.* **27**, 1484–1494.
1003 **Sadate-Ngatchou, P. I., Payne, C. J., Dearth, A. T. and Braun, R. E.** (2008). Cre recombinase
1004 activity specific to postnatal, premeiotic male germ cells in transgenic mice. *Genesis* **46**,
1005 738–742.
1006 **Schmahl, J., Rizzolo, K. and Soriano, P.** (2008). The PDGF signaling pathway controls multiple
1007 steroid-producing lineages. *Genes Dev.* **22**, 3255–3267.
1008 **Serber, D. W., Runge, J. S., Menon, D. U. and Magnuson, T.** (2015). The Mouse INO80
1009 Chromatin Remodeling Complex Is an Essential Meiotic Factor for Spermatogenesis. *Biol.*
1010 *Reprod.*
1011 **Shechter, D., Dormann, H. L., Allis, C. D. and Hake, S. B.** (2007). Extraction, purification and
1012 analysis of histones. *Nat. Protoc.* **2**, 1445–1457.

1013 **Soneson, C., Love, M. I. and Robinson, M. D.** (2016). Differential analyses for RNA-seq:
1014 transcript-level estimates improve gene-level inferences. *F1000Research* **4**, 1521.
1015 **Stanton, B. Z., Hodges, C., Calarco, J. P., Braun, S. M. G., Ku, W. L., Kadoch, C., Zhao, K. and**
1016 **Crabtree, G. R.** (2016). Smarca4 ATPase mutations disrupt direct eviction of PRC1 from
1017 chromatin. *Nat. Genet.* **49**, 282–288.
1018 **Sumi-Ichinose, C., Ichinose, H., Metzger, D. and Chambon, P.** (1997). SNF2beta-BRG1 is
1019 essential for the viability of F9 murine embryonal carcinoma cells. *Mol. Cell. Biol.* **17**, 5976–
1020 5986.
1021 **Tachibana, M., Nozaki, M., Takeda, N. and Shinkai, Y.** (2007). Functional dynamics of H3K9
1022 methylation during meiotic prophase progression. *EMBO J.* **26**, 3346–3359.
1023 **Takada, Y., Naruse, C., Costa, Y., Shirakawa, T., Tachibana, M., Sharif, J., Kezuka-Shiotani, F.,**
1024 **Kakiuchi, D., Masumoto, H., Shinkai, Y. -i., et al.** (2011). HP1 links histone methylation
1025 marks to meiotic synapsis in mice. *Development* **138**, 4207–4217.
1026 **Tolstorukov, M. Y., Sansam, C. G., Lu, P., Koellhoffer, E. C., Helming, K. C., Alver, B. H., Tillman,**
1027 **E. J., Evans, J. a, Wilson, B. G., Park, P. J., et al.** (2013). Swi/Snf chromatin
1028 remodeling/tumor suppressor complex establishes nucleosome occupancy at target
1029 promoters. *Proc. Natl. Acad. Sci.* **110**, 10165–10170.
1030 **Turner, J. M. a.** (2007). Meiotic sex chromosome inactivation. *Development* **134**, 1823–1831.
1031 **Turner, J. M. A., Aprelikova, O., Xu, X., Wang, R., Kim, S., Chandramouli, G. V. R., Barrett, J. C.,**
1032 **Burgoyne, P. S. and Deng, C. X.** (2004). BRCA1, histone H2AX phosphorylation, and male
1033 meiotic sex chromosome inactivation. *Curr. Biol.* **14**, 2135–2142.
1034 **Van Der Knaap, J. A., Kumar, B. R. P., Moshkin, Y. M., Langenberg, K., Krijgsveld, J., Heck, A. J.**
1035 **R., Karch, F. and Verrijzer, C. P.** (2005). GMP synthetase stimulates histone H2B
1036 deubiquitylation by the epigenetic silencer USP7. *Mol. Cell* **17**, 695–707.
1037 **Wang, H., Wang, L., Erdjument-Bromage, H., Vidal, M., Tempst, P., Jones, R. S. and Zhang, Y.**
1038 (2004). Role of histone H2A ubiquitination in Polycomb silencing. *Nature* **431**, 873–878.
1039 **Wang, J., Gu, H., Lin, H. and Chi, T.** (2012). Essential Roles of the Chromatin Remodeling Factor
1040 Brg1 in Spermatogenesis in Mice. *Biol. Reprod.* **86**, 186–186.
1041 **Watanabe, R., Ui, A., Kanno, S. I., Ogiwara, H., Nagase, T., Kohno, T. and Yasui, A.** (2014).

1042 SWI/SNF factors required for cellular resistance to dna damage include arid1a and arid1b
1043 and show interdependent protein stability. *Cancer Res.* **74**, 2465–2475.
1044 **Wilson, B. G., Wang, X., Shen, X., McKenna, E. S., Lemieux, M. E., Cho, Y. J., Koellhoffer, E. C.,**
1045 **Pomeroy, S. L., Orkin, S. H. and Roberts, C. W. M.** (2010). Epigenetic antagonism between
1046 polycomb and SWI/SNF complexes during oncogenic transformation. *Cancer Cell* **18**, 316–
1047 328.
1048 **Wojtasz, L., Daniel, K., Roig, I., Bolcun-Filas, E., Xu, H., Boonsanay, V., Eckmann, C. R., Cooke,**
1049 **H. J., Jasin, M., Keeney, S., et al.** (2009). Mouse HORMAD1 and HORMAD2, two conserved
1050 meiotic chromosomal proteins, are depleted from synapsed chromosome axes with the
1051 help of TRIP13 AAA-ATPase. *PLoS Genet.* **5**,.
1052 **Wu, X., Oatley, J. M., Oatley, M. J., Kaucher, A. V., Avarbock, M. R. and Brinster, R. L.** (2010).
1053 The POU Domain Transcription Factor POU3F1 Is an Important Intrinsic Regulator of GDNF-
1054 Induced Survival and Self-Renewal of Mouse Spermatogonial Stem Cells1. *Biol. Reprod.* **82**,
1055 1103–1111.
1056 **Yamaguchi, T., Cubizolles, F., Zhang, Y., Reichert, N., Kohler, H., Seiser, C. and Matthias, P.**
1057 (2010). Histone deacetylases 1 and 2 act in concert to promote the G1-to-S progression.
1058 *Genes Dev.* **24**, 455–469.
1059 **Yang, F., De La Fuente, R., Leu, N. A., Baumann, C., McLaughlin, K. J. and Wang, P. J.** (2006).
1060 Mouse SYCP2 is required for synaptonemal complex assembly and chromosomal synapsis
1061 during male meiosis. *J. Cell Biol.* **173**, 497–507.
1062 **Yu, G., Wang, L.-G., Han, Y. and He, Q.-Y.** (2012). clusterProfiler: an R Package for Comparing
1063 Biological Themes Among Gene Clusters. *Omi. A J. Integr. Biol.* **16**, 284–287.
1064 **Zhang, Y., Liu, T., Meyer, C. A., Eeckhoute, J., Johnson, D. S., Bernstein, B. E., Nussbaum, C.,**
1065 **Myers, R. M., Brown, M., Li, W., et al.** (2008). Model-based analysis of ChIP-Seq (MACS).
1066 *Genome Biol.* **9**,.
1067
1068

1069 **Figure Legends:**

1070

1071 **Figure 1.** BRG1 is enriched at transcriptionally active and poised regions. (A) Heatmaps with K-
1072 means clustering depicting the relative enrichment of BRG1, H3K4me3 and H3K27me3 across
1073 RefSeq gene TSS ± 4 Kb in P12, P17 and P18 testes. TSS: Transcription start site, Cl-1:Class 1,
1074 Cl-2: Class 2, Cl-3: Class 3. Number (n) of TSS's sites within each cluster are indicated (B)
1075 Metaplots depicting the relative enrichment of BRG1 at P12 and P18 (top row), H3K4me3
1076 (middle row) and H3K27me3 (bottom row), at P12 and P17, at TSS ± 4 Kb, associated with
1077 P12 BRG1 ChIP-seq peaks categorized by the testes temporal expression profile of cognate
1078 genes. (C) P12 and P18 BRG1 enrichment across an 8 Kb window centered at TSS's of X -
1079 linked genes.

1080

1081 **Figure 2.** BRG1 influences transcription during spermatogenesis. (A) Smear plot showing the
1082 Log2 fold change in transcript abundance (y-axis) of genes in the P12 *Brg1*^{cKO} relative to *Brg1*^{WT}
1083 and Log2 transcript abundance in counts per million (CPM; x-axis). Red dots denote
1084 significantly mis-expressed genes (FDR≤0.05). The horizontal blue lines demarcate the 2-fold
1085 change in transcript abundance. (B) Table listing enriched anatomy and gene ontology terms
1086 associated with genes differentially regulated by BRG1. Benjamini – Hochberg, adjusted p
1087 values are indicated within parenthesis next to the corresponding ontology term. (C) Heatmap
1088 depicting the change in transcript abundance of genes associated with arrest of male meiosis
1089 (MP:0008261) and abnormal spermatogonia proliferation (MP:0002685) phenotype ontologies
1090 (labeled along vertical axis), across individual P12 *Brg*^{WT} (WT1-WT4) and *Brg*^{cKO} (KO1-KO4)
1091 replicates (horizontal axis). Transcript abundances are represented as z- scores. (D) P10 *Brg*^{WT}
1092 and *Brg1*^{cKO} testes cryosections, immunofluorescently labeled for ZBTB16 (green) and counter
1093 stained with DAPI (blue). The average number of ZBTB16^{+} cells (type A spermatogonia; SpgA)
1094 ± standard error of mean (SEM) per tubule are indicated below each representative image.
1095 Images were captured using a 25x objective Scale bar: 20 µm. (E) Western blot showing the
1096 abundance of SYCP2 in sub-cellular fractions obtained from P21 *Brg1*^{WT}, *Brg*^{Het} and *Brg1*^{cKO}
1097 spermatogenic cells. Histone- H3 was used as a nuclear loading control. (F) *Brg*^{WT} and *Brg1*^{cKO}
1098 zygotene spermatocytes immunofluorescently labeled for SYCP2 (red) and γH2Ax (green). The
1099 percentage of *Brg1*^{cKO} zygotene spermatocytes (n=212) displaying abnormal SYCP2 filaments
1100 is indicated. Images were captured using a 100x objective Scale bar: 10 µm.

1101

1102 **Figure 3.** BRG1 directly regulates chromatin accessibility at promoters. (A) Bar plot depicting
1103 the Log2 values of normalized ATAC-seq read coverage with added pseudocount (y-axis) at the
1104 promoters (TSS± 0.5Kb) of BRG1 activated and repressed genes (x-axis) in P12 *Brg1*^{wt} (red)
1105 and *Brg1*^{cKO} (blue) spermatogenic cells. *** : Significant p-value ($p<0.001$); NS: not significant,
1106 as calculated by Wilcoxon rank sum test (B) Smear plot depicting the Log2 fold change in
1107 chromatin accessibility (y-axis) and Log2 ATAC read abundance in counts per million (CPM; x-
1108 axis) in the P12 *Brg1*^{cKO} relative to *Brg1*^{WT}. Red dots denote regions displaying significant
1109 differences in chromatin accessibility (FDR≤0.05). Horizontal blue lines denote a 2- fold change
1110 in read abundance. Closed: sites less accessible; Opened: sites more accessible, in the P12
1111 *Brg1*^{cKO} relative to *Brg1*^{WT} (C) Genomic associations of closed and opened sites. Total number
1112 either class of sites are indicated within parenthesis (D) Gene ontology analysis of closed and
1113 opened sites. Benjamini – Hochberg, adjusted p values are indicated.
1114
1115

1116 **Figure 4.** BRG1 physically interacts with SCML2 to regulate gene expression. (A) Silver stained
1117 gel (left) and table (right) summarizing proteins identified by performing mass spectrometry(MS)
1118 on BRG1 Immuno-pulldowns (IP) obtained from nuclear lysates which were prepared from 3-
1119 week-old wild type testes. Peptide counts for proteins detected in IgG pulldown are indicated
1120 within parenthesis (B) SCML2 Co-IP . Nonspecific (ns) IgG was used as negative control.
1121 Lysates were treated with 25 U of universal nuclease (benzonase) prior to IP. Red arrowheads
1122 label proteins detected in IP. Lane numbers are indicated at bottom (C) Metaplots depicting
1123 BRG1 enrichment at P12 (green) and P18 (orange) over at TSS ± 2 Kb, associated with SCML2
1124 activated (pach *Scml2* Act) and repressed (pach *Scml2* Rep) genes in pachytene
1125 spermatocytes (D) Quadrant plot depicting the Log2 fold change in expression (KO/WT),
1126 associated with genes commonly regulated by BRG1 (y-axis) and SCML2 (x-axis). Genes
1127 displaying concordant and discordant expression changes are denoted by green and orange
1128 dots respectively. The number of concordantly expressed genes (n) are indicated. r^2 values
1129 were derived from pearson's correlation test.
1130
1131

1132 **Figure 5.** BRG1 influences the localization of SCML2 to the sex body. P21 *Brg1*^{WT} and *Brg1*^{cKO}
1133 cryosections, immunofluorescently labeled for (A) SCML2 (green) and γH2Ax (red), (B) USP7

1134 (green) and γH2Ax (red). DNA (blue) was stained using DAPI. Arrowheads denote the sex
1135 body labeled with γH2Ax. Magnified image of pachytene spermatocytes are shown in panel
1136 insets (Pa: Pachynema). All images were captured using a 63x objective. Scale bar: 20 µm. (C)
1137 Pachytene spermatocytes spreads from *Brg1*^{WT} and *Brg1*^{cKO} testes, immunofluorescently
1138 labeled for SYCP3 (red) and markers of meiotic sex chromosome inactivation (green) -
1139 BRCA1(left-most), ATR (middle) and MDC1 (right-most) . Magnified image of the sex
1140 chromosomes are shown in panel insets. Images were captured using a 100x objective. Scale
1141 bar: 20 µm.
1142
1143
1144 **Figure 6.** BRG1 regulates H2AK119ub1 and H3K27ac during spermatogenesis. (A) Western
1145 blots depicting H2AK119ub1, H3K27ac, H3K4me3 and H3K27me3, abundance in acid
1146 extracted histones obtained from P12 *Brg*^{WT}, *Brg*^{Het} and *Brg1*^{cKO} testes. H3 was used as a
1147 loading control. (B) Log2 fold change in H2AK119ub1 (green box) and H3K27ac (Orange box)
1148 at BRG1 occupied promoters (TSS± 0.5Kb) categorized by chromosomal location (top panel)
1149 and transcriptional status (bottom panel) in P12 *Brg1*^{cKO} relative to *Brg1*^{WT}. *** :Significant p-
1150 value ($p<0.001$); NS: not significant, as calculated by Wilcoxon rank sum test. (C) The
1151 enrichment of H3K27ac (left) and BRG1 (right) at lost, gained and common H3K27ac peaks
1152 identified by a differential analysis of ChIP-seq peaks between P12 *Brg1*^{WT} and *Brg1*^{cKO}
1153 spermatogenic cells. (D) Western blot depicting the abundance (top panel) and quantification
1154 (bottom) of BRG1, RNF2 , USP3 and HDAC1 in nuclear fractions obtained from P12 *Brg*^{WT} ,
1155 *Brg*^{Het} and *Brg1*^{cKO} spermatogenic cells. Bar plot represents the mean of protein band intensities
1156 in the insoluble nuclear fractions determined from at least two independent trials. Protein levels
1157 are relative to the wild type control and normalized to H3. Error bars represent the standard
1158 error of mean (SEM). * denotes a significant students t-test p value.
1159
1160 **Figure 7.** Model describing the role of SWI/SNF in spermatogenic gene regulation. (A) In the
1161 developing male germ line BRG1 activates genes essential for the maintenance of pluripotent
1162 spermatogonial precursors and several meiotic factors during meiosis, while repressing pre-
1163 meiotic and somatic genes in spermatocytes. (B) During meiosis BRG1 activated gene
1164 promoters (meiotic genes) display robust H3K4me3 enrichment while repressed gene
1165 promoters display hallmarks of bivalent chromatin (H3K4me3 and H3K27me3). BRG1 is
1166 required to maintain promoter accessibility and suppresses H2AK119ub1 while maintaining a

1167 relatively higher level of H3K27ac at target genes. We propose that the repression of somatic
1168 and pre-meiotic genes is achieved through the activity of SCML2, a PRC1 factor that is testes
1169 specific. BRG1 exclusively interacts with SCML2 and influences its localization during meiosis.
1170 As a consequence of this interaction, BRG1 also influences the localization of USP7, a factor
1171 known to interact with SCML2.
1172
1173

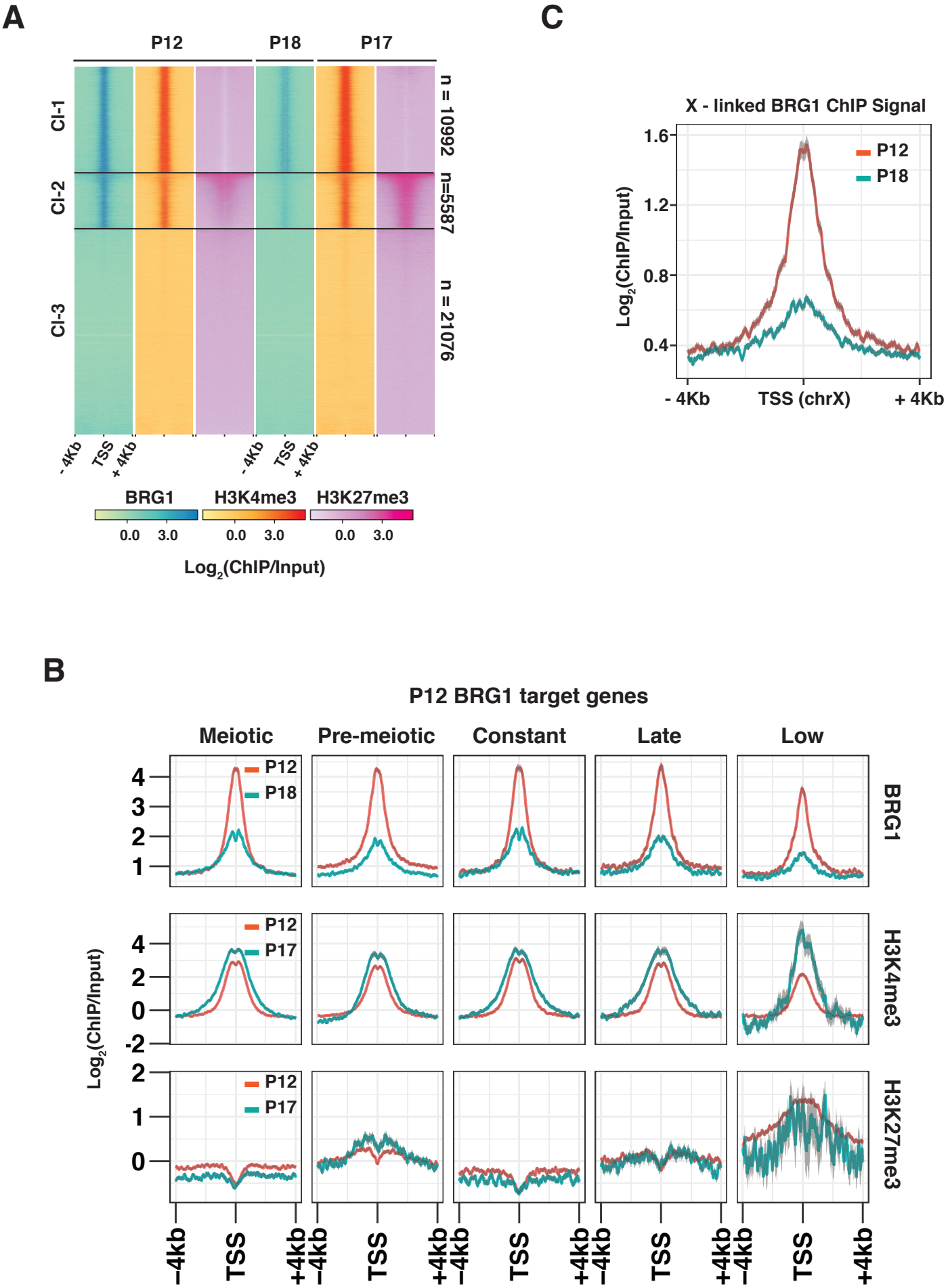
A
P12
P18
P17
Cl-1
Cl-2
Cl-3
n = 10992
n=5587
n = 21076
- 4Kb
TSS
+ 4Kb
BRG1
H3K4me3
H3K27me3
0.0 3.0
Log2(ChIP/Input)
C
X - linked BRG1 ChIP Signal
P12
P18
Log2(ChIP/Input)
1.6
1.2
0.8
0.4
- 4Kb
TSS (chrX)
+ 4Kb
B
P12 BRG1 target genes
Meiotic
Pre-meiotic
Constant
Late
Low
P12
P18
P17
BRG1
H3K4me3
H3K27me3
Log2(ChIP/Input)
−4kb
TSS
+4kb

A

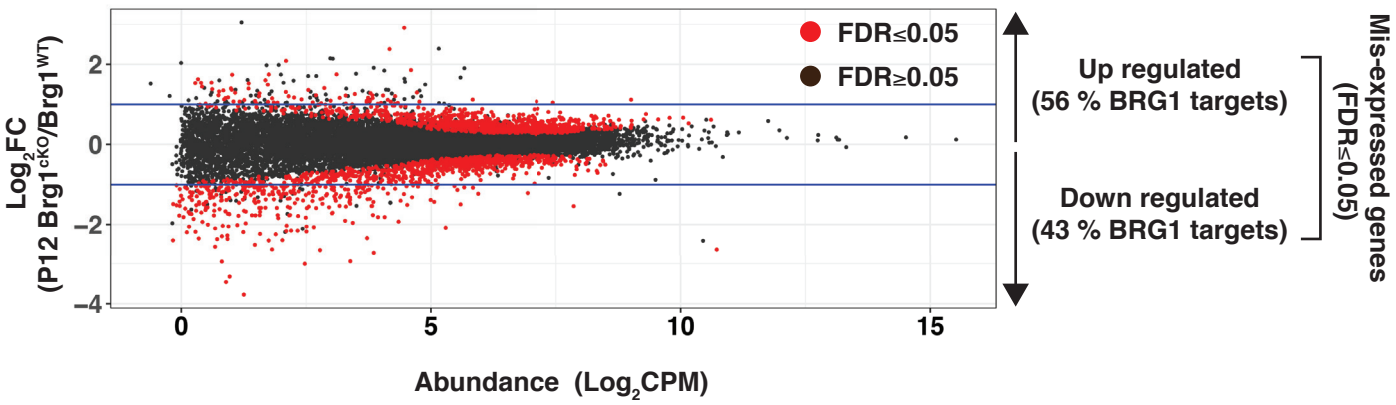

B

	Anatomy Ontology (adj. p value)	Gene Ontology (adj. p value)
Down regulated	Brain (0.0049)	Meiotic cell cycle (2.292e-12)
	Central nervous system (0.0051)	meiotic nuclear division (4.727e-11)
	Gonad (0.0052)	chromosome segregation (1.747e-10)
	Molar (0.0057)	chromosome organization (2.756e-08)
Up regulated	Limb (4.077e-0.9)	Regulation of cell morphogenesis (0.00013)
	Mesenchyme (5.17e-0.9)	Axonogenesis (0.00013)
	Musculoskeletal system (5.27e-0.9)	Developmental cell growth (0.00019)
	Oral region (9.21e-0.9)	Regulation of actib filament-based process (0.00019)

C

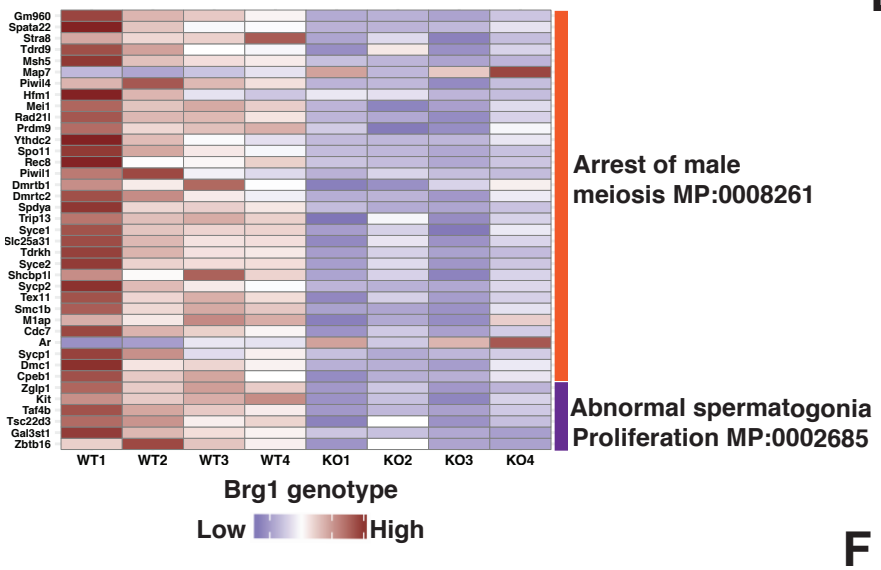

E

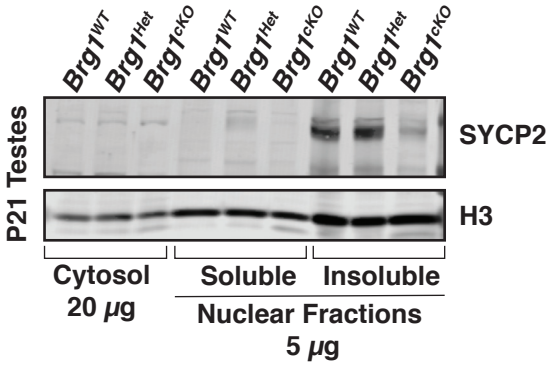

D

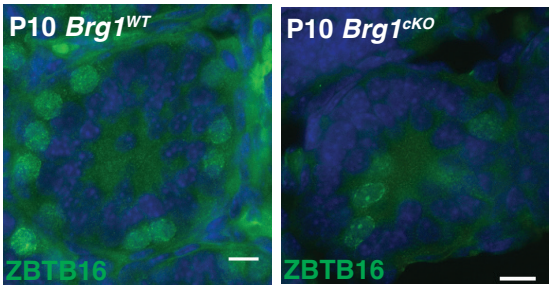

SpgA =13.5 ± 0.2 SpgA =7.4 ± 0.5

F

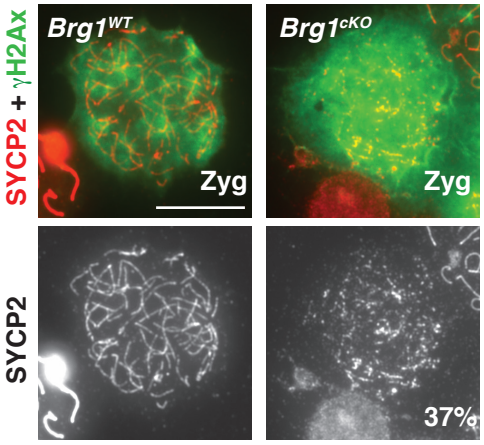

A

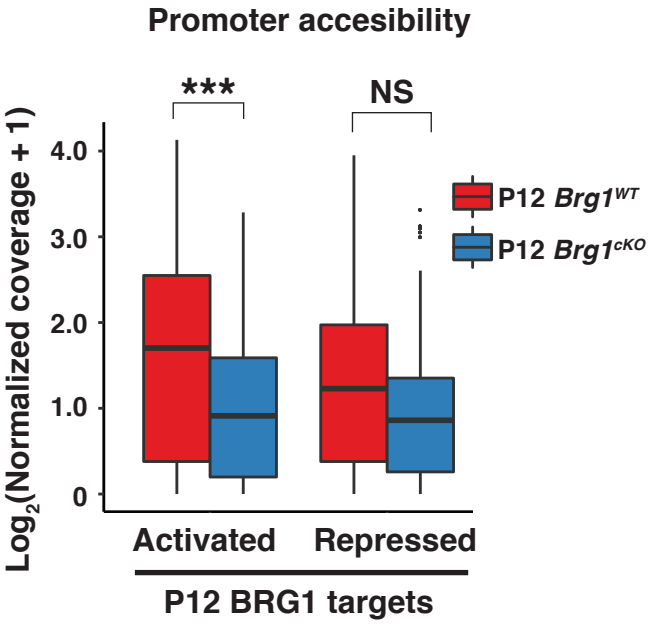

C

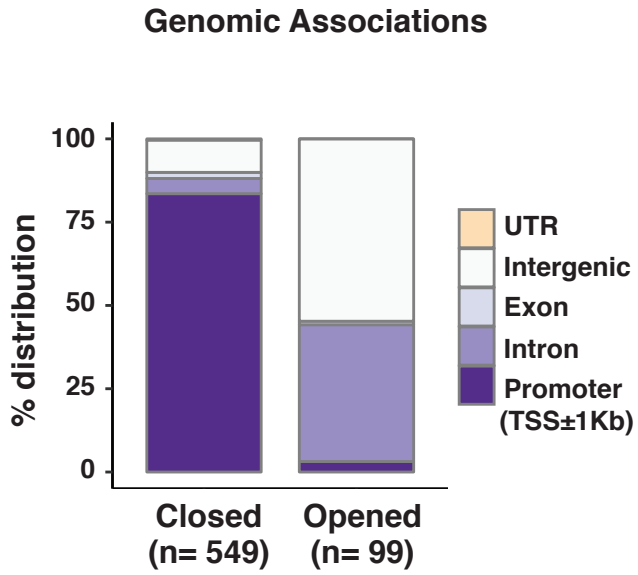

B

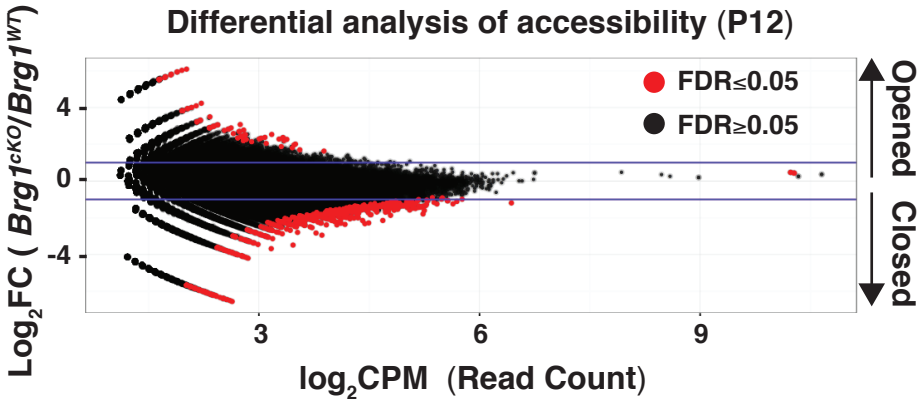

D

	Gene Ontology (Biological Process)	Adj.p value	Candidate Genes
Closed	Meiotic cell cycle	0.0003	*Top6bl, Tex19.1, Brca2*
	DNA repair	0.0009	*Yy1, Ube2n, Fanca, Mus81*
	Chromosome organization	0.0009	*Stag3, Phf13, Ercc3, Ccne2*
Opened	Cardiac muscle tissue development	0.06	*Angpt1,Zfpm2, Pln*
	Fat cell differentiation	0.06	*Jag1, Fndc3b, Igf1*
	Cytoplasm organization	0.06	*Zmiz1,Etv6*

A

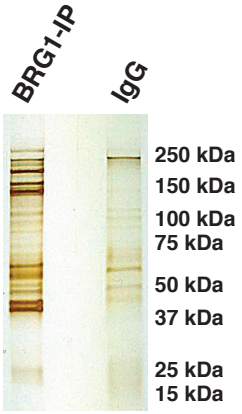

3 week old testes

	Protein	# Unique Peptide	% Coverage
Core	BRG1	63	45
	SNF5	24	70
	BAF155	55	61
	BAF170	49	52
PBAF	ARID2	46	38
	PBRM1	43	35
	BRD7	17	44
BAF	ARID1A	68	42
	ARID1B	45	26
	BRD9	12	33
	BCL7A	5	41
	BCL7B	5	41
	BCL7C	5	46
PRC1	SCML2	11(14)	16(17)

B

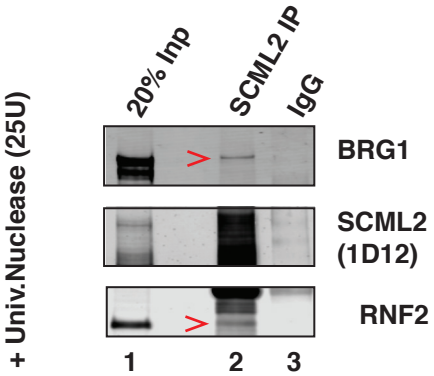

C

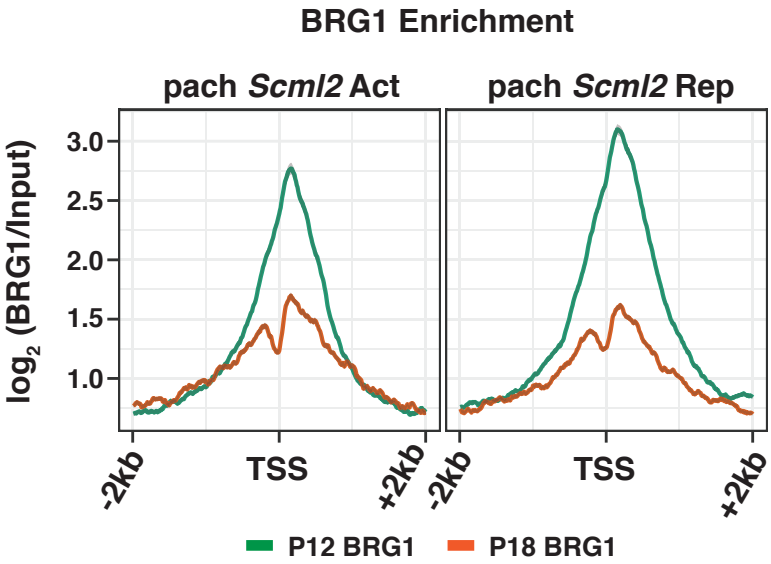

D

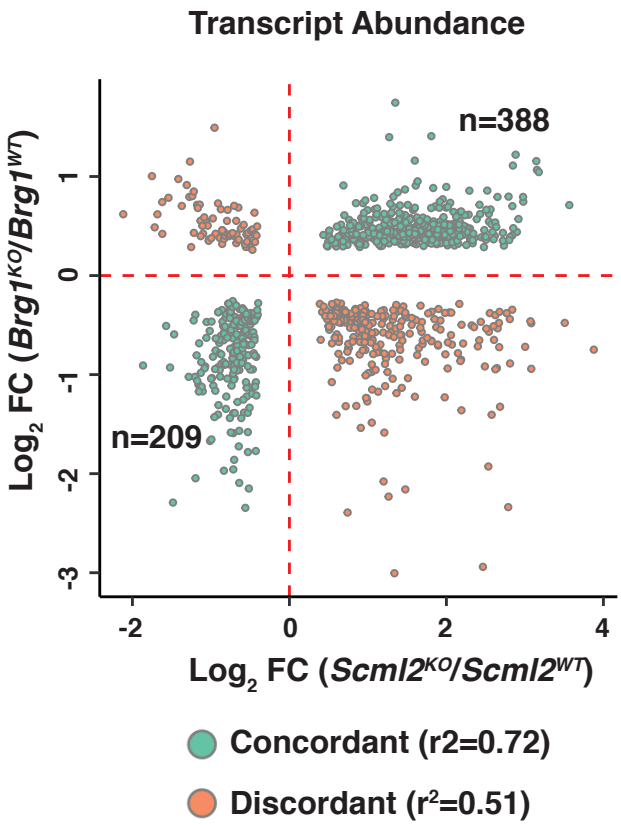

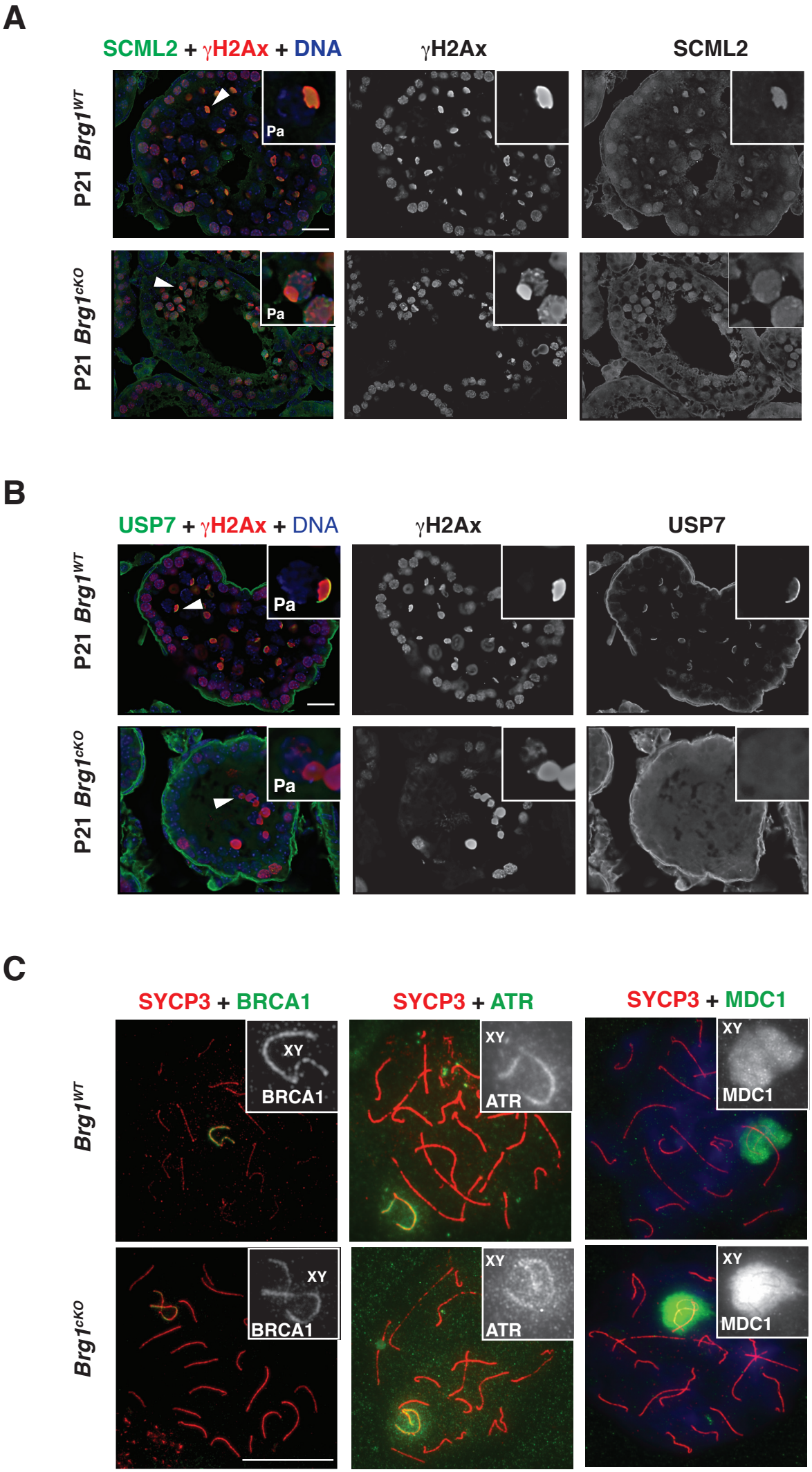
A
SCML2 + γH2Ax + DNA
γH2Ax
SCML2
P21 Brg1WT
P21 Brg1cKO
Pa
B
USP7 + γH2Ax + DNA
γH2Ax
USP7
P21 Brg1WT
P21 Brg1cKO
Pa
C
SYCP3 + BRCA1
SYCP3 + ATR
SYCP3 + MDC1
Brg1WT
Brg1cKO
XY
BRCA1
ATR
MDC1

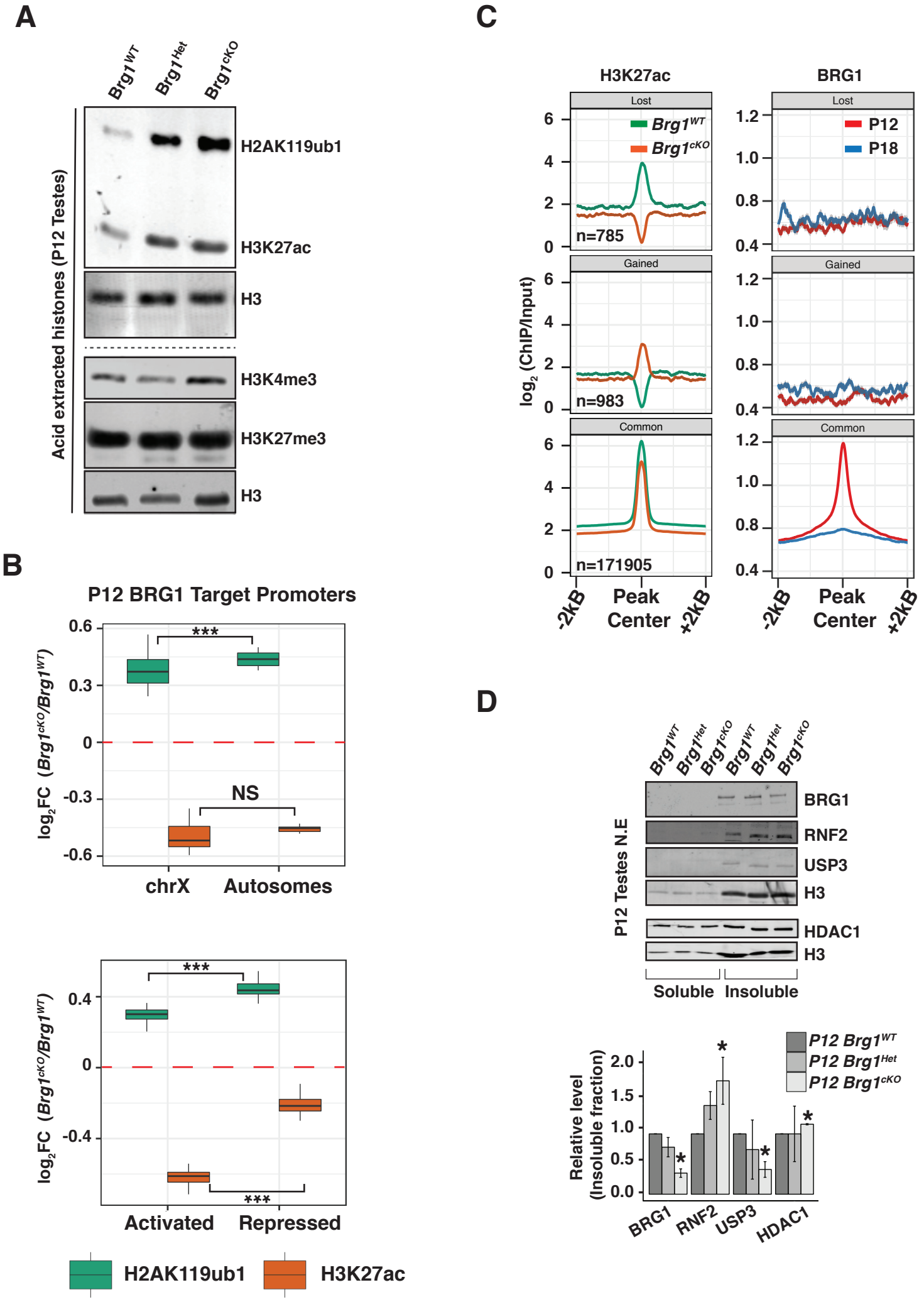
A
Brg1WT
Brg1Het
Brg1cKO
H2AK119ub1
H3K27ac
H3
H3K4me3
H3K27me3
H3
Acid extracted histones (P12 Testes)
B
P12 BRG1 Target Promoters
log2FC (Brg1cKO/Brg1WT)
***
NS
chrX
Autosomes
Activated
Repressed
H2AK119ub1
H3K27ac
C
H3K27ac
BRG1
Lost
Gained
Common
Brg1WT
Brg1cKO
P12
P18
n=785
n=983
n=171905
log2 (ChIP/Input)
-2kB
Peak Center
+2kB
D
P12 Testes N.E
BRG1
RNF2
USP3
H3
HDAC1
H3
Soluble
Insoluble
P12 Brg1WT
P12 Brg1Het
P12 Brg1cKO
Relative level (Insoluble fraction)
BRG1
RNF2
USP3
HDAC1

A

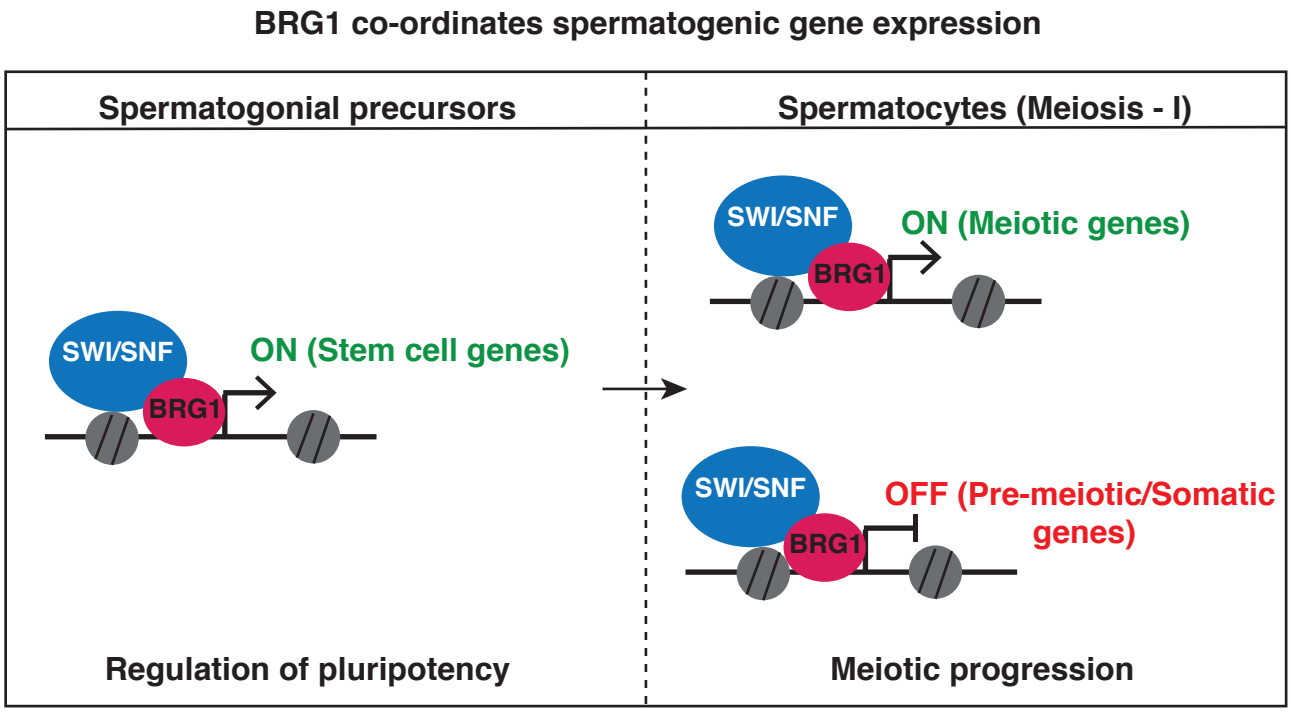
BRG1 co-ordinates spermatogenic gene expression
Spermatogonial precursors
Spermatocytes (Meiosis - I)
SWI/SNF
BRG1
ON (Stem cell genes)
SWI/SNF
BRG1
ON (Meiotic genes)
SWI/SNF
BRG1
OFF (Pre-meiotic/Somatic genes)
Regulation of pluripotency
Meiotic progression

B

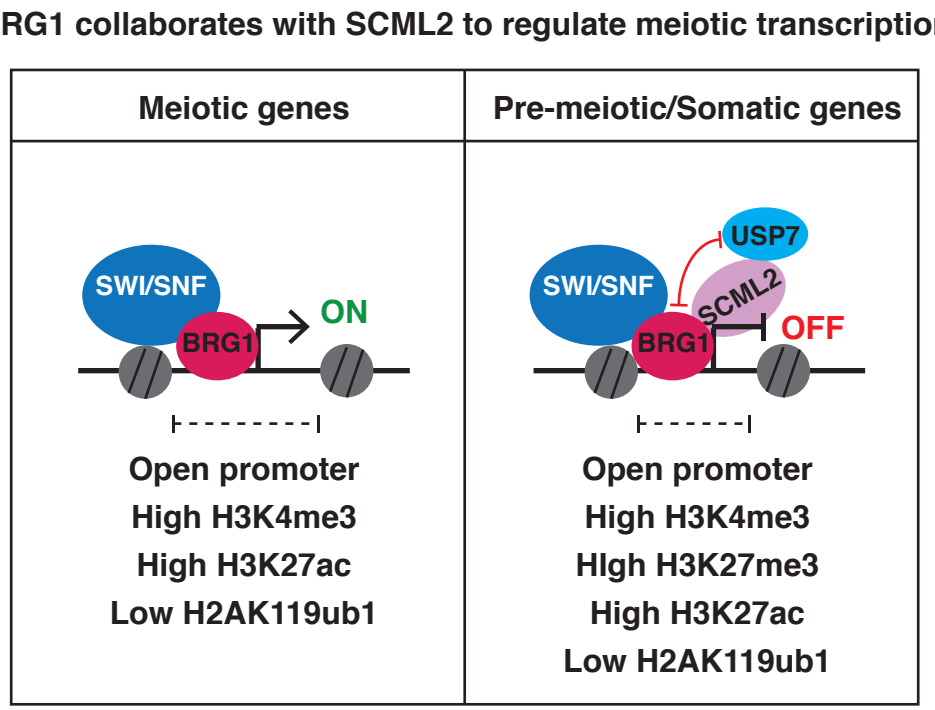
BRG1 collaborates with SCML2 to regulate meiotic transcription
Meiotic genes
Pre-meiotic/Somatic genes
SWI/SNF
BRG1
ON
Open promoter
High H3K4me3
High H3K27ac
Low H2AK119ub1
USP7
SWI/SNF
SCML2
BRG1
OFF
Open promoter
High H3K4me3
HIgh H3K27me3
High H3K27ac
Low H2AK119ub1

Supplemental Information

Mammalian SWI/SNF collaborates with a polycomb-associated protein to regulate male germ line transcription in the mouse

Debashish U. Menon, Yoichiro Shibata, Weipeng Mu and Terry Magnuson

Department of Genetics, and Lineberger Comprehensive Cancer Center, The University of North Carolina at Chapel Hill, Chapel Hill, North Carolina, NC 27599-7264, USA
*Correspondence: trm4@med.unc.edu, Tel 919-962-1319, Fax 919-843-4682

List of supplemental information:

Supplemental figures S1-S10

Figure S1. Features of BRG1 genomic associations.

Figure S2. Transcriptional response to the loss of BRG1 in the male germ line.

Figure S3. BRG1 directed changes in chromatin accessibility

Figure S4. Summary and validation of BRG1 interactions.

Figure S5. Features of BRG1 association with genes differentially regulated by SCML2.

Figure S6. Validation of the role of BRG1 in the recruitment of SCML2 to the sex body.

Figure S7. Analysis of SCML2 localization in meiotic spreads

Figure S8. Temporal regulation of H2AK119ub1 in testes and validation of anti- H2AK119ub1 (clone E6C5).

Figure S9. Genomic associations of lost, gained and common H3K27ac peaks.

Figure S10. BRG1 regulates the expression of epigenetic modifiers of H2AK119ub1, H2BK120ub1 and H3K27ac.

Supplemental tables

Table S1. List of genes differentially regulated by BRG1 at P12 (Excel sheet).

Table S2. List of regions displaying significant differences in chromatin accessibility in the *Brg1*^{cKO} relative to *Brg1*^{WT} (Excel sheet).

Table S3. List of BRG1 ChIP-seq peak calls and the genomic location of sites differentially bound by BRG1 between P12 and P18 testes (Excel sheet).

Table S4. List of antibodies used in this study

Table S5. Sequences of qRT-PCR primers used in this study

Supplemental figure legends

Figure S1. Features of BRG1 genomic associations. (A) Annotation of regions associated with P12 and P18 BRG1 peaks. Number (n) of P12 and P18 peaks are indicated within parenthesis. (B) Distribution of temporal expression profile of genes associated with class 1-3 TSS's. PMei: pre-meiotic, Mei: Meiotic, Const: constant. (C) UCSC genome browser views depicting H3K4me3 and H3K27me3 peak associations with promoters of candidate BRG1 target genes. Thick black bars denote BRG1 Macs2 peak calls. (D) P12 (green line) and P18 (orange line) BRG1 enrichment across an 8 Kb window centered at PRDM9 peaks (purple line).

Figure S2. Transcriptional response to the loss of BRG1 in the male germ line. (A) Quantification of spermatocyte populations per tubule (left panel) staged by γH2Ax immunostaining of *Brg*^{WT} and *Brg1*^{cKO} cryosections obtained from P10 , P13 and P14 testes. The total number of tubules analyzed (n) at each stage is indicated. Abundance (right panel) of spermatogonial and meiotic sub stage specific protein-coding genes (x-axis) between P12 *Brg*^{WT} (red box) and *Brg1*^{cKO} (blue boxes). Transcript abundance is expressed as the Log2 value of counts per million (CPM) added with a pseudo count (y–axis). (B) Quantitative RT-PCR analysis to determine the transcript abundance (y-axis) of candidate stem cell factors (x-axis) in *Brg*^{Het} and *Brg1*^{cKO} relative to *Brg*^{WT} spermatogonia (THY1^{+}). The transcript abundance of candidate factors was normalized to genes whose transcript levels are constantly expressed (*Sdha* and *Ywhaz*). * denotes a p-value < 0.05, calculated using an unpaired students t-test. (C) Western blot showing the abundance of SYCP2 in sub-cellular fractions obtained from P12 *Brg*^{Het} and *Brg1*^{cKO} spermatogenic cells. Histone- H3 was used as a nuclear loading control. (D) *Brg*^{WT} and *Brg1*^{cKO} zygotene spermatocytes immunofluorescently labeled for SYCP2 (red) and SYCP3 (green). Images were captured using a 100x objective Scale bar: 10 µm. (E) Western blot showing the abundance of PDGFRA in cytosolic fractions obtained from P12, P14, P21 *Brg*^{WT}, *Brg*^{Het} and *Brg1*^{cKO} spermatogenic cells. α TUBULIN was used as a loading control.

Figure S3. BRG1 directed changes in chromatin accessibility (A) Metaplots (top) and corresponding heatmaps (bottom) depicting the pairwise comparisons of normalized ATAC-seq signal at RefSeq genes ± 2Kb, between P12 *Brg1*^{WT} and *Brg1*^{cKO} spermatogenic cells, P18 *Brg1*^{WT} and *Brg1*^{Het} (*Brg1*$^{fl/\Delta}$) spermatogenic cells. TSS: Transcription start site, TES: Transcription end site. (B) UCSC browser view of candidate closed and opened regions.

Figure S4. Summary and validation of BRG1 interactions. (A) List of known SWI/SNF subunits identified by IP-MS that are common to BAF and PBAF subcomplexes. (B) Validation of SCML2 antibody (1D12) specificity on nuclear extracts prepared from testes, ovaries and purified spermatogenic cells. Nucleolin (NCL) was used as a nuclear marker. (C) Co-immunoprecipitation of BRG1 and USP7. Nonspecific IgG was used as negative control. All lysates were treated with 25 U of universal nuclease (benzonase) prior to IP.

Figure S5. Features of BRG1 association with genes differentially regulated by SCML2. (A) ATAC seq coverage from P12 *Brg1*^{WT} and *Brg1*^{cKO} at TSS ± 4 Kb, associated with genes regulated by SCML2 in pachytene spermatocytes. (B) Enriched gene ontology terms associated with genes concordantly activated or repressed by BRG1 (P12) and SCML2 (pachynema).

Figure S6. Validation of the role of BRG1 in the recruitment of SCML2 to the sex body. Cryosections prepared from (A) P14 and P21 *Brg1*^{WT} and *Brg1*^{cKO} testes, immunofluorescently labeled for SCML2 (cyan), BRG1(red) and ATR (green), (B) P14 *Brg1*^{WT} and *Brg1*^{Het} testes, immunofluorescently labeled for SCML2 (green) and γH2Ax (red), DNA was stained with DAPI. Arrowheads label pachytene spermatocytes with completely formed sex body. Images were captured using a 63x objective. Scale bar: 20 µm.

Figure S7. Analysis of SCML2 localization in meiotic spreads. Pachytene spermatocyte from *Mvh-Cre* (left panel) and *Stra8-Cre* (right panel) induced *Brg1*^{cKO} and *Brg1*^{WT} testes, immunofluorescently labeled for SCML2 (green) and SYCP3 (red). Arrowheads denote the sex chromosomes and dotted circle outlines the SCML2 signal around the sex body. Images were captured using a 100x objective. Scale bar: 20 µm.

Figure S8. Temporal regulation of H2AK119ub1 in testes and validation of anti- H2AK119ub1 (clone E6C5) . (A) Western blot depicting H2AK119ub1, H3K27ac abundance in acid extracted histones obtained from P8,P10 *Brg*^{WT}, *Brg*^{Het} and *Brg1*^{cKO} testes. H3 was used as a loading control (B) Western blot showing H2AK119ub1 and H3 abundance in acid extracted histones obtained from testes of P12 wild type mice carrying a *Mvh-Cre* transgene and their littermate controls (+/+). (C) Validation of anti-H2AK119ub1 (clone E6C5) specificity by immunoblotting for total H2AK119ub1 in acid extracted histones obtained from *Rnf2*^{WT} and two different *Rnf2*^{KO} ES cell lines. Blots were stained with Ponceau S to show total histone levels. (D) Western blot using anti-H2AK119ub1 (clone E6C5), to show H2AK119ub1 (green) levels in sub-cellular fractions of spermatogenic cells obtained from P12 *Brg*^{WT}, *Brg*^{Het} and *Brg1*^{cKO} testes. H3 (red) was used as nuclear loading control. Dotted rectangle labels the nuclear levels of H2AK119ub1 levels. L: ladder.

Figure S9. Genomic associations of lost, gained and common H3K27ac peaks.

Figure S10. BRG1 regulates the expression of epigenetic modifiers of H2AK119ub1, H2BK120ub1 and H3K27ac. (A) UCSC browser view depicting BRG1 occupancy at *Rnf2*, *Usp3*, *Hdac1* and *Hdac2* promoters. Thick black bars label BRG1 peaks. (B) Transcript abundance (y-axis) of *Rnf2*, *Usp3*, *Hdac1* and *Hdac2* in P12 $Brg1^{WT}$ (red box) and $Brg1^{cKO}$ (blue box). Transcript abundance is expressed as the Log2 value of normalized abundance in counts per million (CPM) added with a pseudo count. (C) Western blot depicting H2BK120ub1 levels in acid extracted histones obtained from P12 Brg^{WT} , Brg^{Het} and $Brg1^{cKO}$ testes. H3 was used as a loading control.

Supplemental_Table_S4.doc

Antibody	Vendor (catalog #)	Application
Rabbit anti-BRG1	Abcam (ab110641)	ChIP-seq (10 µg) IF (1:500)
Rabbit anti- YH2Ax	Cell signaling (9718)	IF (1:1000)
Mouse anti- YH2Ax	Millipore (05-636)	IF (1:1000)
Mouse anti-SYCP3	Abcam (ab97672)	IF (1:500)
Rabbit anti-SYCP3	Abcam (ab154255)	IF (1:500) WB (1:1000)
Rabbit anti-SYCP2	Millipore (ABE2622)	IF (1:500) WB (1:1000)
Goat anti- ATR (N-19)	Santa Cruz Biotech (sc-1887)	IF (1:50)
Mouse anti-SCML2 (1D12)	Developmental Studies Hybridoma Bank (PCRP-SCML2-1D12)	IF (1:10) IP (10 µg)
Rat anti- RNAPII subunit B1 (phosphor CTD Ser-2)	Millipore (04-1571)	IF (1:200)
Mouse anti- H2AK119ub1 (E6C5)	Millipore (05-678)	ChIP-seq (10 µg) WB (1:1000)
Rabbit anti- H3K27ac	Active Motif (39133)	ChIP-seq (5 µg) WB (1:1000)
Rabbit anti- H2BK120ub1	Cell signaling (5546)	WB (1:1000)
Mouse anti- H3K27me3	Abcam (ab6002)	WB (1:1000)
Rabbit anti– H3K4me3	Abcam (ab1012)	WB (1:1000)
Rabbit anti- H3	Abcam (ab1791)	WB (1:5000)
Mouse anti- RNF2	Santa Cruz Biotech (sc-1887)	WB (1:1000)
Mouse anti- USP3	GeneTex (GTX128238)	WB (1:1000)
Mouse anti- USP7	Santa Cruz Biotech (sc-1887)	IF (1:100) IP (2 µg) WB (1:1000)
Mouse anti- HDAC1	Abcam (ab7028)	WB (1:1000)
Rabbit anti- PDGFRA	Cell signaling (3164)	WB (1:1000)
Mouse anti α TUBULIN	Developmental Studies Hybridoma Bank (12G10)	WB (1:1000)
Rabbit anti NCL (Nucleolin)	Bethyl (A300-711A)	WB (1:5000)

Table. S4. List of antibodies used in this study

Supplemental_Table_S5.doc

Gene Symbol	Forward Primer (5' - 3')	Reverse Primer (5' - 3')
Zbtb16	TATCTCGAAGCATTCCAGCGAGGA	ACTCATGGCTGAGAGACCGAAAGA
Id4	CCCGCGCCACCTCTCCAC	CAGAGAATGCTGTCA CCCTG
Pou3f1	TGGGGGCTGTCACTTTATTC	GGAGTTAGAAGGACCCCAGG
Pou5f1	AGCTGCTGAAGCAGAAGAGG	GTGGTCTGGCTGAACACCTT
Foxo1	AAGAGCGTGCCCTACTTCAA	TGCTGTGAAGGGACAGATTG
Sdha	TGGACCTTGTAGTCTTTGGCA	AACCGATTCTTCTCCAGCATT
Ywhaz	GAGAAAAAGCAGCAGATGGC	CTTTCTGGTTGCGAAGCATT
Brg1	GAAGACCATCCAGACCATCG	TTCATACGCCCAGTTTGACA

Table. S5. Sequences of qRT-PCR primer used in this study

Supplemental Materials

ChIP from low input chromatin:

Spermatogenic cells obtained from 12-day-old *Brg1*^{WT} and *Brg1*^{cKO} mice were fixed as described (Raab et al., 2015). Frozen pellets (10^6 cells each) were thawed on ice and then resuspended in 50 µl of nuclear isolation buffer (Sigma NUC-101). For the H3K27ac ChIPs, 5mM sodium butyrate was added to the nuclear suspensions. Samples were mixed by pipetting the cell suspension 15-20 times. 50 µl of nuclear preparations were mixed with 10 µl of MNase digestion buffer [6x MNase buffer (NEB), 8.8 mM DTT, 12 gel units MNase (NEB)] and incubated at 37 C for 15 minutes. The digestion was stopped by adding 1/10th volume of 100 µM EDTA (Ethylenediaminetetraacetic acid). 6.6 µl of a 1% Triton X-100/1% sodium deoxycholate solution was added to the digested chromatin and vortexed gently for 30 seconds after which the samples were held on ice until the next step. In the meantime the DNA content of each chromatin preparation was quantified from 5 ul of chromatin. Briefly, chromatin was mixed with 95 µl H_2O and 100 µl 10% chelex-100 (Bio-Rad) and incubated at 95 C for 10 min. Following RNaseA digestion for 15 min at 37 C, ProteinaseK digestion for 1 hr at 56 C, the DNA was purified using ChIP-DNA clean and concentrator kit (Zymo) and quantified on a qubit. This way we ensured that for each pairwise comparison (wild type versus mutant ChIP), we began with an equal amount of input. We started with 145 ng and 285 ng of input DNA for each H3K27ac and H2AK119ub1 ChIP respectively. Digested chromatin was mixed with complete immnuoprecipitation (IP) buffer (20mM Tris-HCl pH 8.0, 2mM EDTA, 150 mM NaCl, 0.1% Triton X-100, 1x Protease inhibitor cocktail -PIC, 1mM Phenylmethanesulfonyl fluoride -PMSF) such that it comprised less than 25 % of the total volume. Chromatin was pre-cleared with 10 ul of magnetic Protein A (Bio-Rad) or G (Invitrogen/Dynalbeads) beads for 1 hour on a rotator at 4 C. After pre-clearing, 10% chromatin was set aside as input. Pre-cleared lysates were then mixed with antibodies to perform the ChIP. 5µg of rabbit anti-H3K27ac (Active Motif – 39133) conjugated to Protein A beads (Bio-Rad) and 10 µg of mouse anti-H2AK119ub1 IgM antibodies (Millipore E6C5, 05-678) were added to the lysates and left to bind chromatin by rotating the tubes overnight at 4 C. The following day anti-mouse IgM (Millipore, 12-488) conjugated to proteinA/G beads were added to the H2AK119ub1 ChIP samples and rotated at 4 C for 3 hours to capture anti-H2AK119ub1 bound chromatin. Chromatin bound to bead-antibody conjugates from all ChIP samples were isolated using a magnetic separator. Beads were then washed twice in low salt buffer followed by two washes in high salt buffer and eventually re-suspended in 100 µl of elution buffer (1%SDS/100mM $NaHCO_3$) in a 1.5 ml eppendorf tube. DNA was

eluted at 65 C on a shaking incubator (Eppendorf) at 800 rpm for 30 min. Eluate was separated from beads on a magnetic separator. 5 µl of 5M NaCl was added to eluate and incubated in 65 C water bath overnight to reverse crosslinks. ChIP DNA was digested with RNAseA for 30 min at 37 C followed by ProteinaseK digestion for 1 hr at 56 C and then purified using a ChIP-DNA clean and concentrator kit (Zymo) and quantified with a qubit. Libraries were prepared from ChIP and Input samples using the Kapa Hyperprep kit.

ChIP-seq data analysis:

Reads were aligned to mm9 using bowtie/bowtie2 (Langmead and Salzberg, 2012; Langmead et al., 2009). The resulting sam output files were converted to the BAM format using Samtools, version 1.6.0 (Li et al., 2009). The bam files were filtered to remove PCR duplicates using Picard tools, MarkDuplicates (**http://broadinstitute.github.io/picard**). The BAM files were converted to bigwig files for visualization on the UCSC browser (Kent 2002). The bigwig files were generated using DeepTools (Ramírez et al., 2016), bamCompare with a bin size of 10 bp ,extending fragments to 150bp (nucleosome size), filtered for mm9 blacklisted regions and normalized to 1X depth of coverage. Each bigwig file represents the $\log_2$ ratio of ChIP to the corresponding Input sample. For comparison across samples the bigwig files were normalized to effective library size. Replicates were merged into a single bigwig using UCSC tools, bigWigMerge (http://hgdownload.soe.ucsc.edu/admin/exe/). Read coverage over regions of interest were generated from matrix files generated using DeepTools, computeMatrix following which metagene plots were made in R using ggplo2 (Wilkinson, 2011). Peaks from each sample were called using Macs2, version2.1.0, (Zhang et al., 2008) in broadpeak mode with --broad-cutoff 0.05 (FDR ≤ 0.05). Overlapping peaks between replicates were identified using bedtools, intersectBed and were used for subsequent analysis. A list of all BRG1 peak calls are provided (Table S3) Peaks were annotated using HOMER, peakannotate.pl (Heinz et al., 2010). Differential peak analysis was performed on bedgraph files using Macs2, bdgdiff run with default parameters.

ATAC-seq data analysis:

Reads were aligned to the mm9 genome using bowtie, with following paramters: -S –q –m 1 –p 2 –best –strata –chunkmbs 256 (Langmead et al., 2009). The outputed sam files were converted to BAM files using Samtools version 1.3.1. Next Bedtools version 2.25.0 (Quinlan and Hall, 2010), bamtobed was used to convert BAM output files to bed file format to do the subsequent steps . BAM files were converted to bigWig files for visualization on UCSC browser and to generate metagene plots as described above (see supplementary materials on ChIP-seq data analysis).

Differential analysis of chromatin accessibility:

For the differential analysis of chromatin accessibility, we adopted a method described for analyzing significant differences in counts between DNA hypersensitive sites identified by Dnase seq (Shibata et al., 2012). We compared differences in chromatin accessibility between 12 day old (P12) *Brg1*^{WT} and *Brg1*^{cKO} spermatogenic cells . Here the pairwise comparison was performed using edgeR, after obtaining the read counts from each replicate across defined 300 bp windows generated from a union set of the top 100,000 peaks (ranked by F-Seq). We called windows with significantly different counts from the pairwise comparison at a FDR ≤ 0.05. The significantly altered regions were annotated using HOMER, peakannotate.pl (Heinz et al., 2010). Regions with significant differences in open chromatin are provided (Table S2).

Preparation of nuclear lysates for immunoprecipitation:

Spermatogenic cells isolated from 2- to 3-week-old males were washed once in PBS and centrifuged at 600g for 5 min at 4 C. The resulting cell pellet was re-suspended in 20 PCV (packed cell volumes) of buffer A (10mM HEPES-KOH pH7.9, 1.5mM MgCl2, 10mM KCl, 0.1% NP-40, 0.5mM DTT, 0.5mM PMSF, 1x PIC, 0.5) and left on ice to swell for 10 min. Cells were centrifuged at 600g for 5 min at 4 C, resuspended in 2 PCV of buffer A and then homogenized using a dounce (type B). The homogenate containing nuclei were centrifuged at 700g for 10 min at 4 C. Nuclear preparations were washed once again in 10 PCV of buffer A and pelleted at 5000 rpm for 10 min at 4 C. Lysates were extracted from pelleted nuclei at least twice for 1 hour each with an equal volume of high salt buffer C (20mM HEPES-KOH pH7.9, 1.5mM MgCl2,

420mM NaCl, 10mM KCl, 25 % glycerol, 0.2mM EDTA, 0.5mM DTT, 0.5mM PMSF, 1x PIC) on a nutator at 4 C. The resulting nuclear lysates were mixed with 2.8x volume of buffer D (20mM HEPES-KOH pH7.9, 20 % glycerol, 0.2mM EDTA ,0.5mM DTT, 0.5mM PMSF, 1x PIC) following which they were clarified by spinning at 14,000 rpm for 10 min at 4 C, pooled together and snap-frozen in liquid nitrogen and stored at -80 C until further use.

Co-Immunoprecipitation (Co-IP):

100 µl of magnetic protein A beads were initially washed twice in PBS for 5 min each at 4 C followed by one wash in PBS + 0.5% BSA for 10 min at 4 C. The antibodies (tableS3) were then mixed with beads resuspended in 1x volume of PBS + 0.5% BSA and allowed to conjugate for at least 2 hr at 4 C. After this, antibody-bead conjugates were washed once with 500 µl of PBS + 0.5% BSA , followed by two washes in IP buffer (20mM HEPES-KOH pH7.9, 0.15mM KCl, 10 % glycerol, 0.2mM EDTA, 0.5mM DTT, 0.5mM PMSF, 1x PIC) for 5 min each at 4 C. The antibody-coupled beads were stored in IP buffer until the nuclear lysates were processed for IP. Briefly, the lysates were thawed on ice and centrifuged at 14,000 rpm at 4 C to remove any precipitates. 500 µg of nuclear lysate was diluted in IP buffer to make up the volume to 1.3 ml and then incubated with unconjugated protein A beads to pre-clear the lysate. A fraction of lysate was set aside as input and the remaining was transferred to a tube containing the antibody coupled beads and left on a rotator overnight at 4 C. The following day the protein bound antibody-bead conjugates were separated using a magnetic separator and washed on a rotator with a series of buffers in the following order at 4 C for 5 min each: twice in IP buffer, twice in high salt wash buffer (20mM HEPES-KOH pH7.9, <u>300mM KCl</u>, 10 % glycerol, 0.2mM EDTA, 0.1 % Tween-20, 0.5mM DTT, 0.5mM PMSF, 1x PIC), twice in a low salt wash buffer (20mM HEPES-KOH pH7.9, <u>100mM KCl</u>, 10 % glycerol, 0.2mM EDTA, 0.1 % Tween-20, 0.5mM DTT, 0.5mM PMSF, 1x PIC), once in final wash buffer (20mM HEPES-KOH pH7.9, 60mM KCl, 10 % glycerol, 0.5mM DTT, 0.5mM PMSF, 1x PIC). The proteins were eluted by resuspending the beads in 2X Laemmli buffer and incubating them at 70 C for 10 min followed by boiling the samples at 95 C for 5 min.

BRG1-IP and mass spectrometry:

Prior to mass spectrometry the IPs were performed with anti-BRG1 antibody and non-specific IgG (table S4) as described above with a few modifications. After conjugation each antibody

was crosslinked to protein A beads with BS^3 (bis[sulfosuccinimidyl] suberate) crosslinking agent, prepared as per the manufacturer's instructions (Thermo scientific, 21585). Crosslinking with BS^3 significantly reduces IgG elution and improves signal to noise ratio in samples obtained by boiling beads in Laemlli buffer (Sousa et al., 2011). Briefly, antibody coupled beads were washed once in PBS for 5 min at 4 C, followed by two washes in conjugation buffer pH 7.9 (20 mM Sodium Phosphate, 0.15M NaCl). The antibody-coupled beads were resuspended in 250 ul of conjugation buffer containing 5mM BS^3 in a tube and incubated on a rotator for 40 min at room temperature. Antibody crosslinked beads were separated and the crosslinker was quenched with an equal volume of 1M glycine (1x volume of beads). The crosslinked beads were then washed once in PBS at 4 C for 5 min, followed by incubation in 100 ul of 0.11M glycine (pH2.5) for 10 min at 4 C to remove any uncrosslinked antibody. The crosslinked beads were then washed thrice in PBS tween-20 (0.1%) + 0.5 % BSA, followed by another three washes in IP buffer before transferring them to a 15 ml falcon tube containing 4 mg of nuclear lysate made up in IP buffer up to a final volume of 10ml and left on rotator overnight at 4 C. The following day the beads were washed and proteins were eluted as described above. Samples were run on a short gel from which the regions containing the proteins were cut out and processed for mass spectrometry and peptide identification.

In-gel Digestion

Gel slices were cut into 1x1 mm pieces and placed in 1.5 mL eppendorf tubes with 1 mL of water for 30 min. The water was then removed and 50 µL of 250 mM ammonium bicarbonate followed by10 µL of 45 mM 1, 4 dithiothreitol (DTT) were added prior to incubation at 50 ^{o}C for 30 min. The samples were cooled to room temperature and then alkylated with 10 µL of 100 mM iodoacetamide for 30 min. The gel pieces were washed 2x with 1 mL of water, removed and added 1 mL of 50 mM ammonium bicarbonate:acetonitrile (1:1) and allowed to incubate at room temperature for 1 hr. The solution was then removed and 200 µL of acetonitrile was added, removed, and the gel pieces dried by SpeedVac. Gel pieces were rehydrated in 70 µL of 2 ng/µL trypsin (Sigma) and 0.01% ProteaseMAX surfactant (Promega) in 50mM ammonium bicarbonate and incubated at 37 ^{o}C for 21hrs. Supernatant was removed, gel pieces added 100 µL of 80:20 (1% (v/v) formic acid in acetonitrile), combined with the former supernatant, and dried on a SpeedVac. Samples were reconsituted in 25 µL of 5% acetonitrile (0.1% (v/v) trifluroacetic acid) for LC-MS/MS analysis.

LC-MS/MS

Tryptic peptides were dissolved in 0.1% trifluoroacetic acid and directly loaded at 4 µL/min for 7 minutes onto a custom-made trap column (100 µm I.D. fused silica with Kasil frit) containing 2 cm of 200Å, 5 µm Magic C18AQ particles (Michrom Bioresources). Peptides were then eluted onto a custom-made analytical column (75 µm I.D. fused silica) with gravity-pulled tip and packed with 25 cm 100Å, 5 µm Magic C18AQ particles (Michrom). Peptides were eluted with a linear gradient from 100% solvent A (0.1% (v/v) formic acid in water:0.1% formic acid in acetonitrile (95:05)) to 35% solvent B (0.1% (v/v) formic acid in acetonitrile) in 90 minutes at 300 nanoliters per minute using a Waters NanoAcquity UPLC system directly coupled to a Thermo Scientific Q Exactive hybrid mass spectrometer. Data were acquired using a data-dependent acquisition routine of acquiring one mass spectrum (*m/z* 300 -1750) in the Orbitrap (resolution 70,000, 1e6 charges, 30 ms maximum fill time) followed by 10 tandem mass spectrometry scans (resolution 17,500, 1e5 charges, 110 ms maximum fill time, HCD collision energy 27 eV NCE). Dynamic exclusion was employed to maximize the number of peptide identifications and minimize data redundancy.

Data Analysis

Raw data files were processed into peak lists using Proteome Discoverer (version 1.4; Thermo Scientific) and then searched against the Uniprot mouse database with Mascot (version 2.5; Matrix Science) using precursor mass tolerances of 10 ppm and fragment mass tolerances of 0.5 Da. Full tryptic specificity was specified considering up to 2 missed cleavages; variable modifications of acetylation (protein N-term), pyro-glutamination (N-term glutamine), and oxidation (methionine) were considered and fixed modifications of carbamidomethylation (cysteine) were considered. Mascot search results were loaded into Scaffold (Proteome Software) with threshold values of 80% for peptides (1.0% false-discovery rate) and 90% for proteins (2 peptide minimum) for final annotation.

Supplemental references:

Heinz, S., Benner, C., Spann, N., Bertolino, E., Lin, Y. C., Laslo, P., Cheng, J. X., Murre, C., Singh, H. and Glass, C. K. (2010). Simple Combinations of Lineage-Determining Transcription Factors Prime cis-Regulatory Elements Required for Macrophage and B Cell Identities. *Mol. Cell* **38**, 576–589.

Langmead, B. and Salzberg, S. L. (2012). Fast gapped-read alignment with Bowtie 2. *Nat. Methods* **9**, 357–359.

Langmead, B., Trapnell, C., Pop, M. and Salzberg, S. (2009). Ultrafast and memory-efficient alignment of short DNA sequences to the human genome. *Genome Biol.* **10**, R25.

Li, H., Handsaker, B., Wysoker, A., Fennell, T., Ruan, J., Homer, N., Marth, G., Abecasis, G. and Durbin, R. (2009). The Sequence Alignment/Map format and SAMtools. *Bioinformatics* **25**, 2078–2079.

Quinlan, A. R. and Hall, I. M. (2010). BEDTools: A flexible suite of utilities for comparing genomic features. *Bioinformatics* **26**, 841–842.

Raab, J. R., Resnick, S. and Magnuson, T. (2015). Genome-Wide Transcriptional Regulation Mediated by Biochemically Distinct SWI/SNF Complexes. *PLoS Genet.* **11**, 1–26.

Ramírez, F., Ryan, D. P., Grüning, B., Bhardwaj, V., Kilpert, F., Richter, A. S., Heyne, S., Dündar, F. and Manke, T. (2016). deepTools2: a next generation web server for deep-sequencing data analysis. *Nucleic Acids Res.* **44**, W160–W165.

Shibata, Y., Sheffield, N. C., Fedrigo, O., Babbitt, C. C., Wortham, M., Tewari, A. K., London, D., Song, L., Lee, B. K., Iyer, V. R., et al. (2012). Extensive evolutionary changes in regulatory element activity during human origins are associated with altered gene expression and positive selection. *PLoS Genet.* **8**,.

Sousa, M. M. L., Steen, K. W., Hagen, L. and Slupphaug, G. (2011). Antibody cross-linking and target elution protocols used for immunoprecipitation significantly modulate signal-to noise ratio in downstream 2D-PAGE analysis. *Proteome Sci.* **9**, 45.

Wilkinson, L. (2011). ggplot2: Elegant Graphics for Data Analysis by WICKHAM, H. *Biometrics* **67**, 678–679.

Zhang, Y., Liu, T., Meyer, C. A., Eeckhoute, J., Johnson, D. S., Bernstein, B. E., Nussbaum, C., Myers, R. M., Brown, M., Li, W., et al. (2008). Model-based analysis of ChIP-Seq (MACS). *Genome Biol.* **9**,.

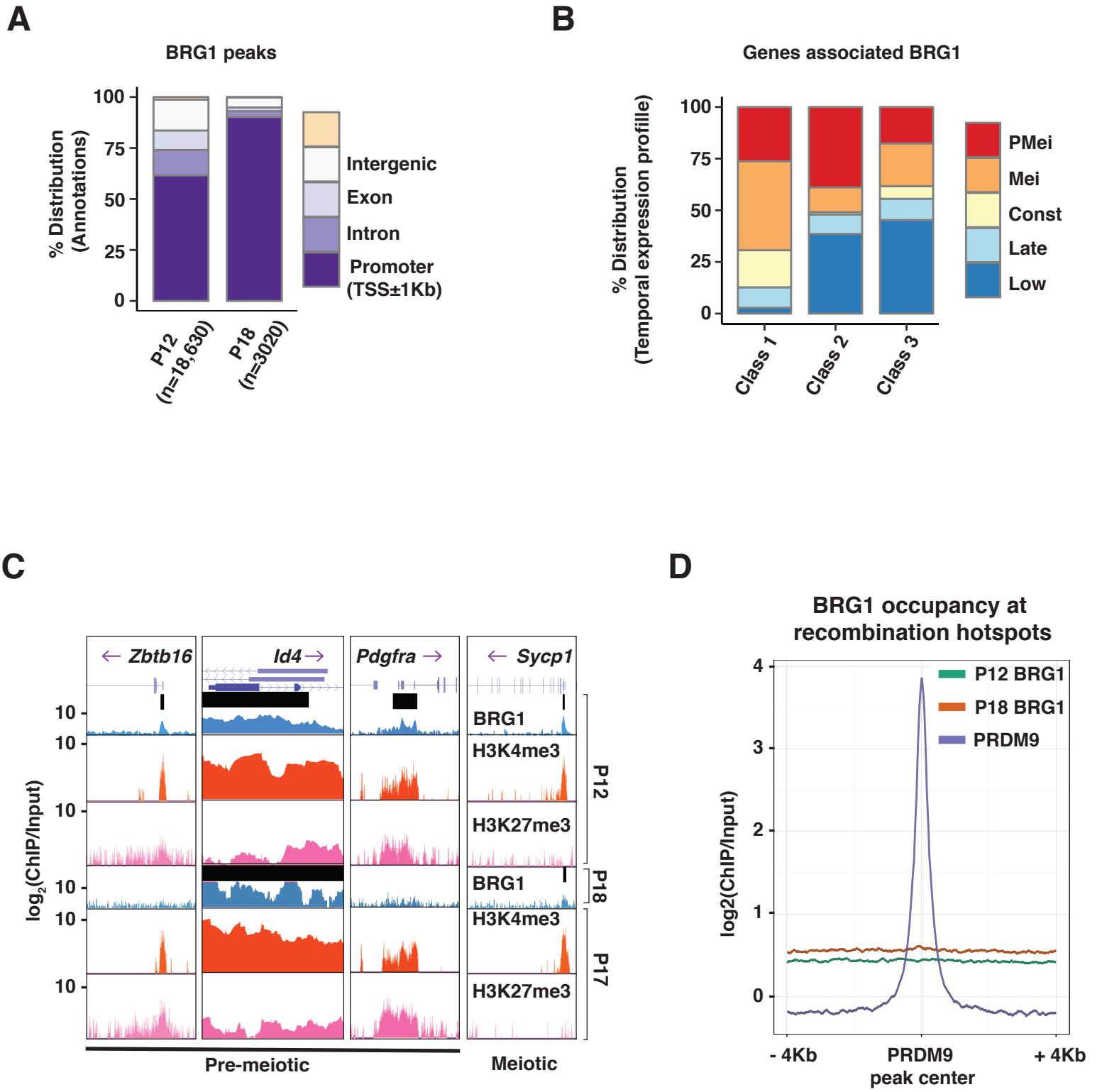
A
BRG1 peaks
% Distribution (Annotations)
100
75
50
25
0
P12 (n=18,630)
P18 (n=3020)
Intergenic
Exon
Intron
Promoter (TSS±1Kb)
B
Genes associated BRG1
% Distribution (Temporal expression profile)
100
75
50
25
0
Class 1
Class 2
Class 3
PMei
Mei
Const
Late
Low
C
Zbtb16
Id4
Pdgfra
Sycp1
BRG1
H3K4me3
H3K27me3
BRG1
H3K4me3
H3K27me3
P12
P18
P17
log2(ChIP/Input)
10
Pre-meiotic
Meiotic
D
BRG1 occupancy at recombination hotspots
P12 BRG1
P18 BRG1
PRDM9
log2(ChIP/Input)
4
3
2
1
0
- 4Kb
PRDM9 peak center
+ 4Kb

A

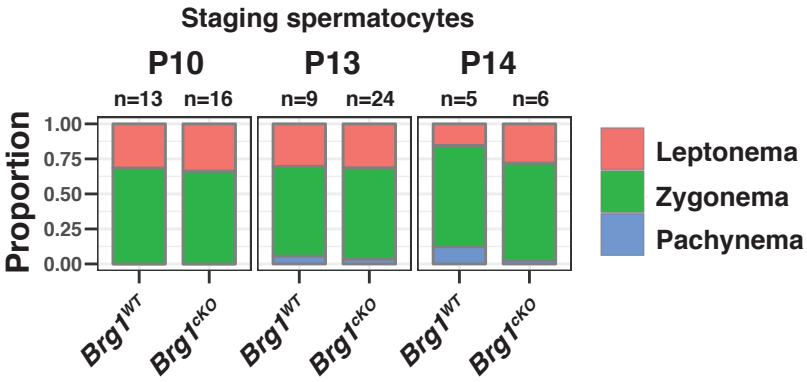
Staging spermatocytes
P10
P13
P14
n=13
n=16
n=9
n=24
n=5
n=6
Proportion
1.00
0.75
0.50
0.25
0.00
Brg1WT
Brg1cKO
Leptonema
Zygonema
Pachynema

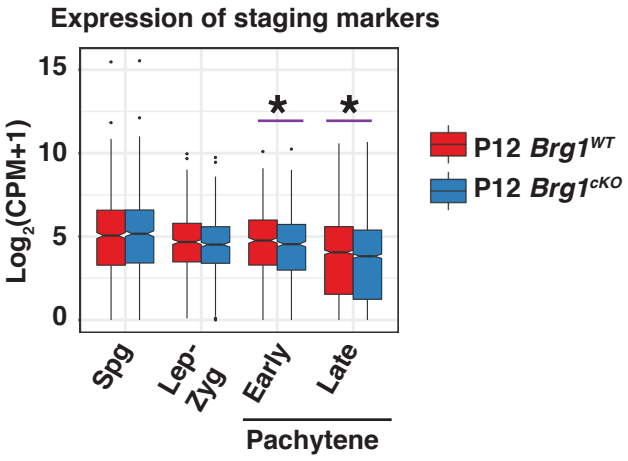
Expression of staging markers
Log2(CPM+1)
15
10
5
0
Spg
Lep-Zyg
Early
Late
Pachytene
P12 Brg1WT
P12 Brg1cKO

B

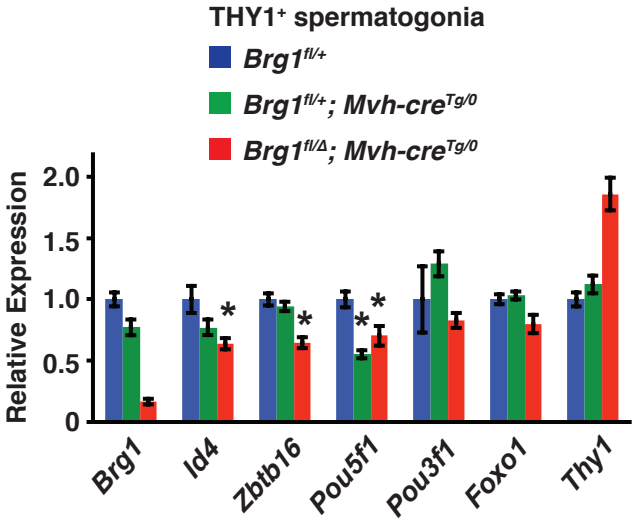
THY1+ spermatogonia
Brg1fl/+
Brg1fl/+; Mvh-creTg/0
Brg1fl/Δ; Mvh-creTg/0
Relative Expression
2.0
1.5
1.0
0.5
0
Brg1
Id4
Zbtb16
Pou5f1
Pou3f1
Foxo1
Thy1

D

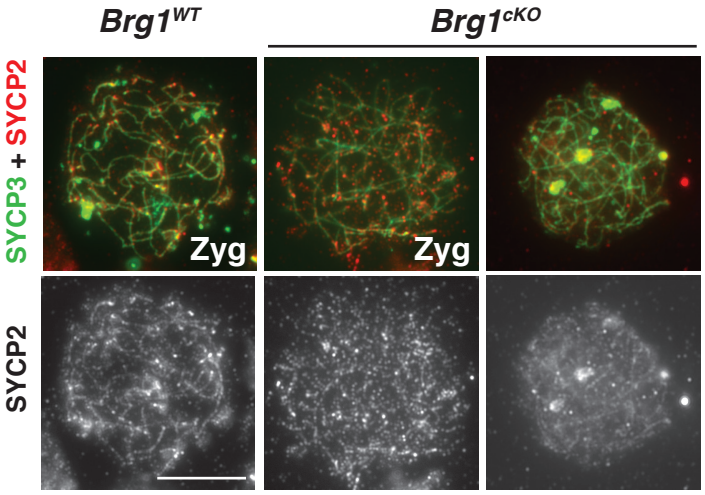
Brg1WT
Brg1cKO
SYCP3 + SYCP2
SYCP2
Zyg
Zyg

C

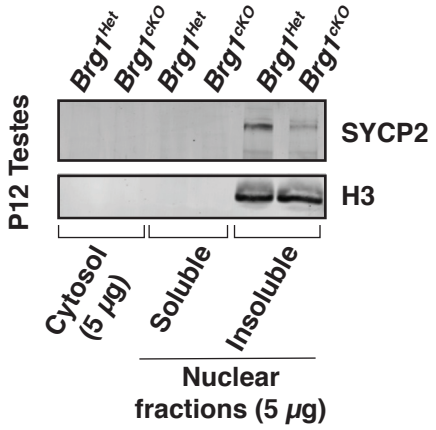
Brg1Het
Brg1cKO
P12 Testes
SYCP2
H3
Cytosol (5 μg)
Soluble
Insoluble
Nuclear fractions (5 μg)

E

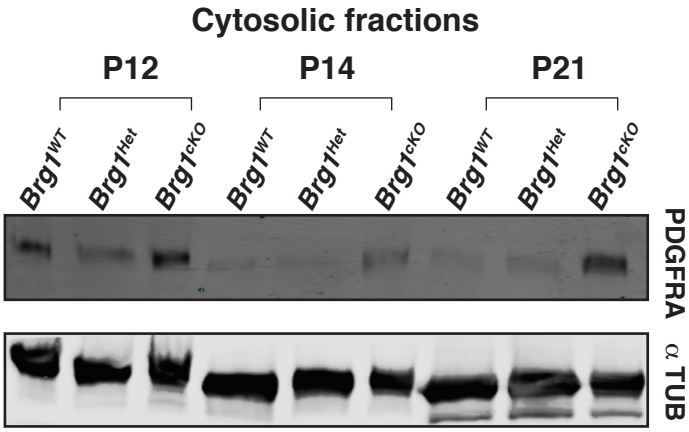
Cytosolic fractions
P12
P14
P21
Brg1WT
Brg1Het
Brg1cKO
PDGFRA
α TUB

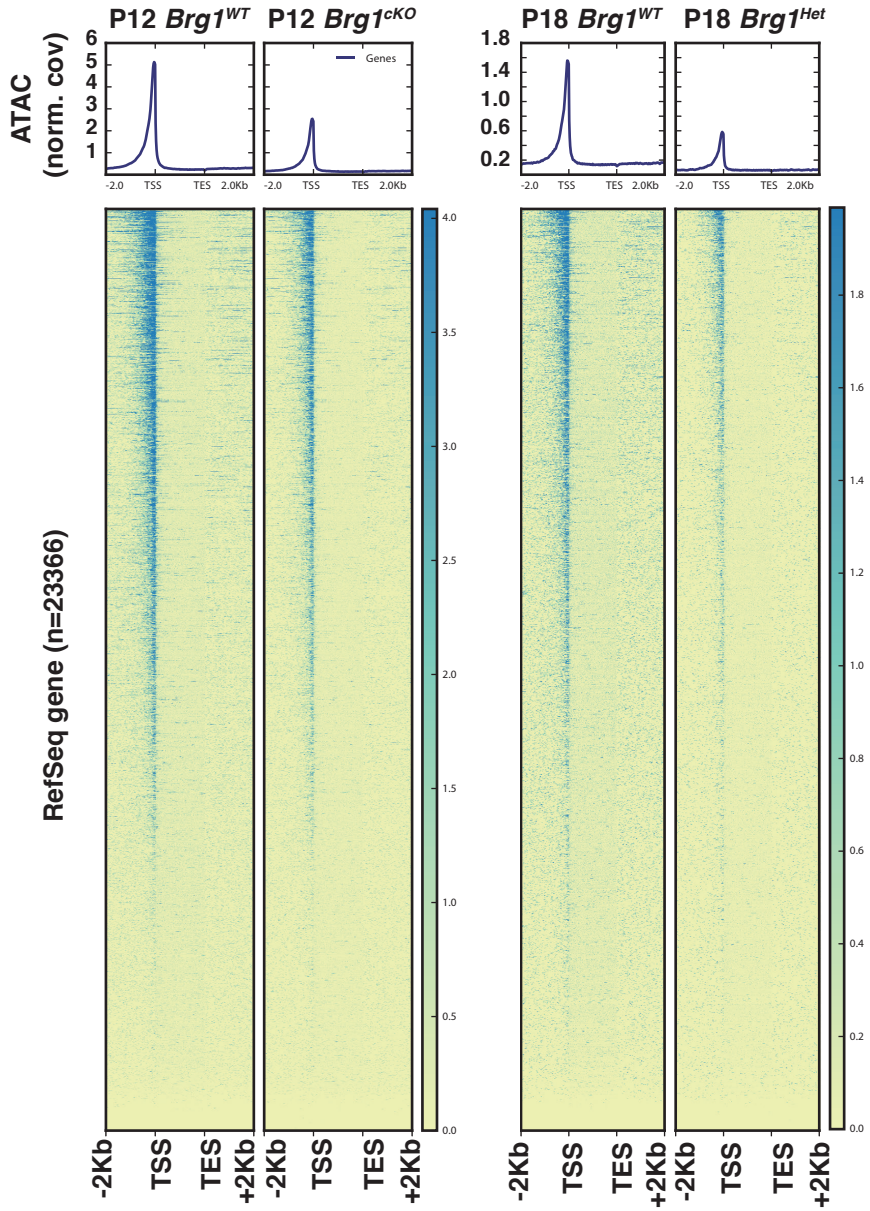
A
P12 Brg1WT
P12 Brg1cKO
P18 Brg1WT
P18 Brg1Het
ATAC (norm. cov)
Genes
RefSeq gene (n=23366)
-2Kb
TSS
TES
+2Kb

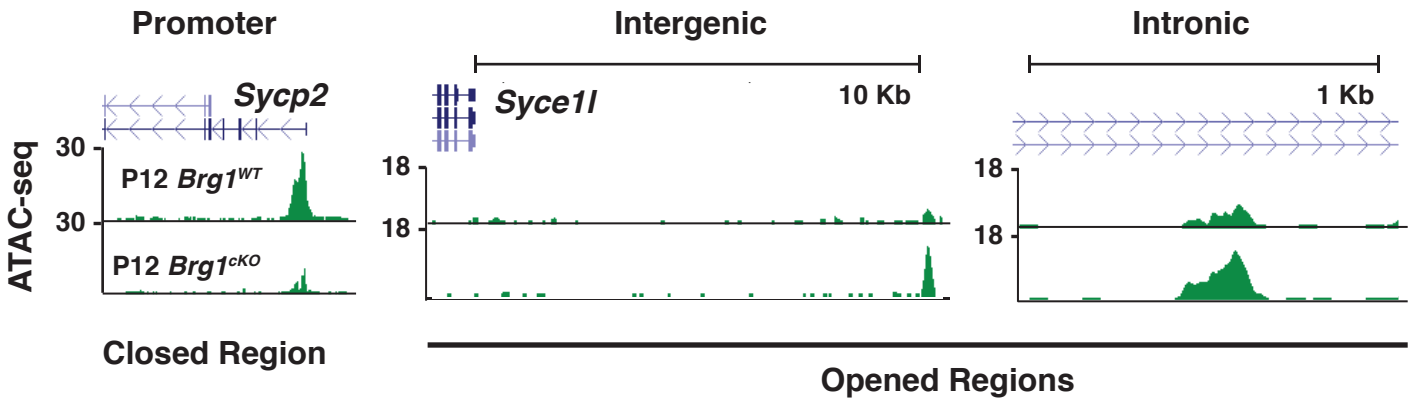
B
Promoter
Intergenic
Intronic
Sycp2
Syce1l
10 Kb
1 Kb
ATAC-seq
P12 Brg1WT
P12 Brg1cKO
Closed Region
Opened Regions

A

	Protein	# Unique Peptide	% Coverage
Shared SWI/SNF sub units	BAF60A	37	82
	BAF60B	26	60
	BAF60C	19	45
	BAF45A	14	36
	BAF45B	10	38
	BAF45C	8	33
	BAF45D	15	49
	BAF57	20	51
	BAF53A	22	55

B

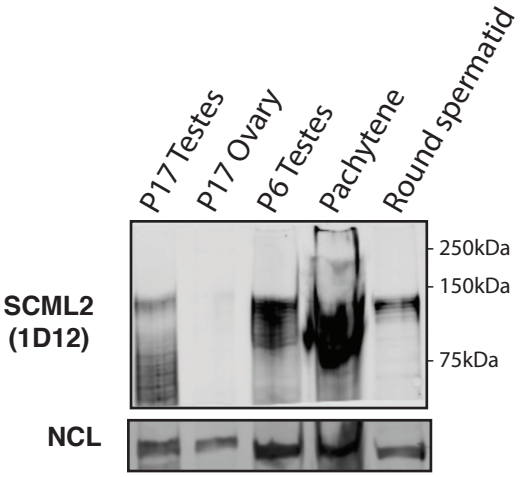

C

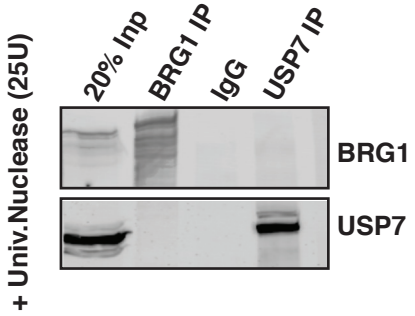

A

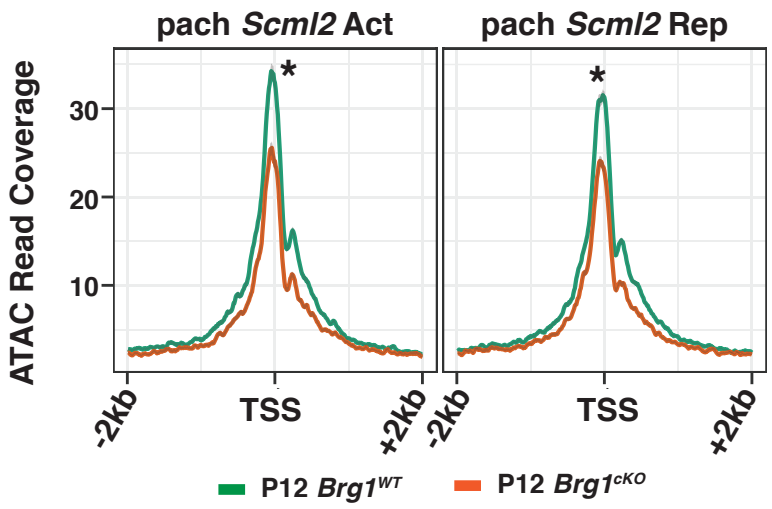
pach Scml2 Act
pach Scml2 Rep
ATAC Read Coverage
30
20
10
*
*
-2kb
TSS
+2kb
-2kb
TSS
+2kb
P12 Brg1WT
P12 Brg1cKO

B

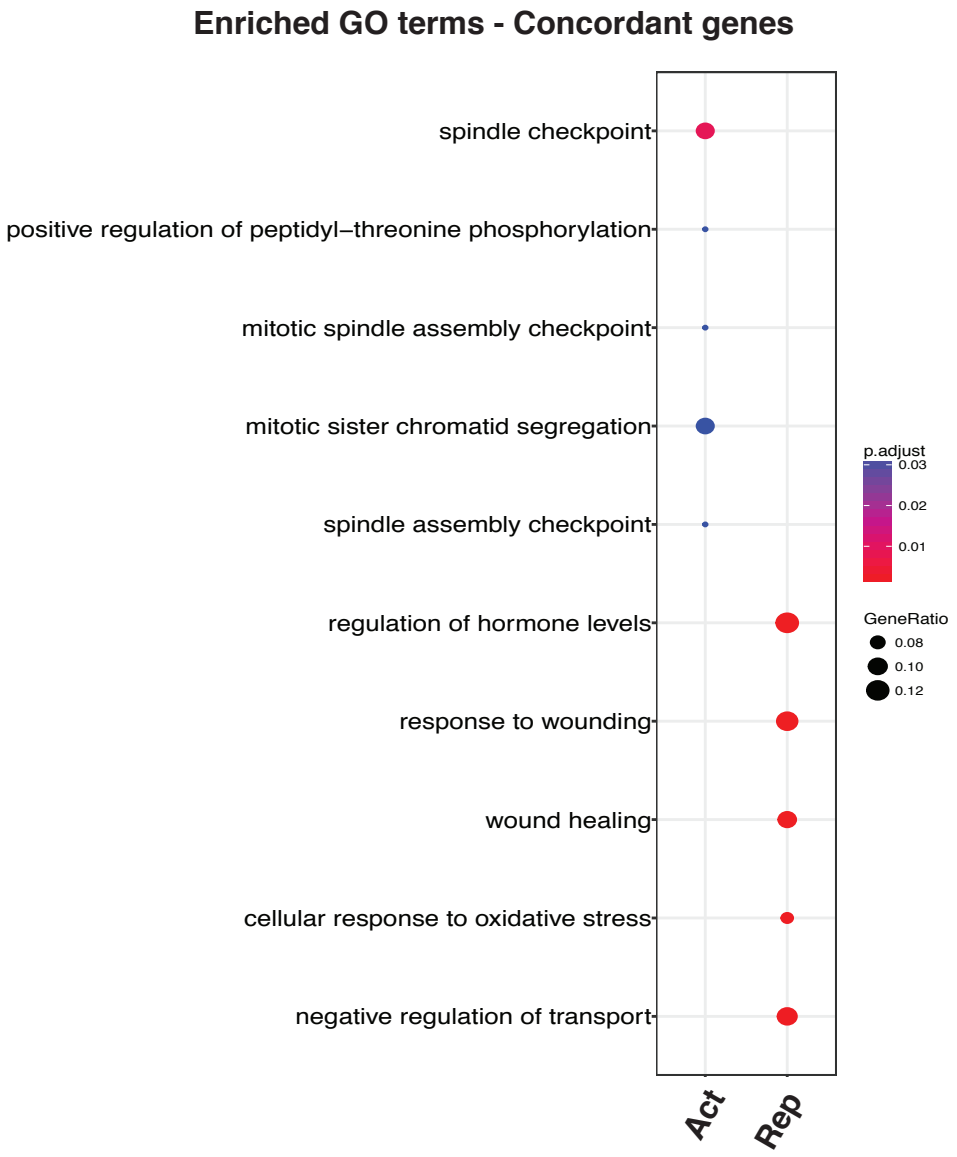
Enriched GO terms - Concordant genes
spindle checkpoint
positive regulation of peptidyl−threonine phosphorylation
mitotic spindle assembly checkpoint
mitotic sister chromatid segregation
spindle assembly checkpoint
regulation of hormone levels
response to wounding
wound healing
cellular response to oxidative stress
negative regulation of transport
Act
Rep
p.adjust
0.03
0.02
0.01
GeneRatio
0.08
0.10
0.12

A

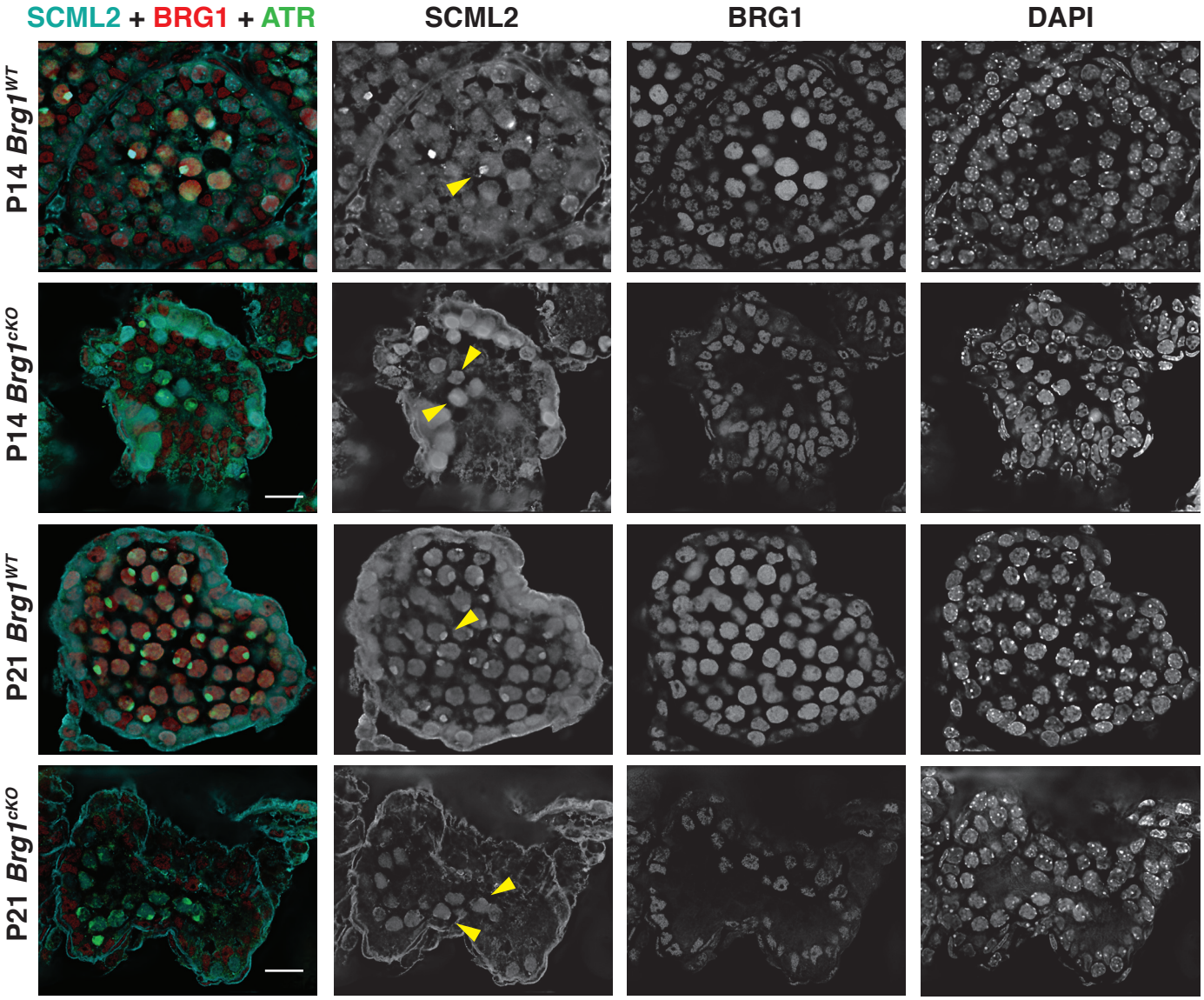
SCML2 + BRG1 + ATR
SCML2
BRG1
DAPI
P14 Brg1WT
P14 Brg1cKO
P21 Brg1WT
P21 Brg1cKO

B

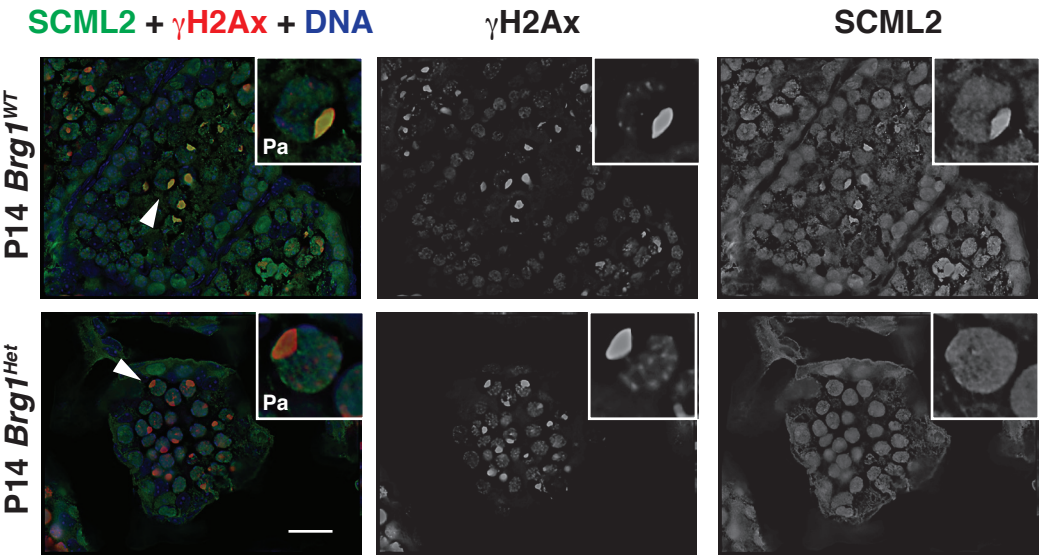
SCML2 + γH2Ax + DNA
γH2Ax
SCML2
P14 Brg1WT
P14 Brg1Het
Pa
Pa

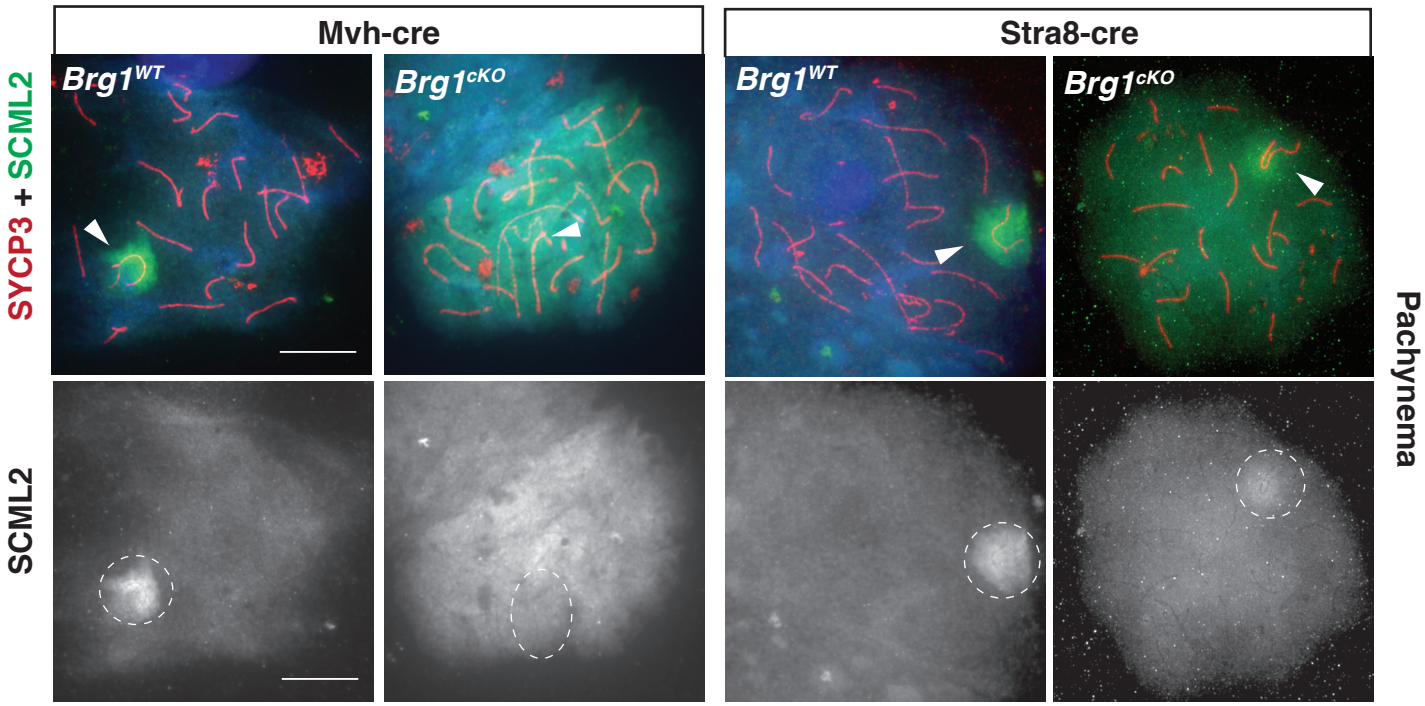
Mvh-cre
Stra8-cre
Brg1WT
Brg1cKO
Brg1WT
Brg1cKO
SYCP3 + SCML2
SCML2
Pachynema

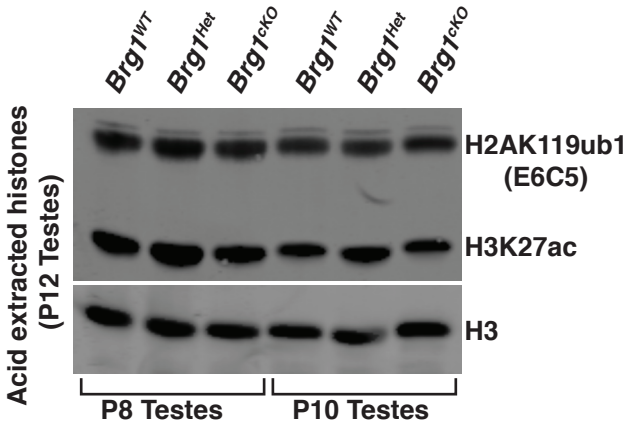
A
Brg1WT
Brg1Het
Brg1cKO
Brg1WT
Brg1Het
Brg1cKO
Acid extracted histones
(P12 Testes)
H2AK119ub1
(E6C5)
H3K27ac
H3
P8 Testes
P10 Testes

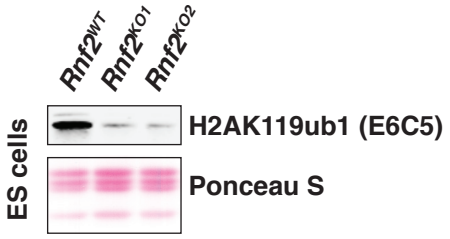
C
Rnf2WT
Rnf2KO1
Rnf2KO2
ES cells
H2AK119ub1 (E6C5)
Ponceau S

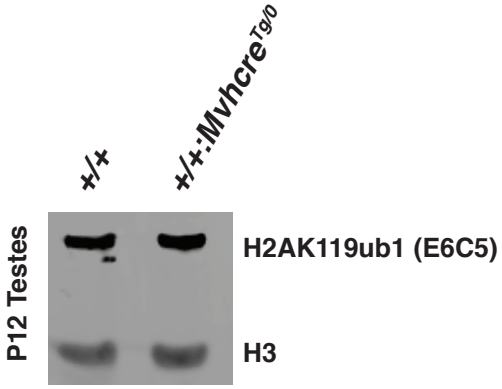
B
+/+
+/+;Mvhcre Tg/0
P12 Testes
H2AK119ub1 (E6C5)
H3

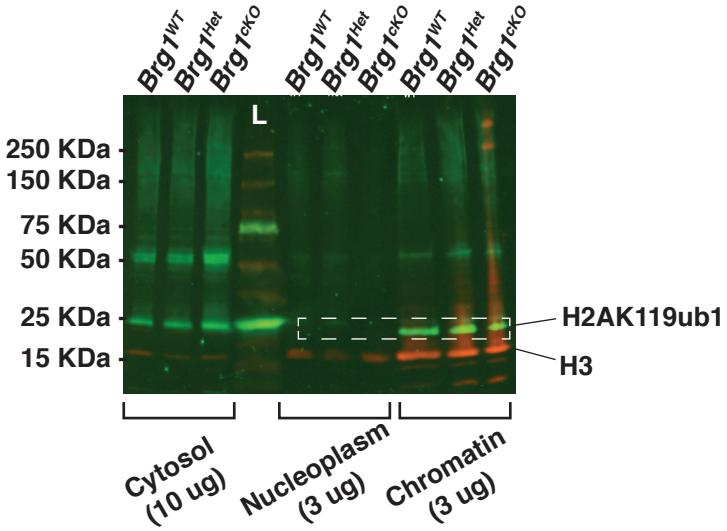
D
Brg1WT
Brg1Het
Brg1cKO
Brg1WT
Brg1Het
Brg1cKO
Brg1WT
Brg1Het
Brg1cKO
L
250 KDa
150 KDa
75 KDa
50 KDa
25 KDa
15 KDa
H2AK119ub1
H3
Cytosol
(10 ug)
Nucleoplasm
(3 ug)
Chromatin
(3 ug)

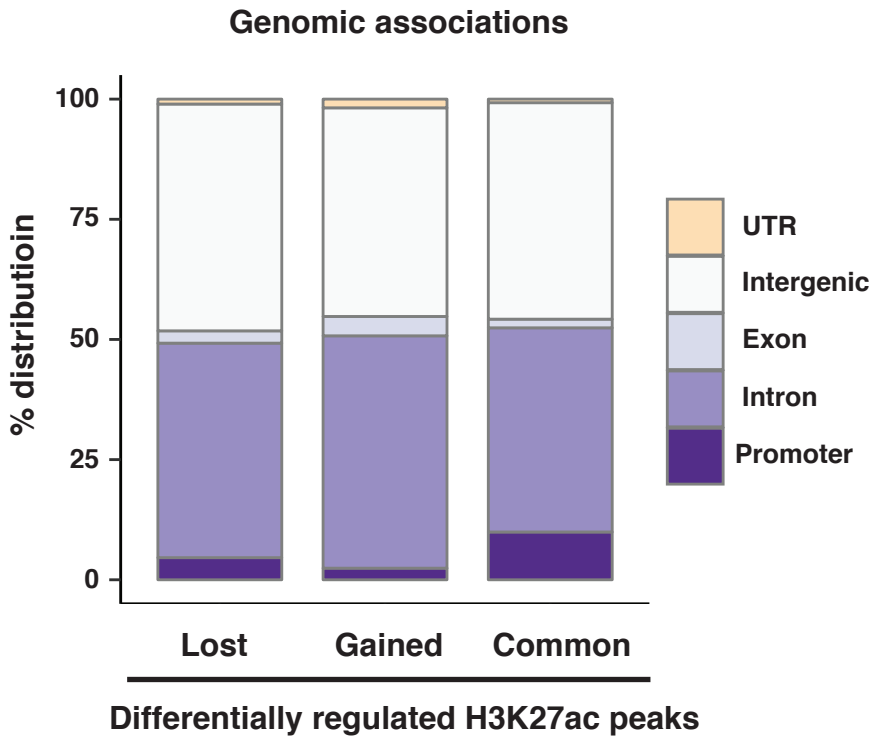
Genomic associations
% distributioin
100
75
50
25
0
Lost
Gained
Common
Differentially regulated H3K27ac peaks
UTR
Intergenic
Exon
Intron
Promoter

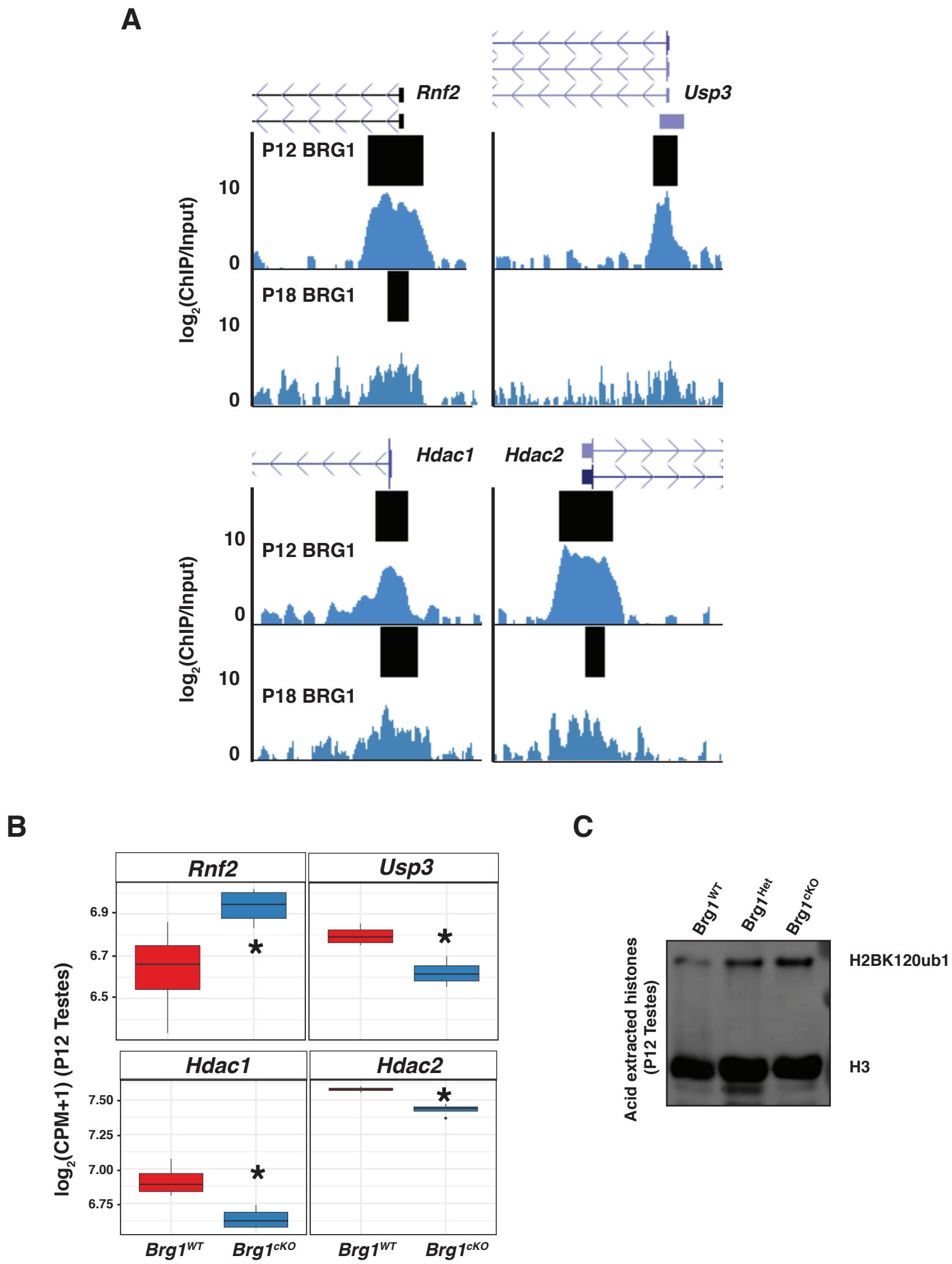
A
Rnf2
Usp3
P12 BRG1
P18 BRG1
log2(ChIP/Input)
10
0
Hdac1
Hdac2
B
Rnf2
Usp3
Hdac1
Hdac2
log2(CPM+1) (P12 Testes)
6.9
6.7
6.5
7.50
7.25
7.00
6.75
Brg1WT
Brg1cKO
C
Brg1WT
Brg1Het
Brg1cKO
Acid extracted histones (P12 Testes)
H2BK120ub1
H3